

Durham E-Theses

The lubrication of porous elastic solids with reference to the functioning of animal joints

Norman, R

How to cite:

Norman, R (1971) *The lubrication of porous elastic solids with reference to the functioning of animal joints*, Durham theses, Durham University. Available at Durham E-Theses Online:
<http://etheses.dur.ac.uk/9083/>

Use policy

The full-text may be used and/or reproduced, and given to third parties in any format or medium, without prior permission or charge, for personal research or study, educational, or not-for-profit purposes provided that:

- a full bibliographic reference is made to the original source
- a [link](#) is made to the metadata record in Durham E-Theses
- the full-text is not changed in any way

The full-text must not be sold in any format or medium without the formal permission of the copyright holders.

Please consult the [full Durham E-Theses policy](#) for further details.

"I could have done it in a much more complicated way", said the Red Queen, immensely proud.

Lewis Carroll, Alice in Wonderland

Science is a subversive activity that flourishes best when no one is looking.

Anon

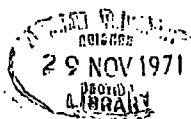
THE LUBRICATION OF POROUS ELASTIC SOLIDS
WITH REFERENCE TO THE FUNCTIONING OF
ANIMAL JOINTS

By

R. NORMAN, B.Sc.

A thesis submitted for the degree of Doctor of Philosophy
in the Department of Engineering Science, University of Durham.

October 1971.



ACKNOWLEDGMENTS

The Author is indebted to the following people whose help and encouragement have made this research possible:

Professor G.R. Higginson for his supervision and suggestions.

The technicians of the Engineering Science Department for their help in constructing the experimental rig.

ABSTRACT

This investigation is concerned with the elasto-hydrodynamic squeeze-films generated by the normal approach of two surfaces. It is inspired by the excellent functioning of healthy animal joints under the adverse conditions of high load and low, or even zero, sliding speeds.

The effects on the film of four features are examined from both the theoretical and experimental viewpoints. These four features are the elasticity of the materials bounding the film, the permeability of these materials, an extreme interpretation of the concept of "weeping" lubrication and the presence of a lubricant enrichment in the film. This latter feature is considered only in its theoretical aspects.

It is shown experimentally that when a thin layer of rubber is used as the soft boundary of the film, entrapment occurs, due to the high poisson's ratio involved. The agreement between theoretical predictions and experimental results for the effects of permeability and of a "weeping" mechanism is good.

The models, as examined, are found to be dominated by viscous forces rather than the inertia of the moving surfaces.

It is found that high permeability of the surfaces tends to decrease film life and that high flexibility tends to increase it. However, very low permeability material appears to promote slight "weeping" tendencies and hence prolong film lives.

The effect of an additive confined to motion in the fluid flow is found to be small unless present at extremely high concentrations and in joints it seems likely to be effective only at very thin films.

When the additive is confined not only to the film but also prevented from flowing in the film, squeeze times are found to be increased by several times. The increase is not considered to be enough to make the mechanism totally convincing as a mode of operation of an animal joint.

CONTENTS

	PAGE
CHAPTER 1	
INTRODUCTION	1
NOTATION	5
CHAPTER 2	
THEORETICAL DEVELOPMENT OF THE MODEL	8
2.1	8
Introduction	
2.2	9
Rigid Impervious Boundaries	
2.3	11
"Weeping" Lubrication	
2.4	15
Impermeable Elastic Layer	
2.5	16
Rigid Permeable Thin Layer	
2.6	18
Permeable Elastic Layer	
2.7	20
Lubricant Additive and Permeable Elastic Layer	
2.8	23
"Dowson" Enrichment Model	
CHAPTER 3	
NUMERICAL SOLUTION OF THE MODEL	24
3.1	24
Introduction	
3.2	25
Normal Approach with an Isoviscous Lubricant and Rigid Boundaries	
3.2.1	25
The Direct Solution of the Equation of Motion	
3.2.2	26
Numerical Problems of the Direct Solution	
3.2.3	27
Indirect Solution of the Equation of Motion	
3.3	29
"Weeping" Lubrication	
3.4	29
Elastic Impermeable Surfaces	
3.5	31
Elastic Permeable Surfaces	
3.6	35
Normal Approach and Variable Viscosity	

	PAGE
CHAPTER 4. DIMENSIONAL ANALYSIS OF NORMAL APPROACH	37
CHAPTER 5 THE EXPERIMENTAL WORK	41
5.1 The Apparatus	41
5.2 Instrumentation	43
5.3 Rigid Impermeable Boundaries	47
5.4 The "Weeping" Thin Layer	48
5.5 The Elastic Impermeable Layer	51
5.6 The Elastic Permeable Layer	54
CHAPTER 6 THEORETICAL PREDICTIONS OF THE MODEL	57
6.1 The Rigid Impermeable Model	57
6.2 The "Weeping" Lubrication Model	58
6.3 The Elastic Impermeable Layer	61
6.4 Elastic Permeable Layers	62
6.5 Enrichment in Normal Approach	64
6.5.1 Enrichment with Permeable Elastic Layers	64
6.5.2 The Concept of "Boosted" Lubrication	66
CHAPTER 7 DISCUSSION	70
7.1 Squeeze Films and Elastic Permeable Thin Layers	70
7.2 The Relevance of this Work to Animal Joints	72
7.3 Conclusions	74
APPENDICES	
I References	R1-2
II The Computer Programme	
III A Finite Element Approach to Laminar Fluid Flow	A1-12

Chapter 1

INTRODUCTION

The aim of hydrodynamic lubrication is the maintenance of a full fluid film between surfaces that move relative to one another. This is as true when the motion is normal approach as when the motion is rolling, sliding or a combination of the two.

Much of the effort in lubrication research has been directed towards problems occurring in rolling and sliding situations; relatively little effort has been expended in studying the other branch of the subject, that of normal approach, in which so-called "squeeze films" are generated.

The study of the behaviour of such films is by no means of purely academic interest since cyclically loaded journal bearings generate squeeze films and these occur whenever reciprocating motion is converted to rotary motion.

Traditional bearing surfaces have been metallic and at low sliding or rolling speeds, the hydrodynamic lubrication tends to break down and damage to the surfaces results. Recent work (1) in the use of a soft layer has shown that full hydrodynamic lubrication can continue in situations of extremely low sliding velocities. A very common example of the bearing in which both low sliding speeds and full film lubrication exist simultaneously is the animal joint. This bearing consists of two thin layers of low modulus material separated by a fluid film and having a stiff backing.

The film is a water-like fluid known as synovial fluid with an additive of extremely high molecular weight called hyaluronic acid. The soft layers are cartilage and exhibit some degree of permeability. The stiff backing is bone.

The various roles that the additive, the permeability and the



elasticity of the cartilage play have by no means been agreed upon and indeed, the two most publicised current theories of the functioning of joints are diametrically opposed (2, 3).

This bearing is of interest to engineers not only because of the long duration of its squeeze films but also because of the extremely low frictional forces observed.

Scope thus clearly exists for an investigation of the basic behaviour of squeeze films in the hope that the action of an animal joint may come to be better understood and also that the design of mechanical bearings in which these films are generated may be improved.

This thesis therefore describes the construction of a mathematical model of a squeeze film, its numerical and partial theoretical solutions, and some experimental comparisons with the theoretical work. The effects on normal approach of permeability and of elasticity of the squeeze film boundary, and of additive in the fluid, are also examined.

Whilst this model was clearly inspired by the efficient behaviour of animal joints, it can lay no claim to describe them accurately or even adequately. The mathematical description of the model is a description only of the model, not of a joint, and thus its predictions relate only to its idealization of a squeeze film.

The work described in this thesis must also be considered as a preliminary, wide-ranging look at the whole field of normal approach. It is to be hoped that rigorous investigations of specific squeeze film situations will follow from this initial work.

Since the two mechanisms proposed in modern times to explain joint lubrication, known as "boosted" and "weeping" lubrication, have so far lacked adequate mathematical description, even in idealized situations, it was hoped that the model would enable comparisons to be made between the two theories to decide which was more effective in maintaining full

film lubrication. It was considered that the model might also be applicable to the squeeze films that occur in machines.

Chapter 2 then, contains the mathematical description of the model, starting with an isoviscous lubricant and rigid impermeable boundaries. An interpretation of the concept of "Weeping" Lubrication is next attempted and the problem of the inclusion of the elastic effects of a thin layer is considered at the same time. Permeability is introduced into the model and finally the effect of an additive, whose flow is confined to the film, is examined.

The assumptions of previous workers that the integral of the pressure distribution over the area of the film is equal to the applied load on the film, and that the time rate of elastic displacement of the thin layer is negligible, are examined with the aim of producing accurate film thickness-time curves.

The few analytical solutions to the governing equations are included in this section.

Chapter 3 is concerned with the numerical solution of the model. The limitations of the numerical methods used, notably in describing accurately the velocity of deformation of the thin layer by a process of numerical differentiation, and the inclusion of this quantity in the solution of the flow in the elastic permeable layer are considered.

Chapter 4 introduces a dimensional analysis of the model based on the use of four repeating variables, the non-dimensional groups including two length parameters instead of the more usual one. Justification of this step is given.

Chapter 5 describes the experimental work that was carried out in order to check the theoretical solutions. The problem of film thickness measurement is considered and observation of the two phenomena, entrapment and cavitation, is described. A comparison of the experimental and

theoretical results is included.

Chapter 6 presents the theoretical predictions of the mathematical model. The effects of permeability and elasticity of the thin layer and of an additive in the lubricant are examined. The implications of these effects on the theories of "weeping" and "boosted" lubrication are discussed.

Chapter 7 contains a discussion about squeeze films in general and the problems of their mathematical treatment. Also included is a continuation from the previous chapter of the discussion of the possible mechanisms operating in animal joints.

Finally a short description of an early simple finite-element, applicable to lubrication problems is given in Appendix III.

NOTATION

The notation listed here refers to the theoretical description of the models and does not necessarily correspond to the symbols used in the computer programme.

A	flexibility of the elastic layer (δ_r/P_r)
\tilde{A}	non-dimensional flexibility (AL/R^2D)
A_1, A_2, A_3	surface areas of an annulus in the plane of the film.
B	$(-Mg/6\pi\eta R^2)$
C_n	n-th coefficient of a power series.
c	concentration of additive in the lubricant film.
D	initial separation of centres of undeformed surfaces.
F	integral of the film pressure over the area of the film.
g	acceleration due to gravity.
h_r	film thickness at radius r .
\tilde{h}_r	non dimensional film thickness (h_r/D)
I	force producing closure of the film with no inertia effects considered.
J_A, J_B	volume of additive in an annular volume of the film before and after a time Δt
k_{1-5}	various numerical constants.
L	a force (Mg) producing closure of the film.
L_A, L_B	volume of an annular region of the film before and after a time Δt
M	mass of the top boundary of the film, produces closure of the film under the action of gravity.

M_r	ratio of viscosity of an additive to the viscosity of the base fluid (η_i / η_o)
N_A, N_B	concentration of an additive in a region of the film before and after a time Δt
P	hydrostatic pressure of the fluid in the porous material.
P_r	pressure in the film at radius r .
P_o	pressure in the film at its centre.
ϕ_1, ϕ_2, ϕ_3	flowrates through the surfaces of an annular region of the film.
R	radius of curvature of the top surface of the film.
r	distance of a point from the axis of symmetry.
S	radius of a flat disc.
T	initial thickness of the soft layer.
t	time.
Δt	increment of time.
\tilde{t}	non-dimensional time $(t L / \eta_i R^2)$
u	radial flowrate in porous material.
V	void ratio of undeformed porous layer.
x	displacement of the centre of the top surface above the undeformed lower surface.
\tilde{x}	non-dimensional displacement (x / D)
\dot{x}	time derivative of above.
$\tilde{\dot{x}}$	non-dimensional derivative $(\dot{x} \eta_i R^2 / L D)$
\ddot{x}	acceleration of the top surface.
$\tilde{\ddot{x}}$	non-dimensional acceleration $(\ddot{x} \eta_i^2 R^4 / L^2 D)$

\dot{x}	a "lumped" approach velocity.
δ_r	a deformation of the thin layer at radius r.
z	axial co-ordinate in porous layer.
ϵ_r	compressive strain in axial direction of porous elastic material.
ϕ_r, ϕ_z	permeability of porous material in radial and axial directions respectively.
η	viscosity of fluid in the film.
η_i	initial viscosity of fluid in the film.
η_0	viscosity of fluid in porous layer, and in the film if no additive present.
η_1	viscosity of pure additive.
w	axial flowrate in porous material.
w_0	velocity of deformation of elastic layer (positive upwards).
w_2	flowrate in axial direction across the boundary of the porous elastic material.

Chapter 2

THEORETICAL DEVELOPMENT OF THE MODEL2.1 Introduction

This discussion is best followed with reference to diagram 1.

One reason that comparatively little work has been done in the field of normal approach lubrication may be found in the fact that the process is time-dependent and both experimental and theoretical work are more difficult than in the steady-state processes of rolling or sliding.

For these steady-state problems, the numerical solution of Reynolds' Equation involves two successive integrations of the equation to find the load carrying capacity (F) of a film. In normal approach, however, these two integrations at time t , say, must be followed by a substitution of F into the equation of motion of the moving surface and this must be integrated twice over a period of time Δt to produce new values of film thickness and relative velocity of approach for a time $t + \Delta t$. The integrations of Reynolds Equation are then repeated and this cycle must be carried out many times to produce a profile of the various parameters, such as film thickness, against time.

Despite the absence of the usual "downstream boundary", calculations in squeeze film situations are very much more difficult than in steady rolling or sliding films.

Two approximations have been made by several people (4, 5) in the tackling of normal approach. First, the mass of the moving surface has been assumed to be zero, i.e. the load applied to the film has no inertia. With this assumption, the variation of film thickness with time is defined by:

$$\int P_r d(\text{area}) = \text{applied force}$$

where the integral is taken over the area of the film.

In 2.2 an expression is derived to show the difference between this assumption and the more accurate one of the moving surface having considerable mass.

The other approximation has been concerned with the evaluation of the rate of deformation of an elastic boundary under the pressures generated in the squeeze film. The relevant term in Reynolds Equation is $(\dot{x} - w_0)$ where \dot{x} is the velocity of the rigid surface and w_0 that of the elastic boundary. \dot{x} is a function of time alone, w_0 however depends on time and radius, being zero for all time at the outside edge of the film and a considerable fraction of \dot{x} near the centre of the film at commencement and termination of the normal approach.

A typical approximation replaces $(\dot{x} - w_0)$ by \dot{x} and Reynolds Equation is then solved for various values of \dot{x} and x , the variation of x with time being found by recourse to the assumption of 'zero inertia' described above. The equations describing normal approach with and without this assumption are presented in 2.3 and 2.4 and compared in 6.2 and 6.3.

2.2 Rigid Impervious Boundaries

The governing differential equations reduce to their simplest form when two rigid, impervious surfaces approach each other through an isoviscous lubricant, see diagram 1 (in which $w_0 = 0$).

Reynolds Equation becomes

$$\frac{\partial P_r}{\partial r} = \frac{6 \eta r \dot{x}}{h_r^3} \quad (1)$$

for any point in time.

If the upper surface is parabolic and the lower flat, then

$$h_r = x + \tau^2/2R \quad (2)$$

whence

$$\frac{\partial h_r}{\partial \tau} = \tau/R$$

and we can integrate (1) to produce

$$P_r = 3\eta R \dot{x} \left(\frac{1}{h_a^2} - \frac{1}{h^2} \right) \quad (3)$$

using the boundary condition $P_r = 0$ at $\tau = \tau_a$

With no loss of generality, we can change the boundary condition to $P_r = 0$ at $\tau = \infty$. Using the former boundary condition, integration of (3) produces

$$F = - \frac{3\pi \eta \dot{x} \tau_a^4}{2 x h_a^2} \quad (4)$$

With the latter boundary condition, a rather simpler integration produces

$$F = - \frac{6\pi R^2 \eta \dot{x}}{x} \quad (5)$$

The equation of motion of the top surface is:

$$F - Mg = M\ddot{x}$$

substituting from (5) we obtain

$$- \frac{6\pi R^2 \eta \dot{x}}{x} - Mg = M\ddot{x} \quad (6)$$

If the system is dominated by viscous forces then a first approximation is found by putting $\ddot{x} = 0$ and integrating. This gives:

$$x = D e^{(-Mg/6\pi\eta R^2)t} \quad (7)$$

where the condition $x = D$ at $t = 0$ has been used. For convenience, let

$$B = - (Mg/6\pi\eta R^2)$$

then

$$\dot{x} = Bx$$

and

$$\ddot{x} = B^2x$$

} (8)

An exact solution can be found to equation (6) by writing

$$x = C_0 + C_1 t + \sum_{n=2}^{n=\infty} \frac{C_n t^n}{n(n-1)} \quad (9)$$

Substitution of this series into (6) and the equating of coefficients yields:

$$C_2 = g \left[\frac{C_1}{B} - C_0 \right] / C_0 \quad (10)$$

$$C_3 = \left\{ g \left[\frac{C_2}{B} - C_1 \right] - C_1 C_2 \right\} / C_0 \quad (11)$$

and

$$C_n = \left\{ g \left[\frac{C_{n-1}}{(n-2)B} - \frac{C_{n-2}}{(n-2)(n-3)} \right] - C_1 C_{n-1} - \sum_{a=2}^{a=n-2} \frac{C_a C_{n-a}}{a(a-1)} \right\} / C_0 \quad (12)$$

(12) being valid for $n \geq 4$

From (6), if the film closes due to an applied force (I) whose inertia is neglected (or zero) then

$$x = D. e^{(-I/6\pi\eta R^2)t}$$

and this is then an exact solution to the equation of motion.

The dominance of the viscous forces in the model and hence the accuracy of (7) is illustrated in Chapter 6.1.

2.3 "Weeping Lubrication"

McCutchen (2) has proposed the concept of "self-pressurized hydrostatic lubrication", known conveniently as "weeping lubrication" to explain the functioning of animal joints. He suggests that, as a

joint is loaded, fluid is expelled from the cartilage into the film. Because the stiffness of cartilage without any fluid in its pores is very low, the rate of expulsion of fluid, and hence the rate of deformation of the cartilage, is controlled by its permeability.

It is possible to devise a simple mathematical model to describe an extreme form of this "weeping lubrication", diagram (2). Such a model requires an elastic layer with zero radial permeability and infinite axial permeability, and whose constituent material is incompressible (i.e. deformation occurs by closure of the pores). As the layer is deformed, fluid is thus forced out of the pores in an axial direction.

Since the material is elastic, we must consider the question of the stress distribution in this layer and its interaction with the fluid pressures.

Were the elastic layer to be considered as a semi-infinite solid, then it would be possible to devise an iterative process solving first the Reynolds Equation and then the elasticity equations. However this process does not always converge (5) and because the material we are considering is a thin layer, then an approximation can be made of the form

$$\delta_r \propto P_r$$

i.e. the deformation at a point is proportional to the local pressure on the surface. Thus

$$\delta_r = A.P_r \quad (13)$$

The development and examination of the accuracy of this step can be traced through references (6), (1) and (7) and a discussion of it is included in Chapter 7.

If we define

$$w_0 = - (\text{rate of deformation of elastic layer})$$

and $W_2 =$ volume rate of flow of fluid out of the porous elastic layer,

then at any point on the surface,

$$W_0 = -W_2$$

Very conveniently, Reynolds Equation

$$\frac{\partial P_r}{\partial r} = \frac{6\eta\tau}{h_r^3} (\dot{x} - W_0 - W_2)$$

becomes

$$\frac{\partial P_r}{\partial r} = 6\eta\tau\dot{x}/h_r^3 \quad (14)$$

Because of the nature of our interpretation of "weeping lubrication", the problem of calculating the rate of deformation of the elastic layer is avoided and it is thus possible to make some progress towards analytical solutions of the squeeze film.

The simplest case of interest is when the top surface of the film is a flat rigid disc of radius S .

Reynolds Equation is

$$\frac{\partial P_r}{\partial r} = \frac{6\eta\tau\dot{x}}{h_r^3}$$

where

$$h_r = x + A.P_r$$

The equation is separable and can be integrated to give:

$$P_r = \frac{x}{A} \left\{ \left[\frac{12\eta\dot{x}A}{x^4} [r^2 - S^2] + \left[1 + \frac{A.P_s}{x} \right]^4 \right]^{1/4} - 1 \right\}$$

if $x > 0$ then $P_s = 0$ and:

$$P_r = \frac{x}{A} \left\{ \left[\frac{12\eta\dot{x}A}{x^4} [r^2 - S^2] + 1 \right]^{1/4} - 1 \right\} \quad (15)$$

if $x < 0$ then $P_s = -\frac{x}{A}$ as a first approximation and:

$$P_r = \frac{x}{A} \left\{ \left[\frac{12 \eta \dot{x} A}{x^4} [r^2 - S^2] \right]^{1/4} - 1 \right\} \quad (16)$$

At the centre of these discs, the film thickness is

$$h_0 = x + A.P_0$$

thus, from (16),

$$h_0 = \left(-12 \eta \dot{x} A S^2 \right)^{1/4} \quad (17)$$

for $x < 0$

Thus for constant speed of approach, the film thickness is constant. At first sight this is a surprising result, in that the displacement, is not involved. However it well illustrates the fact that the film is provided by lubricant 'weeping' from the elastic layer and that the rate of weeping is connected to the rate of deformation.

It is possible to produce a similar solution to the problem when the top surface is paraboloidal with a radius of curvature R.

In this case, the Reynolds Equation is still

$$\frac{\partial P_r}{\partial r} = \frac{6 \eta \tau \dot{x}}{h_r^3}$$

However

$$h_r = x + \frac{r^2}{2R} + A.P_r$$

Numerical integration of this equation for various values of \dot{x} , η and x shows that the pressure curve resembles a parabola over the central region of the film, for values of $x < 0$

If, then, we substitute an expression of the form

$$P_r = k_1 - k_2 r^2$$

into (14) and equate co-efficients of powers of r , we find an expression of the form:

$$P_r = \left(-\frac{6R\dot{x}\eta}{A^2} \right)^{1/3} - \frac{1}{A} \left(x + \frac{r^2}{2R} \right) \quad (18)$$

Since the expression will be in error for large r , it cannot be integrated with respect to r to produce the force F . Thus the equation of motion of the top surface cannot be solved.

However, for $x < 0$, (18) is an excellent fit to the pressure curve over the important central region of the film, see figure (3).

In this central region, the film thickness is

$$h_r = x + \frac{r^2}{2R} + A.P_r$$

and, from (18) this is

$$h_r = \left(-6R\dot{x}\eta A \right)^{1/3}$$

Thus not only is the film thickness constant over the centre of the film, it is also constant for a constant speed of approach, as was found in the case of a flat disc.

2.4 Impermeable Elastic Layer

If the "weeping lubrication" is to be an effective mechanism for maintaining fluid between approaching surfaces, then it should produce substantially thicker films for longer periods of time than other possible mechanisms operating under the same loads and geometry.

One such mode of operation is to consider the thin layer as impermeable in any direction but still retaining its elasticity, see diagram (1).

This gives a Reynolds Equation of the form

$$\frac{\partial P_r}{\partial r} = \frac{6 \eta r}{h_r^3} (\dot{x} - w_o) \quad (19)$$

Once again we must simplify the elasticity equations with expression (13)

so that

$$h_r = x + \frac{r^2}{2R} + A.P_r$$

Now $w_o = -$ (rate of deformation of the thin layer) so that, using (13),

$$w_o = - \frac{\partial \delta_r}{\partial t} = - A \frac{\partial P_r}{\partial t}$$

Several authors (4, 5) have solved similar equations by replacing the awkward function $(\dot{x} - w_o)$ by a velocity of approach \dot{x} , assumed independent of r .

The Reynolds Equation can then be integrated for ranges of values of x and \dot{x} and the life of the film found by assuming F to be a constant with respect to time.

Neither of these assumptions need be made if we maintain the approximation (13). With this approximation, it is possible to integrate (19) twice numerically for some given values of x , \dot{x} and w_o and thence to find new values of these quantities at some later instant of time. The full procedure is described in Chapter 3.

2.5 Rigid Permeable Thin Layer

If we return to the model described in Chapter 2.2 and replace the lower rigid layer by a permeable rigid layer we have the situation described in figure (4), in which $w_o = 0$.

Equation (1) becomes

$$\frac{\partial P_r}{\partial r} = \frac{6 \eta r}{h_r^3} (\dot{x} - w_2) \quad (20)$$

where W_2 is the volume rate of flow of fluid per unit area out of the porous layer into the film.

$$\text{Again } h_r = x + \frac{r^2}{2R}$$

It is now necessary to describe the flow in the porous material. D'arcy's Law for the flow of fluids through porous media,

$$\left. \begin{aligned} u &= - \left(\frac{\phi_r}{\eta_0} \right) \frac{\partial P}{\partial r} \\ w &= - \left(\frac{\phi_z}{\eta_0} \right) \frac{\partial P}{\partial z} \end{aligned} \right\} \quad (21)$$

gives us the flowrates u and w in the radial and axial directions respectively and is a widely accepted description of the behaviour of fluids in porous media.

ϕ_r and ϕ_z are the permeabilities of the material in the radial and axial directions respectively, having units of area and being a function of the size of the passages and their tortuosity.

$$\text{We can now say } W_2 = - \left(\frac{\phi_z}{\eta_0} \right) \frac{\partial P}{\partial z}$$

where $\frac{\partial P}{\partial z}$ is evaluated at the surface.

A relation is needed between u and w and this is provided by the equation of continuity,

$$\frac{\partial u}{\partial r} + \frac{u}{r} + \frac{\partial w}{\partial z} = 0 \quad (22)$$

On the question of permeability, whether the material is isotropic, or not, will depend on its method of manufacture. Thus ϕ_r and ϕ_z will be kept separate in this theory and not be assumed to be equal.

(21) and (22) can now be combined to describe fully the flow in the porous layer, i.e.

$$\frac{\partial^2 P}{\partial r^2} + \frac{1}{r} \frac{\partial P}{\partial r} + \left(\frac{\phi_z}{\phi_r} \right) \frac{\partial^2 P}{\partial z^2} = 0 \quad (23)$$

This is a form of Laplace's Equation.

The use of the co-ordinate x has been confined to describing the film and the motion of the top surface, the co-ordinate z has been introduced to refer only to the porous material.

The boundaries of the region in which the Laplace-type equation (23) must be solved consist of streamlines on three sides and the film on the fourth side.

Wu (8) has considered a similar situation in which two rigid discs approached one another, one disc having a thin porous annular region. He has solved this analytically by separation of variables in Laplace's Equation and produced a series solution for pressure in r and z and thus substituted for w_2 in Reynolds Equation.

Such a solution could be found for equation (23) were our discussion of squeeze films to be confined to isoviscous lubricants and rigid boundaries. However such a solution is somewhat inflexible and cannot easily be adapted to films of non-isoviscous lubricants between elastic solids. Numerical solution of such systems automatically includes the problem of rigid boundaries and constant viscosity fluids as a special case.

2.6 Permeable Elastic Layer

As discussed above, the next complication to consider is the introduction of elasticity effects into the porous material considered above. Equation (22) becomes

$$\frac{\partial u}{\partial r} + \frac{u}{r} + \frac{\partial w}{\partial z} = \frac{-w_0}{(T - A.P_r)} \quad (24)$$

where T is the thickness of the thin layer, and

$$w_0 = -A \frac{\partial P_r}{\partial t}$$

Equations (21) remain valid, but the local values of ϕ_r and ϕ_z will no longer be constant but will become functions of the deformation. Thus under any system of loading on the material, these permeabilities will vary with r (but not with z).

Remembering this, equation (23) changes to

$$\frac{\partial^2 P}{\partial r^2} + \frac{\partial P}{\partial r} \left[\frac{1}{r} + \frac{1}{\phi_r} \frac{\partial \phi_r}{\partial r} \right] + \left(\frac{\phi_z}{\phi_r} \right) \frac{\partial^2 P}{\partial z^2} = - \frac{w_0 \eta}{\phi_r (T - A.P_r)} \quad (25)$$

The variation of ϕ_r and ϕ_z with deformation must now be considered.

Inevitably more assumptions must be introduced. These are:-

- 1) That ϕ_r and ϕ_z are equally affected by surface deformation.
- 2) Deformation of the porous layer is accomplished entirely by closure of the voids in the material, i.e. the actual material of the layer is incompressible.
- 3) The permeability is proportional to the void ratio in the layer.

Thus if V is the fractional volume of voids in the undeformed layer, we can say

$$\phi_r = k_r V \quad , \quad \phi_z = k_z V$$

for the undeformed

material and for the deformed material at some radius r ,

and

$$\left. \begin{aligned} \phi_r &= k_r \left(\frac{V - \epsilon_r}{1 - \epsilon_r} \right) \\ \phi_z &= k_z \left(\frac{V - \epsilon_r}{1 - \epsilon_r} \right) \end{aligned} \right\} (26)$$

where ϵ_r is the compressive strain in the material in the axial direction.

Now $\epsilon_r = \frac{\delta_r}{T} = \frac{AP_r}{T}$ from (14).

Thus in equation (25) we can say that $\left(\frac{\phi_z}{\phi_r} \right)$ remains constant under any loading and that

$$\frac{1}{\phi} \frac{\partial \phi_r}{\partial r} = \frac{-A(1-\nu)T}{(T-AP)(VT-AP_r)} \left(\frac{\partial P_r}{\partial r} \right)$$

The Reynolds Equation is

$$\frac{\partial P_r}{\partial r} = \frac{6\eta\tau}{h_r^3} (\dot{x} - w_0 - w_2) \quad (27)$$

where $w_0 = -A \frac{\partial P_r}{\partial t}$ and $w_2 = -\frac{\phi_z}{\eta_0} \frac{\partial P}{\partial z} \Big|_{\text{SURFACE}}$

w_2 is evaluated as a flowrate relative to the moving surface of the elastic layer.

w_0 is a velocity of the lower surface relative to a co-ordinate system fixed in space and time.

2.7 Lubricant Additive and Permeable Elastic Layer

The lubricant in animal joints is not a simple iso-viscous Newtonian fluid (9). The viscosity is grossly dependent on shear rate and it also contains a low concentration of a substance called hyaluronic acid. This additive has a molecular weight of 10^6 and appears to form 'complexes'

when in solution in the fluid. It cannot flow through the pores of the cartilage and, at very thin films, when the base synovial fluid has been forced away from the high pressure zone, it is believed to form gels of very high viscosity providing a form of boundary lubrication.

This can be modelled in an idealistic manner by enriching the fluid film of the model described in 2.6. The additive will be free to move about the film but not through the porous layer. The non-Newtonian aspects of synovial fluid have been ignored.

If we know the variation of the concentration of this additive with respect to radius, an approximate, new concentration can be found for a time Δt later. Consider the annular volume shown in figure (5). Let the volume of additive in this region be J_A and the concentration of the additive

$$N_A = J_A / L_A$$

Now over a period of time Δt the nett flow out of the annulus of the additive will be

$$\Delta t (\phi_3 A_3 N_A - \phi_1 A_1 N_A)$$

The increase in volume of the annular region will be

$$\Delta t A_2 (\dot{x} - w_0)$$

Thus the new concentration is

$$N_B = \frac{\{J_A - \Delta t (\phi_3 A_3 N_A - \phi_1 A_1 N_A)\}}{\{L_A + \Delta t A_2 (\dot{x} - w_0)\}} \quad (28)$$

Obviously ϕ_3 can be removed by looking at the continuity of the annular volume, i.e.

$$\phi_3 A_3 - \phi_1 A_1 - \phi_2 A_2 + (\dot{x} - w_0) A_2 = 0$$

whence

$$N_B = N_A \left\{ 1 - \Delta t \left\{ \frac{\phi_2 A_2 - \phi_1 A_1 (N_V/N_A - 1)}{L_A + \Delta t A_2 (\dot{x} - w_0)} \right\} \right\} \quad (29)$$

The numerical calculation of the distribution of additive is described in Chapter 3.

It is however necessary to make two final assumptions before the problem can be solved.

- 1) A relationship between concentration of additive and the resulting viscosity of the fluid must be postulated. Workers in the field of joint lubrication (9) have suggested that the relation of synovial fluid viscosity and concentration of hyaluronic acid is a linear one. Thus at a concentration c ,

$$\eta_c = \eta_0 (1 + c (M_r - 1)) \quad (30)$$

where

$$M_r = \eta_1 / \eta_0$$

η_1 being the viscosity of the pure additive

η_0 the viscosity of the solvent.

- 2) The fluid in the porous material is pure solvent at viscosity η_0 . However if the concentration of additive at some point in the film becomes unity, then no flow can occur of fluid from the film into the porous material at that point. Flow can occur though if the concentration is less than unity. For the purposes of numerical computation it is not reasonable to have a step change in flowrate from some current value $w_2 = -\frac{\phi}{\eta_0} \frac{\partial P}{\partial z} \Big|_{\text{SURFACE}}$

to zero as concentration changes from $c < 1$ to $c = 1$. Thus the assumption is introduced that $\phi_2 \Big|_{\text{surface}}$ is proportional to concentration of solvent, i.e. it falls linearly to zero as concentration of additive approaches unity. This complication is described mathematically in Chapter 3.

2.8 'Dowson' Enrichment Model

Dowson (3) has suggested that since the permeability of cartilage appears to play little part in the lubrication of joints, at least until the film is almost closed, the additive, hyaluronic acid, may be bonded in some way to the surface of the cartilage. This would prevent it from moving sideways with the base synovial fluid when the joint is loaded. Thus the concentration will be inversely proportional to the film thickness.

This can be presented mathematically by

$$c = c_i h_i / h$$

where c_i is the initial concentration and h_i is the film thickness at some radius at the commencement of the normal approach.

This model is discussed in detail in Chapter 6.5.2.

Chapter 3

NUMERICAL SOLUTION OF THE MODEL3.1 Introduction

Whilst the analytical formulation of the differential equations involved in normal approach presents no difficulties beyond the introduction of several approximations and assumptions, the numerical or analytical solution of them is extremely difficult. As already mentioned, two basic assumptions in previously published solutions have been the equality of applied load and the load carrying capacity of the film and the neglect of the velocity of deformation of the elastic material.

Neither assumption was made in Chapter 2 and this has led to difficulties in the numerical solution of the equations. The first assumption is not particularly important but an accurate description of the rate of deformation is vital to determine the flow in the squeeze film. In the case of this velocity, the difficulty in describing it accurately has been the major factor in limiting the application of the model to systems with low values of flexibility.

Unfortunately the model does not lend itself to a neat numerical solution. It would have been more elegant to be able to consider the solution of the normal approach as the solution of a rectangular finite difference network, which was to be solved for nodal pressures. One co-ordinate would have been spatial (radial) and the other temporal. (In the case of a porous material the network would have been three dimensional with two spatial co-ordinates (r and z)). However the equations derived in Chapter 2 are not suitable for this type of treatment. The Reynolds Equation links points in the radial direction, with an expression of the form

$$\left[\frac{\partial P_r}{\partial \tau} \right]_t = f \left\{ x, \dot{x}, \frac{\partial P_r}{\partial t} \right\}$$

in which x and \dot{x} are not constants but are dependent on previous values of x , \dot{x} and \ddot{x} . The latter are derived from some evaluation of F , which in turn depends on the integration of previously determined pressures.

The best way to describe the numerical procedure that has been devised to satisfy the Reynolds Equation and the equation of motion is to consider the development of the method starting with the treatment of the simple model with rigid impermeable boundaries and continuing to the more complex models.

The models are treated in the same order as they were in Chapter 2.

3.2 Normal Approach with an isoviscous lubricant and rigid boundaries

3.2.1 This subsection describes the direct method of solution of the equations for this model and the flowchart for this approach is shown in fig. (6).

For given x and \dot{x} at time t , Reynolds Equation is integrated twice from the starting point $\tau = \tau_a$ to the centre of the film. The second integration gives us the value of the quantity F . This is then substituted into the equation of motion to find \ddot{x} at that instant. New values of x and \dot{x} can then be found for a time $t + \Delta t$. The first integration of Reynolds Equation is performed by a 4th-order Runge-Kutta method, the second integration, of the pressure distribution to find F , by Simpson's Rule. The choice of formulae to find x and \dot{x} at $t + \Delta t$ from values of \dot{x} and \ddot{x} at time t is not critical and even the simplest formulae work tolerably well, i.e.

$$\dot{x}_{t+\Delta t} = \dot{x}_t + \ddot{x}_t \cdot \Delta t \quad \text{and}$$

$$x_{t+\Delta t} = x_t + \dot{x}_t \Delta t + \ddot{x} (\Delta t)^2 / 2$$

The initial conditions chosen for the normal approach are $x = \nu$, $\dot{x} = 0$, $\ddot{x} = -g$ at time $t = 0$.

3.2.2 Numerical problems of the direct solution

The curves of distance/time and velocity/time computed from these initial conditions and by the method described above, are shown in fig. (7). It was found that the trajectory eventually becomes unstable for values of $\tilde{t} > 40$.

It is from these curves that a numerical procedure has been devised that supersedes the direct approach before this instability becomes evident and dominates the curves.

The curves can be considered in three parts, the dividing line between the first and second regions occurring at around $\tilde{t} = 3$

The effect of the initial conditions is most marked in this first region ($\tilde{t} < 3$) and here the use of equal increments of time is a suitable approach to the solution of the equation of motion. However, after $\tilde{t} = 3$ the trajectory closely follows that calculated in Chapter 2.2, see figs. (64, 69). We can see that $\ddot{x} \approx B \dot{x}$ and also that $\ddot{x} \ll g$. To calculate \ddot{x} accurately requires that F be known extremely accurately, since 0.01% error in F will produce an error of 1% in \ddot{x} . By reducing Δt in order that x and \dot{x} become more accurate, and hence F becomes more accurate, we introduce more errors by increasing the number of steps needed. Indeed, whatever finite difference method is used to calculate x and \dot{x} , the trajectory finally goes unstable, producing a spurious solution.

This is of course to be expected when solving an equation of the form $\frac{dx}{dt} = kx$ by finite difference methods (10). Obviously a

different approach is required to tackle the trajectory when $\hat{t} > 3$. This can be easily accomplished if some assumptions are introduced regarding the behaviour of the film. These assumptions are

- 1) that \ddot{x} , having risen from $-g$ to $+0.01g$ (approx.) then approaches zero as $\hat{t} \rightarrow \infty$.
- 2) that $(-\dot{x})$, having risen to a maximum, then falls to zero as $x \rightarrow 0$.

These assumptions can be summed up by saying that the trajectory should follow the form described in 2.2.

3.2.3. Indirect Solution of Equation of Motion

We now have a check on whether a calculated acceleration is accurate. From $\hat{t} = 3$ the trajectory can be calculated by using equal increments of velocity instead of time. Thus the velocity reached at $\hat{t} \approx 3$ is divided into about 50 increments and these increments in velocity become the change in velocity between each double integration of Reynolds Equation. Obviously, for each value of \dot{x} for which we calculate F we need to postulate a value of x . This is done in the simplest possible way, i.e.

$$\dot{x}_2 = \dot{x}_1 + \Delta(\dot{x})$$

$$x_2 = 2x_1 - x_0$$

With these values, we can integrate to find F and thus the acceleration

$$\ddot{x}_2 = F_2/M - g \quad (31)$$

Now we are assuming that the trajectory closely follows the solution found in 2.2 so we can say

$$\ddot{x}_2 \simeq B\dot{x} \quad (32)$$

If the values of \ddot{x} in (31) and (32) are equal, within some specified limits, we can then progress to calculate F_3 with:-

$$\dot{x}_3 = \dot{x}_1 + 2 \Delta(\dot{x}) \quad \text{and} \quad x_3 = 2x_2 - x_1$$

If, however, the two values of \ddot{x} are sufficiently different from one another, then the value from (31) must be corrected.

It can be seen then that the method is indirect in that \ddot{x} is not used to calculate the trajectory but only used as a check on its accuracy.

The acceleration is corrected by correcting x_2 in F_2 by an amount proportional to the error in \ddot{x} , since

$$F_2 \approx -6\pi\eta R^2 \dot{x} (\alpha)^{-1} \quad (33)$$

F_2 is then recalculated with the corrected value of \dot{x}_2 and the acceleration compared with (32).

The process is convergent very rapidly because 1% error in $\ddot{x} \Rightarrow$ 0.01% error in F .

The time taken between steps can be found from

$$\Delta t = (x_2 - x_1) / \left(\dot{x}_1 + \frac{\Delta(\dot{x})}{2} \right)$$

As will be realized, the above procedure produces a trajectory very similar to one that would be obtained from the assumption

$$F = I \quad (\text{ie } M = 0)$$

This is because, for the values of B chosen, the model is dominated by viscous forces. For larger B however, the trajectories calculated for the model and for the system $F = I$ would no longer be closely comparable.

Whilst the analytical solution has been found for the above case (if we neglect differences in spatial and temporal boundary conditions), there are no known analytical solutions for the other models proposed in

Chapter 2 and their solution has been based completely on the method outlined above.

3.3 "Weeping Lubrication"

The numerical solution of the model representing "Weeping Lubrication" is very similar to that of 3.2 although the mode of operation of the model appears at first sight to be quite different.

Reynolds Equation remains as

$$\frac{\partial P_r}{\partial r} = 6\eta r \dot{x} / h_r^3 \quad (34)$$

However, $h_r = x + \frac{r^2}{2R} + AP_r$ the last term being the addition

to the problem. This addition has dramatic effects on the film thickness/time curve but the computation is almost unchanged.

The Runge-Kutta method employed in 3.2 is quite suitable for solving (34) even though it is no longer a linear differential equation.

3.4 Elastic Impermeable Surfaces

The equation for the film thickness, h , remains as in 3.3 but it is now necessary to include the rate of deformation of the elastic layer in the Reynolds Equation since calculation of $\left[\frac{\partial P_r}{\partial r}\right]_t$ requires evaluation of $(\dot{x} - w_o)$.

Our treatment of the elasticity part of the problem has produced the simplification

$$w_o = -A \cdot \left(\frac{\partial P_r}{\partial t}\right)_r$$

There is no explicit description available for $\left[\frac{\partial P_r}{\partial t}\right]_r$, thus its value must be implied by the equations of the model and hence these equations must be sufficient to solve the model completely, i.e. $\left[\frac{\partial P_r}{\partial t}\right]_r$ must be

determined from the information already available.

Since the equation of motion is concerned with $\int_{\text{area of film}} P_r d(\text{area})$, the only equation from which $\left[\frac{\partial P_r}{\partial t}\right]_r$ can be obtained is the Reynolds Equation. Unfortunately Reynolds Equation, when integrated once, gives us $[P_r]_t$ and to calculate $\left[\frac{\partial P_r}{\partial t}\right]_r$ from this involves a process of numerical differentiation. A formula of the type

$$\left[\frac{\partial P_r}{\partial t}\right]_r = f \left\{ [P_r]_{t_1}, [P_r]_{t_2}, \dots \right\} \quad (35)$$

must be used.

Numerical differentiation is a process that should be avoided if at all possible. A large time increment will produce truncation errors, a small increment will produce errors due to inaccuracies in the evaluation of $[P_r]_t$, since $[P_r]_{t_1}$ and $[P_r]_{t_2}$ will be almost equal.

Thus it is the problem of calculation of $\left[\frac{\partial P_r}{\partial t}\right]_r$ which is the weak point in the numerical calculation of the trajectory. The weakness is inherent in the existing mathematical treatment of the model and cannot be eliminated by different difference formula, although this approach was tried to the extent of using a least-squares approach (fitting a parabola through five values of pressure at the same r , and successive values of t).

The effect of this weakness makes itself felt in limiting the model to situations of low flexibility, i.e. $\tilde{A} \leq 10^{-3}$.

Besides the errors inherent in the evaluation of $\left[\frac{\partial P_r}{\partial t}\right]_r$ there is an instability which occurs in the Runge-Kutta procedure.

The integration by Runge-Kutta formulae commences at $r = r_a$ and $w_0 = 0$ (since $P_a = 0$ for all t). As the integration approaches the centre part of the film, $w_0 \rightarrow \dot{x}$ and so $\left[\frac{\partial P_r}{\partial t}\right]_r \rightarrow 0$. Thus $w_0 > \dot{x}$ is a condition that must always be satisfied (remembering that \dot{x} is -ve).

When $\left[\frac{\partial P_r}{\partial r} \right]_t \rightarrow 0$, small errors in the evaluation of P_r are sufficient to cause the solution to oscillate and increase exponentially, eventually causing an 'overflow' condition in the computer ($|P_r| > 10^{75}$).

This can be overcome fairly easily by a smoothing process. If, for example, we represent the rate of deformation of the elastic layer by

$$w_0 = \frac{-A}{\Delta t} \left\{ [P_r]_{t_2} - [P_r]_{t_1} \right\} \quad \text{then} \quad \left[\frac{\partial P_r}{\partial r} \right]_t \quad \text{is zero when the relative}$$

velocity of approach of the two surfaces is zero, i.e. $\dot{x} = w_0$.

From this we can find $[P_r]_{t_2}$, i.e.

$$[P_r]_{t_2} = -\frac{\Delta t \cdot \dot{x}}{A} + [P_r]_{t_1}$$

This gives us a limiting value which $[P_r]_{t_2}$ must approach as $\tau \rightarrow 0$. This condition has been written into the programme to suppress the oscillation and is used to calculate $[P_r]_{t_2}$ if either condition

$$1) [P_r]_{t_2} > \left([P_r]_{t_1} - \frac{\dot{x} \Delta t}{A} \right) \quad \text{or} \quad 2) \left[\frac{\partial P_r}{\partial r} \right]_{t_2} > 0$$

occurs while $[P_r]_{t_2}$ is being found by use of the Runge-Kutta procedure. See fig. (60) in which oscillation has been suppressed in $\tilde{\tau} = 1$ and $\tilde{\tau} < 0.035$.

3.5 Elastic Permeable Surfaces

The cases of rigid and elastic permeable layers can be treated together, since the rigid is merely a special case of the elastic (though an important one). The introduction of a permeable layer into the model increases the problem of numerical solution by many times. Typical computing times for the two co-ordinate models (in r, t) are in the region of 15 seconds; for the three co-ordinate problem (r, z, t) the time

can be 9 minutes.

It was decided to represent the pressure distribution in the porous layer by a finite difference technique and to solve the resulting equations by iteration, using the method of successive corrections, simultaneously with the Reynolds Equation integration. This was considered desirable for the following reasons:

- 1) The mesh had to be fine enough to ensure that w_2 was represented accurately in Reynolds Equation.
- 2) The pressure distribution would not change much over the period of one increment of time or velocity (\dot{x}). Thus it would be economical to use a previous pressure distribution as the starting point for the next series of iterations.

For a large matrix, the iterative approach is faster than inverting a matrix and solving exactly for pressure every time. Calculation of the trajectory involves solving the mesh some 50 times and the number of nodes ranged up to 2,737.

The order of solution of the nodes is shown in fig. (8).

Reynolds Equation is altered to

$$\frac{\partial p_r}{\partial r} = \frac{6\eta r}{h_r^3} (\dot{x} - w_0 - w_2) \quad \text{where}$$

$$w_2 = -\frac{\phi_2}{\eta_0} \left(\frac{\partial p}{\partial z} \right)_{\text{SURFACE}} \quad \text{and} \quad \left(\frac{\partial p}{\partial z} \right)_{\text{SURFACE}} = \frac{[p_r]_{t_2} - [p_l]_{t_2}}{\Delta z}$$

in a finite difference approximation.

The smoothing applied to Reynolds Equation, as described in (36), is altered and is derived from

$$(\dot{x} - w_0 - w_2) = 0$$

In the porous layer, equation (25) must be solved and the following finite

difference approximations are used.

$$\left. \begin{aligned} \left[\frac{\partial^2 P}{\partial r^2} \right]_I &= \frac{P_{I-m} + P_{I+m} - 2P_I}{(\Delta r)^2} \\ \left[\frac{\partial P}{\partial r} \right]_I &= \frac{P_{I-m} - P_{I+m}}{2 \Delta r} \\ \left[\frac{\partial^2 P}{\partial z^2} \right]_I &= \frac{P_{I-1} + P_{I+1} - 2P_I}{(\Delta z)^2} \end{aligned} \right\} \quad (37)$$

A one-dimensional matrix was chosen for P_I since it is quicker to "read" and "write" to a one-dimensional array than a two-dimensional one in the computer.

Δr is a constant, chosen as $T/(m-1)$. Δz however will vary with the deformation of the surface and so

$$\Delta z = \frac{T - A.P}{(m-1)} \quad \text{where } m \text{ is the number of nodes in the}$$

z-direction. The number of nodes in the r-direction is $10m-9$, i.e. the mesh has a radial : axial length ratio of 10 : 1.

When the node I is on one of the boundary streamlines, (such as $z=0$ say) then in (37) we replace P_{I+1} by P_{I-1} .

At ($\tau=0$), the quantity $\frac{1}{r} \frac{\partial P}{\partial r}$ in both the Reynolds Equation and the 'Laplacian' (25) is undefined.

Assume the pressure distribution is parabolic about $\tau=0$, then

$$P_r = k_3 + k_4 \tau^2 \quad \text{say.}$$

$$\therefore \left[\frac{\partial^2 P}{\partial r^2} \right] = 2 k_4, \quad \frac{1}{r} \frac{\partial P}{\partial r} = 2 k_4$$

Now $k_3 = P_0$ and $P_r = P_{0r}$ if $\tau = \Delta r$ This can be solved for P_0 in either Reynolds Equation or equation (25).

The convergence of a mesh such as the one described above is approximately first order and this can be speeded up by the use of 'Aitken's δ^2 method', which estimates a final value of

$$P = P_n - (P_n - P_{n-1})^2 / (P_n + P_{n-2} - 2P_{n-1})$$

Obviously the mesh size and the number of iterations required to solve it, to some specified accuracy, has an upper limit, defined by the size and speed of the available computing power.

The number of nodes in the mesh varies as m^2 and the necessary number of iterations will vary approximately as m or m^2 also. Thus halving the step length Δz will increase computing time by 8 or 16 times.

The largest value of m used in the computing was $m = 17$, i.e. total number of nodes in the porous layer = $m(10m - 9) = 2737$. Since the pressure at any one node may only change by a small amount between calculations (i.e. during one increment of time or velocity) a small number of iterations is permissible. Typically the pressure change per increment may be 1%, in which case, 8 or 16 iterations is sufficient to produce film pressures consistent to 0.1%. The shape of the matrix (the radial length being 10 x the axial length) helps to produce a faster rate of convergence than for a square matrix.

There is one instability in what one would imagine to be a well behaved system of equations and this occurs for $A \neq 0$. There are two components to the pressure distribution in a porous region, one due to the applied pressures on the boundary of the region (corresponding to the complimentary function of equation (25)) and the other due to the rate of deformation of the region (corresponding to a particular integral of equation (25)). This latter component involves the term w_0 , i.e. $\left[\frac{\partial P}{\partial t} \right]_r$ the problems of calculation of which we have already discussed. Unfortunately for some values of \tilde{A} and $\tilde{\phi}$, the computer programme is unable to produce a correct trajectory when this particular integral is included in

the calculation. This must be attributed to difficulty encountered in describing w_0 accurately. The solutions in which it has been necessary to neglect this particular integral are clearly marked and the problem is discussed further in Chapter 6.

3.6 Normal Approach and Variable Viscosity

The equations derived in 2.7 were written in finite difference form and, for a given initial distribution of concentration of additive, the concentration at a time Δt later can be found from them. The calculation must commence at the centre of the film, where $\phi_1 = 0$. After this central concentration has been found, ϕ_3 can be calculated and this is substituted into the next innermost annular region as ϕ_1 . The calculation proceeds to $r = r_a$ and takes place immediately before the simultaneous solution of Reynolds Equation and equation (25).

The viscosities are then found from (30). As pointed out in 2.7, it is necessary to assume that the surface permeability declines as the concentration of additive increases. For the purposes of computation, we assume that the permeability is affected to a depth Δz below the surface (see fig. (9)).

$$\text{Whence, as } w_2 = - \frac{\phi_1'}{\eta_0} \left(\frac{P_r - P_i}{\Delta z} \right)$$

$$\text{then } w_2 = - \frac{\phi_2}{\eta_0} (1 - N_0) \left(\frac{P_r - P_i}{\Delta z} \right)$$

where N_0 is the current value of concentration.

The calculation of nodal pressures immediately below the surface is not so straightforward. Consider the continuity of the element shown in fig. (9): for the upper half of the element, we have

$$\frac{\phi_r'}{\eta_0} \left[\frac{\partial^2 P}{\partial r^2} + \frac{\partial P}{\partial r} \left[\frac{1}{r} + \frac{1}{\phi_r'} \left[\frac{\partial \phi_r'}{\partial r} \right] \right] \right] - \frac{(w_a - w_b)}{(\Delta z/2)} = \frac{w_0}{(T - A.P_r)} \quad (38)$$

and for the lower half;

$$\frac{\phi_r}{\eta_0} \left[\frac{\partial^2 P}{\partial r^2} + \frac{\partial P}{\partial r} \left[\frac{1}{r} + \frac{1}{\phi_r} \left[\frac{\partial \phi_r}{\partial r} \right] \right] \right] - \frac{(w_b - w_c)}{(\Delta z/2)} = \frac{w_0}{(T - A.P_r)} \quad (39)$$

Now $w_a = - \frac{\phi_z'}{\eta_0} \frac{(P_r - P_i)}{\Delta z}$

and $w_c = - \frac{\phi_z}{\eta_0} \frac{(P_i - P_2)}{\Delta z}$

also $\phi_r' = \phi_r (1 - N_B)$ and $\phi_z' = \phi_z (1 - N_B)$

so, adding (38) and (39) and simplifying, we have

$$\left\{ \frac{\partial^2 P}{\partial r^2} + \frac{\partial P}{\partial r} \left[\frac{1}{r} + \frac{1}{\phi_r} \frac{\partial \phi_r}{\partial r} \right] + \frac{2 \phi_z}{(\Delta z)^2 \phi_r (2 - N_B)} \right\} (P_r - P_i)(1 - N_B) - (P_i - P_2) = \frac{2 w_0 \eta_0}{(T - A.P_r) \phi_r (2 - N_B)}$$

if $\frac{1}{\phi_r'} \frac{\partial \phi_r'}{\partial r} = \frac{1}{\phi_r} \frac{\partial \phi_r}{\partial r}$

We now have an expression in finite difference form for the evaluation of P_i

Chapter 4

DIMENSIONAL ANALYSIS OF NORMAL APPROACH

The film thickness and pressure at the centre of the film are the quantities in which we are most interested. Their relationship to the other parameters of the system can be expressed in the following manner:

$$h_o, P_o = f_{1,2} \left\{ t, A, \phi_z, \phi_r, L, \eta_i, R, D, V, \tau_a, \eta_1, c, T, \eta_o \right\} \quad (40)$$

where f_1 and f_2 are unknown functions. The three viscosities η_i, η_o, η_1 refer to the film at the commencement of normal approach, to the porous layer, and to the additive respectively.

Examining the Reynolds Equation for a porous layer with an additive present, we have:

$$\frac{\partial P_r}{\partial \tau} = \frac{6\eta_r}{h_r^3} \left(\dot{x} - w_o + \frac{\phi_z}{\eta_o} \left(\frac{\partial P}{\partial z} \right)_{\text{SURFACE}} \right)$$

For the same system, the flow in the porous layer is given by

$$\frac{\partial^2 P}{\partial r^2} + \frac{\partial P}{\partial r} \left[\frac{1}{r} + \frac{1}{\phi_r} \frac{\partial \phi_r}{\partial r} \right] + \frac{\phi_z}{\phi_r} \frac{\partial^2 P}{\partial z^2} = \frac{w_o \eta_o}{T \phi_r}$$

In both equations, η_o only occurs with ϕ_z or ϕ_r . We can thus replace ϕ_r, ϕ_z, η_o in (40) by ϕ_r/η_o and ϕ_z/η_o .

We have reduced the fourteen variables in (40) to thirteen. Normal dimensional analysis would reduce these thirteen to ten dimensionless groups. If, however, we follow the technique due to Morrison, described in detail in (11), these thirteen parameters can be reduced to nine groups. The method is based on the introduction of extra length dimensions, perpendicular to one another. In the system we are considering, the choice of length dimensions is an obvious one since the model is best described in cylindrical co-ordinates and it possesses axial symmetry. Only two length dimensions are needed to describe the model, these are in the radial

and axial directions. All the parameters concerned with the model can now be described in terms of mass (M), a radial length (L_R), an axial length (L_D) and time (t). The ratio L_R/L_D is no longer dimensionless. The choice of dimensions for the parameters of the model is not arbitrary but, for the technique to be valid, must be such that the differential equations of the model are dimensionally homogeneous.

With this in mind, the dimensions of the parameters are presented as:

A	$M^{-1} L_R^2 t^2$
ϕ_z, ϕ_r	L_D^2
L	$M L_D t^{-2}$
$\eta_i, \eta_o, \eta_1, \eta_2$	$M L_D L_R^{-2} t^{-1}$
R, τ_a , τ	L_R
T, h_r , D, x	L_D
\dot{x}	$L_D t^{-1}$
g, \ddot{x}	$L_D t^{-2}$
B	t^{-1}
t	t
c, v	dimensionless.

The derivation of the dimensions for L is straightforward if L is considered as a force in the axial direction. A is defined as S/P , an axial deformation divided by an axial force acting on unit area in the plane of the film.

To explain the units derived for viscosity, we consider Newton's Law of Viscosity, i.e.

$$\tau = \eta \cdot \frac{\partial u}{\partial x} \quad (41)$$

τ is a radial shear stress, with units $M L_R t^{-2} / L_R^2$ (remembering that tangential lengths all have the dimension L_R). $\frac{\partial u}{\partial x}$ has the units

$L_R t^{-1} / L_D$ Inserting these dimensions into (41) gives the dimensions for η shown above.

It remains to decide the dimensions of the various terms containing 'Pressure' in the two governing equations (25) and (27). Consider the terms $\frac{\partial P}{\partial \tau}$ and $\frac{\partial^2 P}{\partial \tau^2}$. When these equations are derived from consideration of the forces acting in a radial direction on an element of fluid, it is implied that P is a pressure acting in a radial direction on a face of that element, the orientation of that face being perpendicular to the radius vector.

The dimensions of P must then be $ML_R t^{-2} / L_R L_D$. Similar arguments are valid for the terms $\frac{\partial^2 P}{\partial z^2}$ and $\frac{\partial P}{\partial z} \Big|_{\text{surface}}$, in which we deduce that the dimensions of P here are $ML_D t^{-2} / L_R^2$. We now have the unusual situation of one parameter "pressure" having two distinct sets of dimensions simultaneously. Morrison argues that this is quite legitimate.

Using the dimensions derived above and η_i , L, R, D as the repeating variables, we can present the non dimensional form of (40) as

$$\left(\frac{h_0}{D}\right), \left(\frac{P_0 R^2}{L}\right) = f_{1,2} \left\{ \frac{tL}{\eta_i R^2}, \frac{AL}{R^2 D}, \frac{\phi_z \eta_i}{\eta_0 D^2}, \frac{\phi_r \eta_i}{\eta_0 D^2}, c, V, \frac{\eta_i}{D}, \frac{I}{D}, \frac{\tau_2}{R} \right\} \quad (42)$$

Ordinary dimensional analysis, using L, R and η_i would replace D everywhere in (42) by R and also introduce the extra group D/R (42) will of course reduce to this form if R and D are merged to produce only one length dimension.

Ultimately, the judgement of any dimensional analysis must be based on its usefulness in understanding the relationships between the various non-dimensional groups. In this respect (42) is an improvement over the simpler approach.

(h/D) is preferable to (h/R) - see the 'rigid' solution in Chapter 2. The equation (7) becomes

$$\tilde{x} = e^{-\tilde{t}/6\pi}$$

and

$$\dot{\tilde{x}} = -\frac{1}{6\pi} e^{-\tilde{t}/6\pi}$$

also

$$\ddot{\tilde{x}} = \left(\frac{1}{6\pi}\right)^2 e^{-\tilde{t}/6\pi}$$

and $\frac{\phi_z \eta_i}{\eta_o D^2}$ and $\frac{\phi_r \eta_i}{\eta_o D^2}$ represent the effect of a permeable layer on film thickness and pressure. Indeed, Wu (8) has chosen to use $\frac{\phi T}{D^3}$

as his non-dimensional group in a squeeze film with rigid boundaries and iso-tropic permeable layers.

It is more convenient to write (42) in the form

$$\tilde{h}_o, \tilde{p}_o = f_{1,2} \left(\tilde{t}, \tilde{A}, \tilde{\phi}_z, \tilde{\phi}_r, c, V, \tilde{\eta}_1, \tilde{T}, \tilde{r}_a \right)$$

\tilde{T} and \tilde{r}_a refer to the geometry of the model and both of these have remained constant, at 20 and $1/6$ respectively in both experimental and theoretical work. V has taken experimentally determined values when the theoretical and experimental results were compared but has remained constant at 0.25 in the theoretical predictions presented in Chapter 6.

Similarly $\tilde{\phi}_z$ and $\tilde{\phi}_r$ were allowed to differ for the purpose of correlating theory and experiment but with one exception, described in Chapter 6.2, the two permeabilities were otherwise considered equal. The range of values of the repeating variables and the non-dimensional groups used in the experimental and theoretical work and also encountered in animal joints is shown in figure (10).

Chapter 5

THE EXPERIMENTAL WORK5.1 The Apparatus

Whilst large computers can now handle programmes which solve complicated mathematical models, it is extremely desirable that an independent check be kept on the results from such numerical procedures. Such a check might be hoped to confirm the hypotheses on which the model had been based or to illustrate inadequacies or over-elaboration in the model. Bearing in mind the number of assumptions introduced in Chapters 2 and 3 concerning squeeze-film behaviour, it was considered important that some experimental results be obtained that could be compared with the predictions of the numerical work.

The transient nature of normal approach lubrication is an added complexity to experimentation and the approach to the design of the experiments has been dictated by practical limitations rather than the concept of an ideal experiment.

The easiest configuration with which to work and one similar to an animal joint was considered to be two surfaces approaching each other under the action of gravity.

The choice of geometries for the film shape lay among these three possibilities.

- 1) Two circular flat surfaces
- 2) One flat and one cylindrical surface
- 3) One flat and one spherical surface.

The first possibility can be ruled out despite its axial symmetry because of the extreme difficulty in preventing the upper surface from rotating about either of its horizontal axes during its approach towards the lower (fixed) surface.

The second possibility lacks axial symmetry but rotation about only one axis needs to be prevented (a horizontal axis perpendicular to the axis of the cylinder).

The third possibility combines axial symmetry and freedom from the rotational difficulties inherent in the other two geometries. It is the obvious choice.

The rig was constructed around this latter geometry and is shown in figures (11 & 12). The lower boundary of the squeeze film (H) consists of a thin disc of test material, some 150 mm diameter bonded on to a flat (surface ground) mild steel plate (E), 9 mm thick and 220 mm by 170 mm in area. This steel plate is fixed rigidly by four Allen screws on to the baseplate. The height of a test piece above the baseplate can be varied in increments of 0.05 mm by insertion of packing between the baseplate and the test piece backing plate. The baseplate is 9 mm mild steel plate, some 0.5 m square and could be levelled by means of four feet which rest on a work-bench.

A horse-shoe electro-magnet (B) with surface ground faces is suspended above the test piece from a rectangular arch (A) constructed of 19 mm square bar. The feet of the arch are screwed to the baseplate at each side of the test piece so that interchange of specimens can be carried out without disturbing any other part of the rig.

Between the magnet and the specimen fits the moving part of the rig. This consists of two halves, the upper half (C) being a flat steel plate, the lower half (D) being the upper boundary of the squeeze film. This upper half clamps against the faces of the electro-magnet and carries the lower half rigidly suspended about 20 mm below it. The lower half has, of course, a spherical lower surface. This spherical form was produced on a copying lathe from a template of 300 mm radius.

Although any horizontal movement or any slight rotation of the

spherical surface about a horizontal line would not change the geometry of the squeeze film, such motion was considered undesirable since the purpose of the experiments was to examine fluid films under pure normal approach. Also the instrumentation of the rig was designed to measure phenomena on the axis of symmetry of the film and any motion of the upper surface, other than vertical translation, would move this axis of symmetry either in a horizontal direction or out of the vertical.

Two constraints then were added to the moving part of the rig to prevent any of these undesirable motions. The first constraint consisted of three horizontal lightweight arms (I) radiating out at 120° intervals from the upper rim of the spherical surface. These arms were pinned to pillars (J) at the outer edge of the baseplate and were of 10 mm width and 1 mm depth. Their length was 300 mm, hence the large size of the baseplate. Free vertical movement of the spherical surface was thus unaffected but horizontal translation was inhibited. Rotation about a horizontal axis was minimized by constructing an arch F from the plate C over the magnet B and its support A. From this arch, a dowel G fitted into a vertical P.T.F.E bush mounted in the crossbar A. Loading of the rig was accomplished by fitting a load carrier (not shown) to each corner of the steel plate C. This completed the construction of the rig.

5.2 Instrumentation

Initially it was hoped to measure three parameters as they varied with time during normal approach. These three were displacement of the upper surface, central film thickness and central film pressure. Not surprisingly, displacement was found to be the easiest to measure. A displacement transducer reading to 0.0025 mm was mounted vertically on the crossbar A and recorded the vertical displacement of F at a point on the axis of symmetry of the film. The transducer was of the inductive type

and its probe was loaded against F by a light spring. This was found to be quite satisfactory and the probe followed the motion of F with no sign of any time-lag. The signal from the transducer was fed to a strain bridge operating at 5 KHz.

Measurement of pressure in the centre of the film was not so straightforward. In rolling or sliding situations where the pressure at any particular point is constant with respect to time, use of a pressure tapping in the wall of the bearing is a satisfactory method to record pressure. However if this method were to be used in a squeeze-film, it would be found unsuitable on three counts. First, the presence of a tapping changes the film shape and hence the pressure gradients in the region of the tapping, second, since all pressure measuring devices require some physical movement of a diaphragm, there will be a flow from the film to the measuring device through the tapping. This flow will have two effects; there will be a pressure difference between the entrance to the tapping and the diaphragm, and the flow into the tapping will lower film pressures near the tapping. The third drawback to this method is that the pressure reading is purely dynamic and is not capable of measuring static stress due to deformation of the thin layer by the spherical surface.

A commercial pressure transducer was connected to the centre of the film via a tapping but it was considered unsuitable for the reasons given above.

To overcome these difficulties, a direct approach was tried by building in a small stiff diaphragm at the centre of the spherical surface, figure (12). The centre of the top face of D was cut away until only a thin circular diaphragm of 5 mm radius and 0.75 mm thickness was left. On to the centre of the back of this diaphragm was mounted a semi-conductor strain gauge, the active part of the device being 0.5 mm by

1.5 mm in size. The gauge factor of the device was nominally 100 and so very small strains could be detected. For fluid pressures of 10^6 N/m^2 , the deformation of the diaphragm was calculated to be 1.5×10^{-3} mm. This was considered an acceptable departure from sphericity for the top surface. The strain gauge and a dummy formed a half bridge which was connected to a strain bridge instrument with a carrier frequency of 5 KHz. Calibration of this transducer was achieved by applying known uniform hydrostatic pressure to the spherical surface. The calibration was linear.

Error will be present in recordings from the transducer because squeeze film pressures will not be uniform over the area of the diaphragm. However peak pressures will occur in the centre of the film and it is in its centre that the diaphragm will be most sensitive. Drift of the half bridge was minimized by creating a sealed environment around each gauge and since the rig operated at a reasonably constant room temperature, variation of gauge factor with temperature was ignored.

The two strain bridges used to measure pressure and displacement had D.C. outputs and these were fed to an Ultra-violet Oscillograph which produced permanent records of the time variation of these parameters. Paper speeds of up to 1000 mm/s could be used and the galvanometers employed had natural frequencies of 100 Hz. They were linear up to 60 Hz in response. However none of the signals recorded had rise-times less than 0.02 s.

Since the problems of measurement of film thickness vary with the nature of the lower surface, the attempts made to measure films are described separately in the following sections.

To continue the pattern of the previous chapters, the various experiments are described in the following order. First, rigid impermeable squeeze films, second, "weeping" lubrication, third, lubrication with an

elastic impermeable layer, and fourth, the squeeze films with elastic permeable layers. No experiments were carried out to test the effect of additives in the lubricants.

All the experiments had several features in common and it is convenient to describe them now. The thickness of the layers of test materials were all nominally 5 mm and the area of each specimen approximately equal to the area of the spherical surface. Each specimen was tested with three different lubricants, all being mineral oils. They were provided by Shell Research Ltd. and denoted as HVI 160, HVI 650, LVI 1100. At room temperature the viscosities were approximately 3 poise, 15 poise and 75 poise giving a ratio of 5 between successive viscosities. Also three loads were applied to the film. The lowest load was 4.330 kg and was merely the weight of the rig with no extra loads applied. The other loadings were 6.145 kg and 7.960 kg. This upper limit corresponded to the highest value of flexibility that the computer programme could accept without going unstable. It was also within the safe limit of pressures generated in the film in the experiments where the stiff plastics and metal were used as the lower surfaces. The initial height of the top surface above the undeformed lower surface was set at nominally 0.25 mm. The various parameters of interest in the experiments are listed together in figures (10 & 71).

Before each run, the current in the electro-magnet coils was reduced to the minimum necessary to support the plate C and spherical surface D. This was to minimize the effects of retentivity in the iron core on the initial part of the normal approach. The only effect of this retentivity was to produce a slight uncertainty in the zero position of the time scale of the pressure and film thickness curves. This was not considered to be important and had no effect on the experimental results.

With regard to experimental error, it was considered that the Ultra-Violet Oscillograph traces could be measured to less than $\pm 1\%$ FSD

(1 mm in 100 mm). The strain-bridge instruments were quoted as being accurate to $\pm 1\%$ FSD also. Thus both pressure and displacement traces will be accurate to within $\pm 2\%$ FSD. Since the film thickness is deduced from the sum of the displacement and deformation (with the latter proportional to pressure), the error in film thickness curves will be $\pm 4\%$ FSD. This value covers most of the scatter on the experimental results.

The dependency of gauge factor in semi-conductor gauges on temperature is well known. However the variation was quoted by the manufacturers (Electro-Mechanisms Ltd.) as being 6% over a 100 F° range. This is negligible since all experiments were conducted at normal room temperatures.

Because the pressure transducer records strain produced by a non-uniform pressure distribution, there will be a systematic error in the recorded pressures. Thus the accuracy of the transducer can only be estimated by comparing the experimental values with computed values. Whilst the agreement in the experiments with rubber was not so good, that in the porous plastic tests was excellent.

5.3 Rigid Impermeable Boundaries

The lower surface of the squeeze film in this case was a mild steel plate that was surface ground to a roughness of 0.25 microns c.l.a. If the surfaces are considered rigid, the film thickness can be derived directly from the recording of displacement. This assumption has been used to plot the curves of film thickness and pressure, shown in figures (13) and (14). The staggering of the origin of co-ordinates has been done in the interests of clarity, and the three graphs could equally well have been grouped together under headings of load rather than viscosity.

The results from all three oils have produced a reasonable agreement between measured and theoretical film thicknesses and the main discrepancy occurs after $\tilde{t} = 30$ when the experimental values are 0.025 - 0.05 greater

than the theoretical. Possible causes of this are first: friction due to the constraints fitted to the upper surface, and second: deflection of the diaphragm under the generated film pressures. There is no evidence of friction being present in the experiments described later with other materials and a look at the various pressure/time curves suggests that the flexibility of the system is not quite zero. Departure of the experimental curves from the theoretical occurs at $\tilde{t} \approx 25$ and the final static pressures recorded were $\tilde{p} \approx 4000$. Thus the model has produced film thicknesses greater and pressures less than the theory would lead one to predict.

If we consider the diaphragm as being of uniform thickness and built in on its edge, its deflection (δ) under a central load (L) is given by

$$\delta = L a^2 \cdot 12(1-\nu^2) / 16 \pi E h^3$$

where a is the radius and h the thickness. For the loads used in the experiments, this expression produces a deflection at the centre of 4.3×10^{-3} mm. This is 0.017 expressed as a non-dimensional film thickness and is sufficient to account for most of the observed discrepancies.

It was considered that the high pressures predicted by the theory might damage the diaphragm or its strain gauge and so these experiments were conducted as the final part of the experimental work.

5.4 The 'Weeping' Thin Layer

As described in Chapter 2, the concept of self-pressurized hydrostatic lubrication can be realized in its extreme form by a thin layer of material on a rigid backing, the thin layer having zero radial permeability and infinite axial permeability. It was attempted to produce a material which had these properties in the following way:

On to a steel plate was cast a disc of silicone rubber (Silcoset 101 manufactured by ICI Ltd.), some 150 mm dia and 5 mm thick. The surface of the steel was primed to achieve bonding between the rubber and steel - addition of a curing agent caused the liquid rubber to set over a period of 24 hours. Care was taken to remove air from the liquid by subjecting it to a pressure of 5-10 mm mercury for 30 minutes.

Against the upper surface of the liquid rubber was pressed a clean unscratched perspex surface. After setting of the rubber the perspex was removed by prising it free from the surface. In the central region of the rubber disc, 2500 vertical holes were punched to model the concept of weeping lubrication. The pattern of holes was a grid 50 mm square containing 50 holes per side. The spacing of the holes was thus 1 mm and the diameter of each about 0.6 mm at the surface. Production of the grid was achieved by using the table of a milling machine which was indexed in both horizontal directions.

For the actual manufacture of each hole, a large bore hyperdermic needle (0.6 mm bore) was used with the tip ground by trial and error to a shape which produced a clean round hole.

Drilling of the rubber was found to be quite unsatisfactory and it produced a very rough, torn surface. For the first few holes punched, the core was removed by the needle but since these early cores blocked the bore of the needle, later cores were merely pushed down into the rubber as shown in diagram (15). This caused a slight rising of the punched surface above that of the untouched surroundings. To fill the holes with fluid, the fluid was poured on to the surface and the specimen placed under vacuum for several hours.

Measurement of the flexibility of the material was done directly on the rig. The rigid spherical surface was lowered towards the rubber until just touching. On releasing the top surface, the deformation of the soft layer was measured. This was repeated several times and for

three values of load.

The flexibility for the theoretical comparison was calculated from this deformation, knowing the load applied and assuming a parabolic pressure distribution. (This latter assumption is already implicit in the treatment of the elasticity equations in the programme and indeed in all the theory of Chapter 2.) Slightly different values for A were found for the three loads indicating a decrease in flexibility as the deformation increased. These values are shown in the graphs of results for this model, figs. (16-21).

It was also necessary to measure an 'experimental' value of flexibility. In the absence of a direct measurement of film thickness, it became necessary to deduce it from the measured displacement curve and a calculated deformation curve. Since deformation and pressure have been assumed proportional throughout this work, the central deformation of the soft layer could be found in an experiment from the measured pressure and an experimental flexibility.

This flexibility was calculated from the recorded static pressure and the measured static deformation (described as above). Since the predicted final pressures were $\sim 20\%$ greater than the recorded static pressures, the values of flexibility for the theoretical and experimental models were not equal. They are shown in figs. (16-21).

Initial separation of the surfaces was found from the final value of displacement and the total deformation either measured statically or calculated from the final recorded value of pressure.

The same method of production of the thin layer and calculation of film thickness was used for the experiments with an elastic impermeable layer (with the exception of the hole punching).

Originally it was attempted to measure film thickness directly by recording the capacitance between the steel upper surface and a small electrode buried 0.1 - 0.05 mm below the rubber surface. In order that

only the central film thickness would be measured, the electrode was 6 mm square and had four holes drilled in it before insertion in the liquid rubber during casting. However it was found that the presence of the electrode disrupted the pattern of holes in the rubber and also that its area was so small that the peak capacitance measured was of the order of 1 - 2 pf. Consequently there was substantial drift associated with the measurement of this signal. Also the capacitance varied with the deformation of the rubber even in static conditions. The direct measurement of film thickness was thus abandoned and replaced by the indirect method described above.

With this indirect approach, the main source of error was in measuring the total displacement of the top surface. Whilst 95% of the displacement occurs within 3 seconds of release, even with the LVI 1100 oil, the other 5% may take up to several minutes.

The results are plotted with the corresponding theory in figs. (16-21). Since the non-dimensional flexibility contains the quantity L , there are three separate graphs for film thickness and pressure. This applies to the presentation of the results for the elastic impermeable material also.

The agreement between theory and experiment is excellent. However the results are shown only to $t = 120$ and as already mentioned, the theoretical final pressure attains a value somewhat in excess of the static experimental values ($t \rightarrow \infty$). This could be due to the non-uniform pressure distribution applied to the diaphragm (parabolic in the theory but not necessarily so in practice) and also to the fact that the calibration of the diaphragm was based on a uniform hydrostatic pressure.

5.5 The Elastic Impermeable Layer

The material for the thin layer for these experiments was identical to that used for the 'weeping' lubrication tests, with the exception of the holes. Direct measurement of film thickness was attempted but failed

for the reasons previously given. However it was of use in a qualitative manner for an interesting phenomenon which occurred during testing of the rig.

It was found that rapid separation of the two boundaries of the film produced cavitation of the fluid in the central region of the film. This manifested itself on the pressure and film capacitance traces in a most peculiar manner and the relevant traces are shown in fig. (22). It should be noted that both curves are a qualitative record of events since the position and severity of the cavitation was variable.

Presumably the dip in the pressure trace occurs as the bubble is forced out of the central region - replacement of the air by oil would lead to a slower rate of closure of the film.

Confirmation of the presence of air was found by removal of the magnet, the crossbar and all the moving part of the rig and replacing the latter by a perspex disc with a lower surface of spherical form with the same radius of curvature as used in the steel version. By closing and opening the film by hand, a small cavitated region could be induced to form at the centre of the film. A photographic record of this formation is presented in fig. (23).

During actual experiments, care was taken to avoid rapid separation of the surfaces and consequent formation of air bubbles. The phenomenon was more readily inducible in the models with higher viscosities.

The results are shown in figs. (24-29). The pressure traces show some deviation from the theoretical at large values of \tilde{t} , as happened in the experiments with the "weeping" material. However the gross discrepancy is found in the curves of film thickness. For all three flexibilities of the model (i.e. the three loading situations), the difference between theory and mean experiment values is five or six times the standard deviation of the experimental curves. This is significant and it requires some explanation.

It is proposed that the cause of this discrepancy lies in the phenomenon of entrapment. This effect has been described and experimental evidence obtained for it by Christensen (5) and Dowson & Jones (12).

The approximation inherent in all the work in this thesis is that the surface deformation of a thin layer is proportional to the fluid pressure at that point on the surface. In the case of the "weeping material" the presence of the holes produces two results. One is that the transfer of strain from one small deformed region to another is rendered more difficult because of the small amount of material left between successive holes. The other result is that the Poisson's Ratio of the layer will be almost zero despite any solid piece of the constituent material - the rubber, having a value of 0.495. This is due to the rubber being able to expand sideways into the holes when compressed, resulting in a decrease in the volume of the holes. Indeed this effect has been assumed in the theoretical treatment of the "weeping" model. The overall result of the punching of the holes is thus to make the resulting layer agree well with the theoretical analysis.

However the situation in the solid rubber layer is very different. With a Poisson's Ratio of 0.495, the material is virtually incompressible under the loads applied in the experiments. Thus compression of the central region of the thin layer must result in a rise in the surface level elsewhere. This was illustrated when the spherical surface was in dry contact with the rubber. The resulting area of contact was considerably greater than that calculated from the measured deformation.

Direct evidence for entrapment, however, was considered to be necessary and, to this end, two qualitative optical experiments were carried out to examine film shape during normal approach.

The first of these experiments was extremely simple and is shown in fig. (30A).

The two boundaries of the film were a semi-reflecting glass plate

and a silvered piece of silicone rubber that had been cast in a 'watch-glass'. Interference fringes were observed and were circular, but instead of moving outwards from the centre, as one would expect from the theory, they were observed to be moving inwards and outwards from a narrow annular region. A sketch of them is shown in fig. (31A). Although semi-silvering of the glass plate and silvering of the rubber improved the definition of the fringes, they could be observed with neither surface coated. Despite the rapid movement of the fringes during the squeeze process, 50 were counted moving inwards from the annulus and it appeared that about 25 could be seen between this annulus and the centre at any one time.

The other experiment was slightly more sophisticated and involved using a Vickers Microscope - the optical set-up is shown in fig. (30B). The fringe pattern was projected on to a screen and initially, fringes could be seen moving outwards from the centre but, as the sphere approached the rubber, entrapment could be seen to occur (31B). In the first experiment, the loading, the flexibility and the radius of curvature of the system were all similar to the values used in the rig during the experiments. In the second experiment, the load was not known but was less than 5 Newtons and the radius of curvature was only 15 mm.

Since the loads in the theoretical analyses and corresponding experimental models were equal, it would seem that higher pressures exist in the central region and lower pressures elsewhere in the film than are predicted by the computed theory. Clearly a full theoretical treatment and an experimental record of the development of the entrapment (perhaps on cine film) is called for in systems of high flexibility.

5.6 The Elastic Permeable Layer

To test that part of the programme describing the effect of a permeable layer on squeeze film behaviour, experiments were carried out

with two permeable polythenes, both being 5 mm thick and manufactured by Porvair Ltd. Specimens 150 mm square were bonded on to steel plates to form the test pieces. Measurement of the permeabilities of these two materials presented some difficulties.

Axial permeability was easily measured in both cases but the radial permeability presented two problems, neither of which was immediately obvious.

Initially test pieces were prepared as shown in fig. (32A) and the values of permeability derived from these tests were found to be very small - about 1% of the axial permeability. Microscope examination of the faces of the specimens (through which fluid had to flow) showed that the heat generated in the mechanical cutting of the faces during the preparation of the specimens had melted the surface material and virtually sealed both faces.

To overcome this problem, new specimens were prepared, see fig. (32B), in which fluid could flow through surfaces whose structure had not been altered in any way. Due to the small flowrates expected with mineral oils, water was used initially for the tests and gave very inconsistent results due probably to a swelling reaction between the polythene and water.

The use of water was thus abandoned and a mineral oil HVI 55 was used as the fluid. A pressure head of 2 m of liquid was used (instead of the original 300 mm) and measurable flow-rates obtained. It was found that the ratio ϕ_s/ϕ_r was 2.26 for the more permeable material and 2.31 for the less permeable one.

The void ratio of the two materials was found by weighing samples before and after impregnation with oil.

The calculation of flexibility of the polythenes presented various problems since deformation due to loading by the spherical surface was too small (0.025 - 0.035 mm) to be measured accurately and was anyway subject to some time variation. Also the final static pressures differed somewhat

from specimen to specimen although the flexibility of all must have been the same. (It was necessary to use one specimen for each oil since once a lubricant had been forced into the polythene by vacuum technique, it could not be removed.)

Fortunately, however, it was found that the pressure trace of the actual results could be divided into two parts. The first part corresponded to a hydrodynamic lubrication regime, the second part to elastic contact of the two boundaries of the film. The recorded pressures during the hydrodynamic regime were substantially lower than the elastic contact pressures in all cases so it was decided that the highest value of flexibility calculated from elastic contact pressures would be used in the calculation of experimental film thicknesses and also in producing the theoretical trajectory. Since the flexibilities of the elastics were at least an order of magnitude lower than those of the rubbers, it was not vital that they were known with high accuracy. The results are presented in figs. (33-44) and show excellent agreement with the theory over the lubrication regime. There was of course no theory developed for the rise in pressure after contact, neither were any experiments carried out with enriched lubricants.

Chapter 6

THEORETICAL PREDICTIONS OF THE MODEL

Before discussing the details of the various theoretical models examined, some general comments can be made about the results.

In order that the large computing timetable could be completed, it was considered necessary to ensure that "turn-round" time for each programme submitted to the computer was less than 24 hours. This imposed an upper limit of 10 minutes on the running time for any one programme. The time limit produced problems only for the models in which permeability was involved, and, in these cases, the permeability was assumed to be zero over the initial part of the trajectory ($\tilde{t} < 6$). This assumption effectively halved the running time and brought all models within the 10 minute time limit.

Only for the extremely permeable models did this approximation noticeably affect any of the trajectories. In these cases a separate computer run over the period $0 < \tilde{t} < 6$ was performed in which the actual value of permeability was used. This corrected any discrepancy.

The end of all the curves was caused by either impact of the top surface on the lower, completion of the calculation or lack of computing time. This lack of time was due to a rapid rise in sensitivity of acceleration to small changes in position when the film thickness was small.

To maintain the continuity of the previous chapters, the same order of discussion of models is used, starting with the rigid impermeable model and ending with various concepts of enrichment in the lubricant.

6.1 The Rigid Impermeable Model

This was the simplest model to solve numerically and the resulting

variations of film thickness and pressure with time agree well with that predicted by the simple "exponential" solution to the equation of motion derived in Chapter 2.

This is due to the predominance of viscous forces in the models examined and the resulting accelerations being correspondingly small.

Comparisons between the analytical and the computed solutions can conveniently be divided into two parts; showing the effect of spatial and temporal boundary conditions respectively. Figures (7) and (45) show how the velocity, displacement and pressure curves develop when the normal approach commences. The effect of the condition $\tilde{x} = 0$ at $\tilde{t} = 0$ is clearly shown and seems limited to $\tilde{t} < 3$. Figures (64) and (69) show small discrepancies between analytical and computed values over the rest of the trajectory ($\tilde{t} > 3$). This is no doubt due to the different radial boundary conditions in the two cases.

In the analytical solution the radial boundary condition was $\tilde{P}_r = 0$ at $\tilde{r} = \infty$, in the computed model it was $\tilde{P}_r = 0$ at $\tilde{r} = 1/6$. The value of $\int 2\pi\tilde{r} \cdot \tilde{P}_r d\tilde{r}$ for $1/6 < \tilde{r} < \infty$ is not necessarily negligible.

6.2 The "Weeping" Lubrication Model

The only progress towards an analytical solution to the weeping model was an approximate expression for the pressure profile with a condition $\tilde{x} < 0$. This expression has been applied to two arbitrarily chosen instants of time in two computed solutions of the model - see fig. (3). The agreement is excellent.

The description of the rest of the results from the programme can be conveniently divided into two parts, pertaining respectively to models whose flexibilities are equal to or less than 10^{-3} and those greater than 10^{-3} . This division is due to the fact that the behaviour of models with elastic thin layers can only be calculated for values of flexibility not greater than 10^{-3} . Thus the more flexible weeping models have no

corresponding impermeable models with which to compare.

$$\underline{\underline{\tilde{A} \leq 10^{-3}}}$$

The initial accelerations developed in the weeping model for $\tilde{A} = 10^{-3}$ can be seen to be very similar to those for the rigid model. This also applies to the variations of central pressure, velocity and displacement with time, see figs. (45-48).

Figures (49) and (50) show the variation of pressure and film thickness with time and the shape of the curves, as shown, is quite unexceptional. For $\tilde{A} \leq 10^{-3}$, the resemblance to those of the elastic impermeable model is quite striking. These two models are compared in fig. (51). The effect of the "weeping" material can be seen to be quite small and ineffective in maintaining substantially thicker films than the impermeable model.

Thus, for $\tilde{A} \leq 10^{-3}$ at least, the claim of a 'weeping' model in improving squeeze film lubrication is quite unjustifiable, especially when it is remembered that the experimental work produced sound evidence for entrapment, and consequent thicker films, in the impermeable model.

The 'weeping' model that was proposed in Chapter 2 can be considered as the extreme case of an elastic porous material whose radial permeability is very low and its axial permeability very high. Thus any deformation of the material must be accompanied by flow of fluid out of the surface of the layer.

In figures (52) and (53) the curves of film thickness and pressure are shown for two such layers, also, for comparison, the 'weeping', impermeable and two isotropic permeable models of equal \tilde{A} have been included.

It can be seen that these anisotropic permeable models behave very similarly to the weeping model. Due to numerical difficulties in the initial stages of the squeeze film, it was necessary to make $\tilde{\phi}_z = 0$

over the period $\tilde{t} < 6$. Since the difference between the 'weeping' and impermeable curves at $\tilde{t} = 6$ is small, this was not thought to affect the resulting curves significantly.

To return to the 'weeping' material, the film thickness for $\tilde{t} < 6$ is shown in fig. (47) The shape is surprising and not at all what would be expected. Confirmation of this behaviour with the anisotropic model was attempted but failed.

Numerical difficulty in this was due to the presence of the term $\frac{w_0 \eta_0}{\phi_r (T-A.P.)}$ in the equation for evaluating pressures in the porous material (equation 25).

$$\underline{\underline{\tilde{A} \geq 10^{-3}}}$$

Due to the absence of the term w_0 in the Reynolds Equation for this model, the difficulties encountered in the other models with regard to its evaluation are avoided and hence the behaviour of the 'weeping' model can be calculated for extremely large values of \tilde{A} ($\tilde{A} \approx 1$), typical of human joints.

Film thickness and pressure is shown in fig. (54) for some of these very high values.

The curves are most extraordinary and it is very debatable whether such an increase in film thickness does occur in practice. It is difficult to explain the curves in physical terms although it must be attempted.

On initiation of the normal approach, several events occur quite rapidly. These are: the acceleration rapidly changes from $\ddot{x} = -g$ to $\ddot{x} = g/30$ and thence slowly falls to zero as the normal approach proceeds. The pressures - which must rise quickly to reduce the absolute magnitude of the acceleration - produce large deformations due to the high values of flexibility. Also the displacement changes only slowly since the rapid change in acceleration produces quite small velocities and since the difference between deformation and displacement of the top

surface is positive, the film thickness increases over the period of initial pressure rise.

The rapid rise in pressure is not prevented by considerations of the rate of deformation of the elastic layer since fluid always flows out of the surface at a rate equal to the rate of deformation.

Since the material is very flexible, the displacement, x , soon becomes negative and hence the expression for film thickness, derived in Chapter 2.3, becomes valid. Thus the film is parallel over all but the initial stages of the trajectory. (For $\tilde{A} = 0.5$, $x < 0$ when $\tilde{t} > 9$.) If cartilage were found to behave in such a manner, then 'weeping' lubrication would be a very effective mechanism in Joint performance. Indeed one might say that the thin layer in the model is being 'wrung out' by the application of the load. For $\tilde{A} = 0.5$, the final compressive strain in the thin layer is 0.69. It would be useful to perform some experiments in which film thickness could be measured, or calculated, for very flexible weeping materials in order to investigate this phenomenon further.

6.3 The Elastic Impermeable Layer

The pressure and film thickness curves for this model are shown in figures (56) and (55). Their shape is much as would be expected with the more flexible systems producing thicker films and lower pressures.

Development of the pressure profile is shown in fig. (57). It can be seen that the distribution slowly approaches that of the static elastic-contact parabolic shape as $\tilde{t} \rightarrow \infty$

Figure (58) shows the rate of deformation of the elastic surface and the most important feature is that nowhere could this velocity be considered constant by any stretch of the imagination. The device of a velocity of approach constant with respect to radius has been used by several authors, as discussed in Chapter 2.

More interesting features of the model are found in its behaviour immediately after the commencement of the normal approach. For $\tilde{t} < 6$, the system is completely dominated by the effect of w_0 in the Reynolds Equation. This term prevents rapid change in pressure with respect to time (as observed above), and the overall effect is that the model appears to behave as if it had less "damping" than the weeping model (in which w_0 is absent).

This is best seen in the curves of acceleration and central pressure in figures (46) and (45). Both graphs show oscillations whose severity increases as A increases. The central velocity of deformation of the elastic layer is shown in fig. (48) along with the corresponding curve of \tilde{x} . The condition $\tilde{w}_0 \geq \tilde{x}$ (both normally negative) causes \tilde{w}_0 to equal \tilde{x} until the pressures have risen sufficiently to produce small values of \ddot{x} . This occurs until $\tilde{t} = 3$ in the system $\tilde{A} = 10^{-3}$. Thereafter \tilde{w}_0 decreases in magnitude and is normally less than $\tilde{x}/10$ for the rest of the trajectory. Corresponding to this behaviour of w_0 , the film thickness remains constant over the period $\tilde{t} < 3$ and the pressure profile is flat in the central region - this is shown in figure (59).

Whilst neither of these last two features is intuitively obvious, or readily acceptable, they are consistent with the treatment of the elasticity equations in Chapter 2.

6.4 Elastic Permeable Layers

As already mentioned, the introduction of the term $\frac{w_0 \rho_0}{\phi_r (T - A.P.)}$ into the differential equation describing flow in the porous material produces an instability in the numerical analysis. This instability results in longer running times on the computer and also to more frequent programme failures.

Thus the bulk of the results presented represent models in which this term has been ignored. To investigate this approximation three computer

runs were attempted, at $\tilde{A} = 10^{-3}$, with this term included. They are shown in figures (60) and (65). It is seen that the total effect is small, it is of course zero for $\tilde{\phi}_z = 0$. The effect on the other curves ($\tilde{A} < 10^{-3}$) will be less and will be zero for $\tilde{A} = 0$.

Therefore the curves presented in figures (60-69) are an accurate representation of the effect of a permeable elastic layer.

The most interesting feature is that the central pressure actually declines before closure of the film in the more permeable cases. The film pressure in the region $\frac{\partial p}{\partial z} \Big|_{\text{surface}} < 0$ will however tend to increase to counteract the effect of this decline on the force exerted on the top surface by the fluid.

Also interesting is that the film thickness, and thus time taken for the film to close, increases as \tilde{A} increases.

Whilst these curves are for values of \tilde{A} far smaller than those that occur in joints, it is interesting to note that $\phi_{\text{joint}} \simeq 2 \times 10^{-7}$, a value which would produce curves indistinguishable from those of $\tilde{\phi} = 0$ for any of the values of \tilde{A} shown, if the term $\frac{w_o \tau_o}{\phi_r (T - A.P.)}$ is excluded.

Without this term, flow will always be from the centre of the film into the porous layer and then radially outwards. This is because equation (23) cannot have a maximum (or minimum) except on its boundaries. However this is no longer true when the equation is changed to (25). Now we can have a maximum pressure inside the material. Such a maximum could produce "weeping" and the curves shown in figures (60) and (65) for isotropic layers of $\tilde{A} = 10^{-3}$ and $\tilde{\phi} = 2 \times 10^{-7}$, and $\tilde{\phi} = 10^{-4}$ appear to be doing just this, although only marginally.

Thus a material with $\tilde{A} = 10^{-3}$ and a permeability similar to that of cartilage can act as a "weeping" layer. Since the effect will be less marked at lower \tilde{A} , then presumably it will increase with increase in \tilde{A} .

Finally, one point should be noted. In the impermeable cases, it has been assumed that the layer behaves solely as described by $\delta_r \propto P_r$ i.e. the constituent material can be compressed. However, in the permeable models, the equations demand that any change in the volume of an element be accompanied by an equal outflow of fluid from that element. Thus if the permeability of an elastic porous layer were decreased, then its response to loading would become slower and at zero permeability, the material would be effectively rigid. This slight contradiction is present throughout this work but it only affects layers of low permeability and low void ratio.

6.5 Enrichment in Normal Approach

The examination of enrichment was accomplished with two slightly different models of squeeze films. The first corresponded to that described in Chapter 2 where an additive is included in the fluid, the molecules of which are too large to be able to flow in the porous layer. The unenriched fluid can of course flow through this region.

The other model was one suggested by Dowson (5) and, by its nature, expected to be much more effective in maintaining fluid films. Here the additive is considered bound in some way to the surface of the elastic layer whose permeability is taken to be zero.

6.5.1 Enrichment with permeable elastic layers

The relevant parameters for this model are flexibility, permeability (the material considered to be isotropic), initial concentration of additive in the fluid, and the ratio of the viscosity of the additive to that of the unenriched fluid.

Since the purpose of examination of these models is to attempt to draw some conclusions about joint behaviour, the highest flexibility for which the programme would work (10^{-3}) was chosen for all the calculations.

Also, from exploratory runs of the programme, it was found that the effect of an additive was not marked over the range of time that the trajectory could be calculated.

Thus the highest possible value (10^4) that could be deduced from published values was chosen for the ratio of viscosities (3). Also the quantity $\frac{w_0 \eta_0}{\phi_r (T - A.P.)}$ in equation (25) was ignored since its inclusion would not have helped increase the additive's concentration in the central region of the film.

Of the other parameters, three values of permeability and initial concentration were chosen; 2×10^{-7} , 10^{-5} , and 5×10^{-4} for the permeability giving a ratio of 50 between successive runs and 3.5×10^{-3} , 3.5×10^{-2} and 3.5×10^{-1} for the initial concentrations, spaced at one order of magnitude intervals. The first values of these quantities are those most widely quoted as typical of animal joints (9, 13).

It should be noted that no value has been published for the radial permeability and, for the purposes of this model, the material has been assumed isotropic. Also the concentration of 3.5×10^{-3} is a gravimetric value and may not be accurate as a volumetric ratio, given the nature of the Hyaluronic Acid molecule.

The initial viscosity used in all these computing runs and in the non-dimensional groups was that produced by adding the initial concentration of additive to the base fluid.

Of the values used in the model, only the extreme case of highest permeability and highest concentration produced results discernibly different from those models with no additive. The relevant curves are shown in figure (70).

At $\tilde{t} \approx 60$, the central region attains a concentration of unity with a consequent rise in pressure and cessation of flow into the porous layer. The film remains parallel and entrapment, due to high central pressures, does not occur.

The conclusion we can draw from this is that enrichment with permeability and concentration corresponding to typical joint values will only be effective at very thin films, when it will produce boundary lubrication.

This conclusion is of course only valid for the flexibility 10^{-3} and a typical joint value is 0.5, which is many times greater than the model value.

6.5.2 The concept of "Boosted Lubrication"

"Boosted Lubrication" was first proposed by Dowson (3) and in concept is extremely simple. The system is considered impermeable and the additive is considered to be bound in some way such that it cannot flow sideways (i.e. radially). Thus for $c < 1$, we can say $c < \frac{1}{h}$, as already given in Chapter 2.

It was originally intended to compute results for this mechanism for elastic models. However the radial variation of viscosity produced problems in evaluating w_0 accurately and forced this approach to be abandoned. Various models with zero flexibility have already been examined by Dowson (3), but it is worth repeating the analysis in a slightly different format.

For the model of Chapter 2.2,

$$\frac{\partial P_r}{\partial r} = 6 \eta \tau \dot{x} / h_r^3 \quad (1)$$

and

$$c = c_i h_i / h_r \quad (c < 1)$$

also

$$\eta = \eta_0 (1 + c (M_r - 1)) \quad (30)$$

whence

$$\eta = \eta_0 (1 + c_i h_i (M_r - 1) / h_r) \quad (43)$$

Now $h_i = D + r^2/2R$ where h_i is the film thickness at $t = 0$.

Also $h_r = x + r^2/2R$ for all t

so

$$h_i = h_r + (D - x)$$

$$\begin{aligned} \eta &= \eta_0 \left\{ 1 + c_i(M_r - 1) + \frac{c_i(D - x)(M_r - 1)}{h_r} \right\} \\ &= \eta_i \left\{ 1 + k_s \frac{(D - x)}{h_r} \right\} \end{aligned} \quad (44)$$

It can be seen that the effect of enrichment is represented by one parameter, k_s

$$\text{where } k_s = \left\{ \frac{1}{1 + \frac{1}{c_i(M_r - 1)}} \right\}$$

since $0 \leq c_i \leq 1$ then $0 \leq k_s \leq 1$

It is interesting to note that the values quoted for joints, $c_i = 0.0035$ and $M_r = 10^4$, give $k_s = 0.974$, a value very near to the upper limit of $k_s = 1$.

Integrating (1),

$$\tilde{p}_0 = -\frac{3\tilde{x}R}{\tilde{x}^2 D} \left\{ 1 + \frac{2k_s}{3} \left(\frac{1}{\tilde{x}} - 1 \right) \right\} \quad \text{where}$$

$\tilde{p}_r = 0$ at $\tilde{r} = \infty$

Two further integrations give:-

$$\tilde{t}_{k_s} = 2\pi k_s \left\{ \frac{1}{\tilde{x}} - 1 + \left(\frac{3 - k_s}{k_s} \right) \log \frac{1}{\tilde{x}} \right\} \quad (45)$$

in which $\tilde{t}_{k_s} = 0$ at $\tilde{x} = 1$

if $k_s = 0$, $\tilde{t}_0 = 6\pi \log \frac{1}{\tilde{x}}$ which is the same as (7). Letting $k_s = 0.974$, and $\tilde{x} = 0.1$,

then
$$\frac{\tilde{t}_{0.974}}{\tilde{t}_0} = 1.95$$

for $\tilde{x} = 0.01$

$$\frac{\tilde{t}_{0.974}}{\tilde{t}_0} = 7.66$$

If we change the model to one which is perhaps more realistic in terms of animal joints, i.e. two parallel circular rigid plates, then we have

$$\tilde{P}_0 = -\frac{3\tilde{x}S^2}{\tilde{x}^3 D^2} \left\{ 1 + k_s \left(\frac{1}{\tilde{x}} - 1 \right) \right\}$$

where $\tilde{x} = x/D$, $\tilde{x} = \frac{\dot{x} \eta_i S^2}{F \cdot D}$ and $\tilde{P} = \frac{PS^2}{F}$

Two integrations give

$$\tilde{t}_{k_s} = \frac{\pi S^2}{4D^2} \left\{ \frac{1}{\tilde{x}^2} \left[3(1 - k_s) + \frac{2k_s}{3} \right] - (3 - k_s) \right\} \quad (46)$$

where

$$\tilde{t}_{k_s} = 0 \quad \text{at} \quad \tilde{x} = 1$$

putting $k_s = 0.974$ and $\tilde{x} = 0.1$ we get:-

$$\frac{\tilde{t}_{0.974}}{\tilde{t}_0} = 6.58$$

for $\tilde{x} = 0.01$,

$$\frac{\tilde{t}_{0.974}}{\tilde{t}_0} = 65.0$$

It is seen then that the mechanism works quite well in retarding closure of the film.

This latter example of parallel circular flat plates has been treated by Dowson (3) and he has calculated an improvement of 126 for $\tilde{\lambda} = 0.1$, compared with the value of 6.58 quoted above.

The discrepancy between results is due not to the calculation of 'boosted' squeeze film times but to the model with which the 'boosted' mechanism is compared. Equations (45) and (46) have been deduced by considering the 'non-boosted' model to operate with a constant viscosity η_i .

Dowson's comparisons have been with a model of constant viscosity η_o . The difference between η_i and η_o is sufficient to account for the difference in squeeze-film ratios.

Chapter 7

DISCUSSION

This chapter can be conveniently divided into two parts, the first relating generally to elastohydrodynamic squeeze films and the second particularly to squeeze films in animal joints.

7.1 Squeeze films and elastic permeable thin layers

The work described in this thesis has been a preliminary investigation of normal approach and the effect on the generated squeeze films of several types of thin layers. Inevitably the treatment of the subject has been broad at the expense of depth. This has manifested itself in the major approximation inherent in the work, the description of the behaviour of thin layers under load.

The accuracy of the statement $\delta \propto P$ can be examined by solving the full elasticity equations for a thin layer deforming under fluid pressure. This has been done for a Journal Bearing by Hooke, Brighton and O'Donoghue (7). They found that the approximation was valid for a Poisson's Ratio (ν) of 0.4 or less but gave large errors for a value of 0.495, a value typically found in Rubbers.

Further justification can be found by examining the correlation between experiments and theoretical predictions using this approximation. The evidence from this source confirms the findings of Hooke. Bennett (1) found good agreement between experimental and theoretical friction values using plastics of Poisson's Ratio of 0.4. The tests described in Chapter 5 using the porous plastics agreed well with the programme but due to low A , hardly constituted a rigorous test of the approximation.

The tests with the "weeping" layer with $\nu \simeq 0.0$ gave excellent agreement, but the experiments with the solid rubber $\nu \simeq 0.495$ gave large discrepancies.

In conclusion then, the approximation $\delta \propto \rho$ is justifiable as a first step in the investigation of squeeze films with low moduli thin layers of $\nu \leq 0.4$. Consideration of future theoretical work in this field would appear to face severe difficulties.

Hooke (6) has said that the full analysis is only 12 times longer than the simplified in terms of computing time but this is an average figure and at high eccentricities the ratio was considerably higher. This increase in computing time might be acceptable in the two-dimensional case (r, t) but is out of the question for the three dimensional (r, z, t) .

Closely connected with this question is the problem of evaluating the rate of deformation of the elastic layer. In the case of high flexibility, where both surfaces will move many times their initial separation, i.e. $A \frac{\partial \rho}{\partial t} \approx -\dot{x}$, a full elasticity treatment would fail if it did not describe the rate of deformation accurately.

It would also be desirable to tackle the problem of calculating squeeze films near the end of the approach when both surfaces have very low (nearly equal) velocities. The programme described in Chapter 3 became slower and slower in converging at these thin films. Christensen (3) has described similar troubles with his numerical methods.

On a more cheerful note, the neglect of the inertia of the top surface by Herrebrugh, Christensen (2, 3) has been shown to be a reasonable assumption in squeeze film calculations. The dominance of viscous forces in the rigid impermeable model has been well illustrated for the loads examined.

Comparison of the 'weeping' model described in Chapter 2 with anisotropic porous models suggests that it gives a fairly accurate description of the extreme case

The effect of flexibility on the squeeze film has been seen to be

much as expected, with thicker films and lower pressures than the rigid case. Also the presence of a porous layer has been shown in most cases to close the films faster although with interesting pressure/time variations. The exceptions to this are discussed in the next section.

On the experimental side, whilst the results have been generally satisfactory with regard to agreement with theory, there are two situations which require further exploration. Both are concerned with film thickness measurement. The first is an optical study of normal approach towards solid thin layers of materials with varying Poisson's Ratio to study the occurrence of entrapment. The second is a model with high flexibility ($\tilde{A} \simeq 0.1 - 0.5$) and with the "weeping" characteristics produced in the experimental work by punching holes in a rubber layer. This latter model would attempt to confirm experimentally the surprising results of the corresponding theoretical model described in Chapter 6.2.

7.2 The relevance of this work to animal joints

It remains only to discuss whether understanding of the operation of animal joints has been increased by the work described in this thesis.

An indication of the baffling complexity of the subject is that two authorities (2, 3) can propose diametrically opposed theories of their operation.

Whilst the models that have been examined, both theoretically and experimentally, bear some relationship to the structure of animal joints, it is not the author's intention to pronounce definitely in favour of one or the other. It is possible however to make some comments on the concepts of 'boosted' and 'weeping' lubrication.

The most striking feature of the theoretical models examined was found in the 'weeping' model described in Chapter 2. At high flexibilities (0.1 - 0.5), dramatically thick films developed which would suggest that

such a material would constitute an ideal layer for a low-friction bearing. However, until some experimental evidence is forthcoming that such a material can be found and shown to operate in this manner, the model must remain an interesting theoretical speculation.

Of more relevance are the results from the model in which additives have enriched the film. From the curves shown and discussed in the previous chapter, it is clear that such an enrichment mechanism will only be effective with very thin films. It will form an excellent boundary lubrication mechanism at the termination of normal approach.

The system proposed by Dowson (3) is much more powerful in retarding closure of the film, as equations (45) and (46) show; it operates for the apparently quite low values of concentration and viscosity of additive found in animal joints. Further evidence about the role of Hyaluronic Acid in actual joints is needed, however, before one can accept the mechanism as being an accurate representation of physical processes.

The computer runs with concentrations higher than 0.0035 are not necessarily just of academic interest because 0.0035 is a gravimetric concentration and the programme is designed to use a volumetric value. The shape and activities of the Hyaluronic Acid molecule - or molecular complex - appear to be quite complicated (9).

Another possible model for an animal joint is represented by an elastic isotropic porous layer in which the term $(w_0 \eta_0 / \phi_r (T - A P_r))$ has been included. This is probably the closest model to the concept of "weeping lubrication" as expounded by McCutchen (4). The behaviour of the high permeability models is unexceptional but for the lower values (2×10^{-7} , 10^{-4}) it appears that the film thickness is marginally greater than for the impermeable model. Thus the material is showing slight signs of "weeping". The lower value of permeability (2×10^{-7}) corresponds to a value typically quoted for cartilage.

One crucial quantity which it appears has not yet been measured is

the permeability in a radial direction. All figures that have been quoted refer to the axial direction - no doubt due to the difficulty of radial measurements. A value of ϕ_r / ϕ_z greater than unity would encourage "boosted" lubrication, a value lower than unity would suggest "weeping". Clearly a theoretical analysis at high flexibility and varying radial and axial permeabilities would help decide this conflict of theories.

7.3 Conclusions

This investigation has shown that it is possible to examine squeeze films and the effect on them of various types of boundary in reasonable detail. It is to be hoped that it lays a firm foundation for future investigations into normal approach in general and in particular, investigations of the phenomena of entrapment in elastic impermeable surfaces and of the increase in film thickness with respect to time as found in the "weeping" models of high flexibility. Also the extension of the computing beyond $\tilde{A} = 10^{-3}$ would be a major development.

One other extension of the models considered would be to examine the effect of large scale surface undulations on the squeeze film; Dowson has suggested that such roughness is an important feature of joints (14). This effect could be simulated by allowing the thin layer surface to undulate sinusoidally with radius.

From the point of view of animal joint operation, this work can be looked upon as a synthesis of the various features involved in their efficient operation. The synthesis approach was considered to be more logical, and easier, than attempting the analysis of the complete, and very complex, animal joint when operating under natural conditions.

APPENDIX I

REFERENCES

1. Hydrodynamic Lubrication of Soft Solids.
A. Bennett and G.R. Higginson
Journal of Mechanical Engineering Science, Vol. 12 No. 3, 1970.
2. Physiological Lubrication.
C.W. McCutchen
Proceedings I. Mech. E. 1966-67, Volume 181, Part 35.
3. Analysis of Boosted Lubrication in Human Joints.
D. Dowson, A. Unsworth, V. Wright
Journal of Mechanical Engineering Science, Vol. 12 No. 5, 1970.
4. Elastohydrodynamic Squeeze Films Between Two Cylinders in Normal Approach.
K. Herrebrugh, Paper 69 - Lub. - 13.
A.S.M.E. Journal of Lubrication Technology.
5. The Oil Film in a Closing Gap.
H. Christensen
Proc. Royal Society, A Vol. 266, pp.312-338, 1962.
6. The Theoretical Effects of Elastic Deformation of the Bearing Liner on Journal Bearing Performance.
G.R. Higginson, Paper 1. Elastohydrodynamic Lubrication.
Proc. Instn. Mech. Engrs. 1965-66. 180 (Part 3B), 31.
7. The Effect of Elastic Distortions on the Performance of Thin Shell Bearings.
C.J. Hooke, D.K. Brighton, J.P.O'Donoghue
Instn. Mech. Engrs. Nottingham Symposium 20-22nd Sept. 1966, P.87.
8. Squeeze Film Behaviour for Porous Annular Discs.
H. Wu
Journal of Lubrication Technology, Oct. 1970, P.593.
9. Properties of Synovial Fluid.
D.V. Davies
Proc. Instn. Mech. Engrs. 1966-67, Vol. 181, Part 35.
10. Numerical Methods, Vol. II
B. Noble
Oliver and Boyd Ltd., 1964.

11. Generalized Dimensional Analysis and Similarity Analyses.
F.A. Morrison Jr.
Bull. Mech. Eng. Educ. Vol. 8, pp.289-300, 1969.

12. An Optical Interference Method of Measurement of Time-Dependent
Elastohydrodynamic Film Profiles.
D. Dowson and D.A. Jones. Rep. 3 Symp. Exptl. Methods in Tribology.
Proc. Instn. Mech. Engrs. 1967-68. 182 (Part 3G), 49.

13. Physical Characteristics of Articular Cartilage.
J. Edwards
I. Mech. E. Proceedings 1966-67. Vol. 181, Part 35.

14. Boosted Lubrication of Human Joints by Fluid Enrichment and Entrapment.
M.D. Longfield, D. Dowson, P.S. Walker and V. Wright
Bio-Medical Eng. Nov. 1969, P.517.

APPENDIX II

The Computer Programme

The following listing is the computer programme that was used for all the results quoted in this thesis. The language is P.L:1 (Programming Language One) and was run on the Northumbrian Universities Multiple Access Computer (NUMAC), an I.B.M. 360/67 machine.

The programme has been divided into small sections with headings of 'comment cards' to clarify its structure. It is, however, basically two nested 'Do-Loops', the outer one controlling the number of steps taken to calculate the trajectory, the inner one controlling the number of iterations on the pressure matrix for any particular model.

It should be noted that a few internal alterations must be made to the programme to run certain models - e.g. the "Weeping" mechanism.

```

> 1 RN7:PROC OPTIONS(MAIN);
> 2
> 3 /* DECLARATION OF SYMBOLS USED IN PROGRAMME */
> 4 DCL(CONC(300),VOL(300),STORR(3,300),VISC(300),P(3000),VU(300)
> 5 VL(200),KKK(200),S(300),ACCEL(300),TIME(300),ZIZ(300),RAD(
> 6 300),Z(300),DELTA(4),HAT(3000),MAT(3000),Y(300),Q(300),SS(200),
> 7 RR(200),QQ(200),QQQ(200),RRR(200),SSS(200),JJJ(200),TTT(200),
> 8 TT(200))FLOAT;
> 9 DCL(VISCO,AREA1,AREA2,AREA3,FLOW1,FLOW2,ALPH1,ALPH2,MMV,
> 10 SPEED,DVISC,RADIUS,FLOATM,STEP,DATUM,PERM,HALFP,PLOAD,MASS,
> 11 TIM,KK,V,W,T,FL,K3,K4,B,KD,KE,KF,A,H,ALPH3,ALPH4,DUD,H1,
> 12 H2,DIFFP,ALPH5,VV,PIP,DDATUM,DACCEL,DVU,DVL,DPLoad,DPTOT,
> 13 DAPTOT,DFILM,DTIME)FLOAT;
> 14 DCL(ENRICH,GIG,GOG,D,E,CORRM,TOTAL,LENGTH,TZ,II,JJ,NN,X,C,
> 15 L,N,I,J,K,M,AIT1,AIT2)FIXED BIN;
> 16
> 17 /* INPUT OF PHYSICAL PARAMETERS IN C.G.S. UNITS */
> 18 A=1.0E-9; /* FLEXIBILITY OF THIN LAYER */
> 19 MASS=8E3; /* MASS OF TOP SURFACE */
> 20 V=0.25; /* VOID RATIO */
> 21 DATUM=2.5E-2; /* INITIAL SEPARATION */
> 22 RADIUS=30; /* CURVATURE OF SPHERICAL SURFACE */
> 23 T=0.5; /* THICKNESS OF THIN LAYER */
> 24 VISC=15; /* INITIAL VISCOSITY */
> 25 MMV=1; /* RATIO OF ADDITIVE'S VISCOSITY TO BASE VALUE */
> 26 CONC=0.0; /* INITIAL CONCENTRATION */
> 27 DIFFP=1; /* RATIO OF AXIAL PERMEABILITY TO RADIAL */
> 28 PERM=6.25E-6; /* AXIAL PERMEABILITY */
> 29
> 30 /* INTERNAL PROGRAMME CONSTANTS */
> 31 /* BASE VISCOSITY */
> 32 VISCO=VISC(1)/(1+CONC(1))*(MMV-1);

```

```

33 > TIM=1E-4;
34 > ENRICH=0;
35 > AIT1=10;
36 > AIT2=20;
37 > PIP=0.9;
38 > GIG=98;
39 > GOG=112;
40 > H2=16;
41 > H1=8;
42 > M=17;
43 > Y=PERM/V;
44 > H=30;
45 > E=0;
46 > SS=0.0;
47 > RR=0.0;
48 > QQ=0.0;
49 > SSS=0.0;
50 > RRR=0.0;
51 > QQQ=0.0;
52 > KKK=0.0;
53 > ACCEL(1)=-981;
54 > TIME(1)=0.0;
55 > S(1)=DATUM;
56 > VU(1)=0;
57 > W=1;
58 > P=0;
59 > CORR=0;
60 > TOTAL=10*M**2-9*M;
61 > LENGTH=(10*M)-9;
62 > FL=LENGTH;
63 > X=1;
64 >

```

```

65 PLOAD=0;
66 VL=0;
67 FLOATM=M;
68 STEP=RADIUS/(60*(FLOATM-1));
69 DO N=1 TO LENGTH-1;
70   B=N;
71   RAD(N)=(1-(B-1)/(FL-1))*RADIUS/6;
72   Z(N)=DATUM+((RAD(N)**2)/(2*RADIUS));
73 END;
74
75 /* PRINTOUT OF INPUT DATA AND PROGRAMME CONSTANTS */
76 PUT SKIP DATA(PERM,RADIUS,MASS,DATUM,A,V,T,MMV,
77 CONC(1),VISCO,VISC(1),DIFFP);
78 PUT SKIP;
79 PUT SKIP;
80 PUT SKIP DATA(M,W,TOTAL,LENGTH,STEP,TIM,ENRICH,Y,HL,
81 H2,H,GIG,GOG,PIP,AIT1,AIT2);
82 PUT SKIP;
83
84 /* PRINTOUT OF HEADINGS */
85 PUT SKIP EDIT('TRAJECTORY RESULTS')(X(30),A(19));
86 PUT SKIP;
87 PUT SKIP EDIT('X','DATUM','ACCEL','VU(X)','VL(X)CENTRE',
88 'PLOAD','CENTRE PRESS','CENTRE DEFN','CENTRE FILM','TIME')
89 (X(2),A(2),X(3),A(12),A(12),A(12),A(12),A(12),A(12),
90 A(12),A(12),A(12));
91 PUT SKIP;
92 PUT SKIP EDIT(X,DATUM,ACCEL(X),VU(X),VL(X),PLOAD,P(TOTAL-M+1),
93 A*P(TOTAL-M+1),DATUM+A*P(TOTAL-M+1),TIME(X))(X(2),F(2),
94 E(12,4),E(12,4),E(12,4),E(12,4),E(12,4),E(12,4),
95 E(12,4),E(12,4));
96 PUT SKIP;

```



```

129 > Y=PERM/V;
130 > IF (CONC(1)>10**8) THEN ENRICH=1;
131 > H=H2;
132 > END;
133 > PINK:IF (X>(GOG-1)) THEN TIM=(S(X)-S(X-1))/(VU(X-1)+SPEED/2);
134 >
135 > /* RATE OF DEFORMATION FOR PART 'A' */
136 > IF X=2 THEN KK=2*A/TIM;
137 > IF X=3 THEN DO;
138 > KK=3*A/(2*TIM);
139 > DO N=2 TO LENGTH;
140 > KKK(N)=2*A*RRR(N)/TIM;
141 > JJJ(N)=2*A*RR(N)/TIM;
142 > END;
143 > END;
144 > IF X=4 THEN DO;
145 > KK=3*A/TIM;
146 > DO N=2 TO LENGTH;
147 > KKK(N)=2*A*QQ(N)/TIM;
148 > JJJ(N)=2*A*QQ(N)/TIM;
149 > END;
150 > END;
151 > IF ((X>4)&(X<GOG)) THEN DO;
152 > KK=54*A/(70*TIM);
153 > DO N=2 TO LENGTH;
154 > KKK(N)=A*(27*RRR(N)+40*QQ(N)+13*TTT(N)-26*SSS(N))/(70*TIM);
155 > JJJ(N)=A*(27*RRR(N)+40*QQ(N)+13*TT(N)-26*SS(N))/(70*TIM);
156 > END;
157 > END;
158 > /* RATE OF DEFORMATION FOR 'PART 'B' */
159 > IF X>GOG THEN DO;
160 >

```

```

161 > KK=A/TIM;
162 > IF CORR=0 THEN DO;
163 > DO N=2 TO LENGTH;
164 > KKK(N)=A*TT(N)/TIM;
165 > JJJ(N)=A*TT(N)/TIM;
166 > END;
167 > END;
168 > IF CORR=1 THEN DO;
169 > DO N=2 TO LENGTH;
170 > KKK(N)=KKK(N)*(DATUM-S(X-1))/(S(X)-S(X-1));
171 > JJJ(N)=JJJ(N)*(DATUM-S(X-1))/(S(X)-S(X-1));
172 > END;
173 > END;
174 > END;
175 > GREEN:
176 >
177 > /* *****ENRICHMENT CALCULATIONS***** */
178 > /* CONCENTRATION AT CENTRE OF FILM */
179 > IF (ENRICH=1)&(CORR=0) THEN DO;
180 > J=LENGTH;
181 > AREA3=3.14159*(STEP/2)*(DATUM+Z(J-1)+A*(P((J-1)*M+1)+
182 > P((J-2)*M+1)));
183 > FLOW2=-Y(J)*(V*T-A*P((J-1)*M+1))*(P((J-1)*M+1)-P((J-1)*M+2))/
184 > ((T-A*P((J-1)*M+1))*(STEP-A*P((J-1)*M+1)/(M-1))*VISCO);
185 > AREA2=(3.14159*STEP**2)/4;
186 > VOL(J)=AREA2*(3*DATUM+3*A*P((J-1)*M+1)+Z(J-1)+A*P((J-2)*M+1))/4;
187 > STORR(1,J)=CONC(J);
188 > STORR(3,J)=AREA2*(VU(X-1)-VL(J));
189 > STORR(2,J)=(AREA2*FLOW2*(1+CONC(J-1)/CONC(J))+STORR(3,J)*
190 > (1-CONC(J-1)/CONC(J)))/2;
191 > CONC(J)=STORR(1,J)*(1-TIM*STORR(2,J))/(VOL(J)+TIM*STORR(3,J));
192 > FLOW1=(STORR(2,J)-STORR(3,J))/AREA3;

```

```

193 > IF (CONC(J)>1.0) THEN DO;
194 > CONC(J)=1;
195 > PUT EDIT(J)(F(4));
196 > END;
197 > VISC(J)=VISCO*(1+CONC(J)*(MMV-1));
198 > Y(J)=PERM*(1-CONC(J))/(V*(1-CONC(1)));
199 > IF (CONC(J)<CONC(1)) THEN Y(J)=Y(1);
200 >
201 > /* CONCENTRATION OVER REST OF FILM */
202 > DO J=(LENGTH-1) BY -1 TO 2;
203 > AREA1=AREA3;
204 > FLOW2=-Y(J)*(V*T-A*P((J-1)*M+1))*(P((J-1)*M+1)-P((J-1)*M+2))/
205 > ((T-A*P((J-1)*M+1))*(STEP-A*P((J-1)*M+1))/(M-1))*VISCO);
206 > AREA2=2*3.14159*RAD(J)*STEP;
207 > VOL(J)=AREA2*(Z(J)+A*P((J-1)*M+1));
208 > STORR(1,J)=CONC(J);
209 > STORR(3,J)=AREA2*(VU(X-1)-VL(J));
210 > STORR(2,J)=(AREA2*FLOW2*(1+CONC(J-1))/CONC(J))+FLOW1*AREA1*
211 > (CONC(J-1)-STORR(1,J+1))/CONC(J)+STORR(3,J)*(1-CONC(J-1)/
212 > CONC(J))/2;
213 > CONC(J)=STORR(1,J)*(1-TIM*STORR(2,J))/(VOL(J)+TIM*STORR(3,J));
214 > AREA3=3.14159*(RAD(J)+STEP/2)*(Z(J)+Z(J-1)+A*(P((J-1)*M+1)
215 > +P((J-2)*M+1)));
216 > FLOW1=(FLOW2*AREA2+FLOW1*AREA1-STORR(3,J))/AREA3;
217 > IF (CONC(J)>1.0) THEN DO;
218 > CONC(J)=1;
219 > PUT EDIT(J)(F(4));
220 > END;
221 > VISC(J)=VISCO*(1+CONC(J)*(MMV-1));
222 > Y(J)=PERM*(1-CONC(J))/(V*(1-CONC(1)));
223 > IF (CONC(J)<CONC(1)) THEN Y(J)=Y(1);
224 > END;

```

```

225 > END;
226 >
227 > /* ADJUSTMENTS TO CONCENTRATION IN PART 'B' IF
228 > ACCELERATION IS INACCURATE */
229 > IF (ENRICH=1)&(CORRN=1) THEN DO;
230 >   DO J=2 TO LENGTH;
231 >     CONC(J)=STORR(1,J)*(1-TIM*STORR(2,J))/(VOL(J)+TIM*STORR(3,J));
232 >   IF (CONC(J)>1.0) THEN DO;
233 >     CONC(J)=1;
234 >     PUT EDIT(J)(F(4));
235 >   END;
236 >   VISC(J)=VISCO*(1+CONC(J)*(MMV-1));
237 >   Y(J)=PERM*(1-CONC(J))/(V*(1-CONC(1)));
238 >   IF (CONC(J)<CONC(1)) THEN Y(J)=Y(1);
239 > END;
240 > END;
241 > DATUM=S(X);
242 > DO N=1 TO LENGTH-1;
243 >   Z(N)=DATUM+((RAD(N)**2)/(2*RADIUS));
244 > END;
245 >
246 > /* ZERO-ISING OF RATE OF DEFORMATION AT CHANGEOVER
247 > FROM PART 'A' TO PART 'B' */
248 > IF (X=GOG) THEN DO;
249 >   JJJ=0;
250 >   KKK=0;
251 >   KKK=0;
252 > END;
253 >
254 > /* RELAXATION SOLUTION OF PRESSURE MATRIX AND FIRST
255 > INTEGRATION OF REYNOLDS' EQUATION */
256 > DO C=1 TO H;

```

```

257 D=0;
258
259 /* FIRST COLUMN OF NODES */
260 DO J=2 TO (M-1);
261   P(J)=P(J)-(W/4)*(4*P(J)-P(J-1)-P(J+1)-2*P(J+M));
262 END;
263 P(M)=P(M)-(W/2)*(2*P(M)-P(M-1)-P(M+M));
264 K=0;
265 I=1;
266 DO J=(M+1) TO (TOTAL-M);
267   K=K+1;
268   IF (K=1) THEN DO;
269     I=I+1;
270
271 /* REYNOLDS' INTEGRATION BY RUNGE-KUTTA */
272 DELTA(1)=(-6*STEP*RAD(I-1)*VISC(I-1)/(Z(I-1)+A*P(J-M))**3)*(
273 (VU(X)-KKK(I-1)+KK*P(J-M)+E*VL(I-1)+(Y(I-1)/VISCO)*
274 (V*T-A*P(J-M))*(P(J-M)-P(J-M+1))
275 /((T-A*P(J-M))*(STEP-A*P(J-M)/(M-1)))));
276 HALFP=P(J-M)+DELTA(1)/2;
277 DELTA(2)=(-STEP*6*(RAD(I-1)-STEP/2)*((VISC(I-1)+VISC(1))/2)/((
278 DATUM+((RAD(I-1)-STEP/2)**2)/(2*RADIUS))+A*HALFP)**3))*((VU(X)
279 -JJJ(I)+KK*HALFP)+
280 ((Y(I-1)+Y(I))/(2*VISCO))*(V*T-A*HALFP)*
281 (HALFP-P(J-M+1)/2-P(J+1)/2)/((T-A*HALFP)*(STEP-A*HALFP
282 / (M-1))));
283 HALFP=P(J-M)+DELTA(2)/2;
284 DELTA(3)=(-STEP*6*(RAD(I-1)-STEP/2)*((VISC(I-1)+VISC(1))/2)/((
285 DATUM+((RAD(I-1)-STEP/2)**2)/(2*RADIUS))+A*HALFP)**3))*((VU(X)
286 -JJJ(I)+KK*HALFP)+
287 ((Y(I-1)+Y(I))/(2*VISCO))*(V*T-A*HALFP)*
288 (HALFP-P(J-M+1)/2-P(J+1)/2)/((T-A*HALFP)*(STEP-A*HALFP

```

```

289 > / (M-1));
290 > HALFPP=P(J-M)+DELTA(3);
291 > DELTA(4)=(-STEP*6*RAD(1)*VISC(1)/((Z(1)+A*HALFP)**3))*(
292 > (VU(X)-KKK(1)+KK*HALFP+E*VL(1))+Y(1)/VISCO)*
293 > (V*T-A*HALFP)*(HALFP-P(J+1))/((T-A*HALFP)*(STEP-A*HALFP
294 > / (M-1)));
295 >
296 > /* INSTABILITY SUPPRESSION OF RUNGE-KUTTA INTEGRATION */
297 > IF((DELTA(1)<0)|(DELTA(2)<0)|(DELTA(3)<0)) THEN D=1;
298 > IF (DELTA(4)<0) THEN D=1;
299 > IF ((D=0)&(DELTA(3)>3*DELTA(2))) THEN DELTA(3)=3*DELTA(2);
300 > IF ((D=0)&(DELTA(4)>3*DELTA(2))) THEN DELTA(4)=3*DELTA(2);
301 > IF ((D=0)&(DELTA(1)>3*DELTA(2))) THEN DELTA(1)=3*DELTA(2);
302 > IF D=1 THEN DO;
303 > ALPH1=Y(1)*(V*T-A*P(J-M))/((T-A*P(J-M))*(STEP-A*P(J-M))
304 > / (M-1))*VISCO);
305 > P(J)=((P(J+1)*ALPH1)-VU(X)+KKK(1)-VL(1)*E)/(KK+ALPH1);
306 > P(J-M)=(2*P(J-M)+P(J)+P(J-2*M))/4;
307 > END;
308 > ELSE DO;
309 > P(J)=P(J-M)+(DELTA(1)+2*DELTA(2)+2*DELTA(3)+DELTA(4))/6;
310 > END;
311 > GOTO ZED;
312 > END;
313 >
314 > /* PRESSURE AT FIRST LAYER OF NODES UNDER THE SURFACE */
315 > IF (K=2) THEN DO;
316 > KD=1/RAD(1)-A*(P(J-1-M)-P(J-1))*(1-V)*T/(STEP*(V*T-A*P(J-1)
317 > )*(T-A*P(J-1)));
318 > IF PERM<10**-20 THEN ALPH5=0.0; ELSE
319 > ALPH5=DIFFPP*VISCO*(STEP**2)*(KKK(1)-KK*P(J-1))/(T*PERM);
320 > ALPH4=DIFFPP*(STEP**2)*(1-COINC(1))/(2-COINC(1)-CONC(1))*

```

```

321 > ((STEP-A*P(J-1))/(M-1))**2));
322 > ALPH3=2*ALPH4*(1-CONC(1))/(1-CONC(1));
323 > P(J)=(P(J-M)*(1+KD*STEP/2)+P(J+M)*(1-KD*STEP/2)+2*P(J+1)*
324 > ALPH4+ALPH3*P(J-1)-ALPH5)/(2+ALPH3+2*ALPH4);
325 > ALPH4=DIFFP*(STEP**2)/((STEP-A*P(J-1))/(M-1))**2);
326 > GOTO ZED;
327 > END;
328 >
329 > /* PRESSURE AT BASE OF THIN LAYER */
330 > IF (K=M) THEN DO;
331 > K=0;
332 > P(J)=(P(J-M)*(1+KD*STEP/2)+P(J+M)*(1-KD*STEP/2)+2*P(J-1)
333 > *ALPH4-ALPH5)/(2+2*ALPH4);
334 > GOTO ZED;
335 > END;
336 >
337 > /* PRESSURE AT OTHER NODES */
338 > P(J)=(P(J-M)*(1+KD*STEP/2)+P(J+M)*(1-KD*STEP/2)+ALPH4*(P(J+1)
339 > +P(J-1))-ALPH5)/(2+2*ALPH4);
340 > ZED:END;
341 >
342 > /* CENTRE LINE CALCULATIONS */
343 > J=TOTAL-M+1;
344 >
345 > I=I+1;
346 >
347 > /* FILM PRESSURE */
348 > ALPH1=Y(I)*(V*T-A*P(J-M))/(T-A*P(J-M))*(STEP-A*P(J-M)
349 > / (M-1))*VISCO);
350 > ALPH2=3*(STEP**2)*VISC(I)/((DATUM+A*P(J-M))**3);
351 > P(J)=(P(J-M)-ALPH2*(VU(X)-KKK(I)+VL(I)*E-ALPH1*P(J+1)))/
352 > (1+ALPH2*(ALPH1+KK));
IF (P(J)<P(J-M)) THEN DO;

```

```

353 P(J)=(P(J+1)*ALPH1)-VU(X)+KKK(I)-VL(I)*E)/(KK+ALPH1);
354 P(J-M)=(2*P(J-M)+P(J)+P(J-2*M))/4;
355 END;
356
357 /* PRESSURE AT FIRST NODE UNDER SURFACE */
358 J=TOTAL-M+2;
359 IF PERM<10**20 THEN ALPH5=0.0; ELSE
360 ALPH5=DIFFP*VISCO*(STEP**2)*(KKK(I)-KK*P(J-1))/(T*PERM);
361 ALPH4=DIFFP*(STEP**2)*(1-CONC(I))/(2-CONC(I))*
362 ((STEP-A*P(J-1))/(M-1)**2));
363 ALPH3=ALPH4*(1-CONC(I))/(1-CONC(I));
364 P(J)=(2*P(J-M)+ALPH3*P(J-1)+ALPH4*P(J+1)-ALPH5)/(2+
365 ALPH3+ALPH4);
366 ALPH4=DIFFP*(STEP**2)/((STEP-A*P(J-1))/(M-1)**2);
367
368 /* PRESSURE AT REST OF NODES */
369 DO J=(TOTAL-M+3) TO (TOTAL-1);
370 P(J)=(4*P(J-M)+ALPH4*(P(J-1)+P(J+1))-ALPH5)/(4+2*ALPH4);
371 END;
372
373 /* PRESSURE AT BASE */
374 J=TOTAL;
375 P(J)=(4*P(J-M)+2*ALPH4*P(J-1)-ALPH5)/(4+2*ALPH4);
376 GOTO ZIP;
377 CHANGE:L=J;
378 PUT SKIP EDIT('EXCESSIVE DEFORMATIONS')(X(10),A(24));
379 GOTO FINN;
380
381 /* AITKENS D-SQUARED CONVERGENCE FOR WHOLE MATRIX */
382 ZIP:IF ((C=(AIT1-2))|(C=(AIT2-2))) THEN DO;
383 DO J=2 TO TOTAL;
384 MAT(J)=P(J);

```

```

385 > END;
386 > END;
387 > IF ((C=(AIT1-1)|(C=(AIT2-1))) THEN DO;
388 > DO J=2 TO TOTAL;
389 > HAT(J)=P(J);
390 > END;
391 > END;
392 > IF ((C=AIT1)|(C=AIT2)) THEN DO;
393 > ON ZERODIVIDE BEGIN;
394 > PUT LIST('BUZZ');
395 > END;
396 > TZ=1;
397 > DO J=2 TO TOTAL;
398 > TZ=TZ+1;
399 > IF (TZ=(M+1)) THEN DO;
400 > TZ=1;
401 > GOTO FIZZ;
402 > END;
403 > IF ((HAT(J))>(P(J)*(1-10**--5))&((HAT(J))<(P(J)*(1+10**--5))))
404 > THEN GOTO FIZZ;
405 > MAT(J)=(HAT(J)-MAT(J))/(P(J)-HAT(J));
406 > IF (MAT(J)>1.021) THEN MAT(J)=2/(MAT(J)-0.979);
407 > /* 'CONVERGENCE FACTOR' */
408 > ELSE MAT(J)=47.619;
409 > P(J)=P(J)+MAT(J)*(P(J)-HAT(J));
410 > FIZZ:END;
411 > END;
412 > IF C>18 THEN DO;
413 > DO N=(TOTAL-M+2) BY 2 TO TOTAL;
414 > PUT LIST(P(N));
415 > END;
416 > END;

```

```

417 > END;
418 > ZZZ:
419 >
420 > /* INTEGRATION OF FILM PRESSURES TO FIND 'F' */
421 >   II=1;
422 >   JJ=1;
423 >   PLOAD=0;
424 >   DO NN=(M+1) BY M TO (TOTAL-2*M+1);
425 >     II=II+1;
426 >     JJ=JJ+1;
427 >     IF (JJ=2) THEN DO;
428 >       JJ=0;
429 >       PLOAD=PLOAD+4*P(NN)*RAD(II);
430 >     END;
431 >     IF (JJ=1) THEN PLOAD=PLOAD+2*P(NN)*RAD(II);
432 >     END;
433 >   PLOAD=PLOAD*STEP*2.0944E+00;
434 >   ACCEL(X)=PLOAD/MASS-981;
435 >
436 > /* PREDICTOR-CORRECTOR TREATMENT OF TRAJECTORY FOR PART 'A' */
437 > IF ((X>5)&(X<GOG)) THEN DO;
438 >   VV=VU(X-1)+(TIM/24)*(9*ACCEL(X)+19*ACCEL(X-1)-5*ACCEL(X-2)+
439 >   ACCEL(X-3));
440 >   PUT SKIP DATA(VV);
441 >   S(X)=S(X-1)+(TIM/2)*(VU(X-1)+VV)+(TIM**2/12)*(
442 >   ACCEL(X-1)-ACCEL(X));
443 >   IF ((1-VV/VU(X))<0.010)&((1-VV/VU(X))>>-0.010) THEN DO;
444 >     VU(X)=VV;
445 >     GOTO BROWN;
446 >   END;
447 >   ELSE DO;
448 >     VU(X)=VV;

```

```

449 > GOTO GREEN;
450 > END;
451 > END;
452 >
453 > /* DISPLACEMENT CORRECTION FOR PART 'B' */
454 > IF (X>(GOG-1)) THEN DO;
455 > IF ((ACCEL(X))>(ZIZ(X)+9)) | ((ACCEL(X))<(ZIZ(X)-9)) THEN DO;
456 > PUT SKIP EDIT(A*P(TOTAL-M+1),S(X),ACCEL(X))(X(11),E(12,4),
457 > E(12,4),E(12,4));
458 > S(X)=S(X)+PIP*(S(X)+A*P(TOTAL-M+1))*(ACCEL(X)-ZIZ(X))/(981+
459 > ZIZ(X));
460 > CORR=1;
461 > GOTO PINK;
462 > END;
463 > TIME(X)=TIME(X-1)+(S(X)-S(X-1))/(VU(X-1)+SPEED/2);
464 > END;
465 > BROWN:
466 >
467 >
468 > /* LEAST-SQUARES TREATMENT OF FILM PRESSURES FOR RATES OF
469 > DEFORMATION -PART 'A' ONLY */
470 > IF X=2 THEN DO;
471 > DO N=2 TO LENGTH;
472 > SSS(N)=0;
473 > SS(N)=0.0;
474 > RRR(N)=P(M*(N-1)+1);
475 > IF N=2 THEN RR(N)=(6*P(M+1)-P(2*M+1))/8;
476 > IF N=LENGTH THEN RR(N)=0.0;
477 > ELSE RR(N)=(9*(P(M*(N-1)+1)+P(M*(N-2)+1))-P(M*(N-3)+1)-
478 > P(M*N+1))/16;
479 > END;
480 > END;
481 > IF X=3 THEN DO;

```

```

481 > DO N=2 TO LENGTH;
482 > QQ(N)=P(M*(N-1)+1);
483 > IF N=LENGTH THEN QQ(N)=0.;
484 > IF N=2 THEN QQ(N)=(6*P(M+1)-P(2*M+1))/8;
485 > ELSE QQ(N)=(9*(P(M*(N-1)+1)+P(M*(N-2)+1))-P(M*(N-3)+1))-
486 > P(M*N+1))/16;
487 > END;
488 > END;
489 > IF X=4 THEN DO;
490 > DO N=2 TO LENGTH;
491 > TTT(N)=P(M*(N-1)+1);
492 > IF N=LENGTH THEN TT(N)=0;
493 > IF N=2 THEN TT(N)=(6*P(M+1)-P(2*M+1))/8;
494 > ELSE TT(N)=(9*(P(M*(N-1)+1)+P(M*(N-2)+1))-P(M*(N-3)+1))-
495 > P(M*N+1))/16;
496 > END;
497 > END;
498 > IF X>4 THEN DO;
499 > DO N=2 TO LENGTH;
500 > SSS(N)=RRR(N);
501 > RRR(N)=QQQ(N);
502 > SS(N)=RR(N);
503 > RR(N)=QQ(N);
504 > QQQ(N)=TTT(N);
505 > QQ(N)=TT(N);
506 > IF N=LENGTH THEN TT(N)=0;
507 > IF N=2 THEN TT(N)=(6*P(M+1)-P(2*M+1))/8;
508 > ELSE TT(N)=(9*(P(M*(N-1)+1)+P(M*(N-2)+1))-P(M*(N-3)+1))-
509 > P(M*N+1))/16;
510 > TTT(N)=P(M*(N-1)+1);
511 > END;
512 > END;

```

```

513 > /* VELOCITY OF DEFORMATION THROUGH THE FILM */
514 > DO N=2 TO LENGTH;
515 > VL(N)=KKK(N)-KK*P(M*(N-1)+1);
516 > END;
517 > CORR=0;
518 >
519 >
520 > /* PRINTOUT OF TRAJECTORY PARAMETERS IN C.G.S. UNITS */
521 > PUT SKIP EDIT(X,DATUM,ACCEL(X),VU(X),VL(LENGTH),PLOAD,
522 > P(TOTAL-M+1),
523 > A*P(TOTAL-M+1),DATUM+A*P(TOTAL-M+1),TIME(X))(F(4),
524 > E(12,4),E(12,4),E(12,4),E(12,4),E(12,4),E(12,4),
525 > E(12,4),E(12,4));
526 >
527 > /* NON-DIMENSIONAL PARAMETERS */
528 > DDATUM=DATUM/(2.5*10**-2);
529 > DACCEL=ACCEL(X)*(VISC(1)**2)*(RADIUS**4)/((2.5*10**-2)*
530 > ((MASS*981)**2));
531 > DVU=VU(X)*(RADIUS**2)*VISC(1)/((2.5*10**-2)*(MASS*981));
532 > DVL=VL(LENGTH)*DVU/VU(X);
533 > DPLOAD=PLOAD/(MASS*981);
534 > DPOT=P(TOTAL-M+1)*(RADIUS**2)/(MASS*981);
535 > DAPTOT=A*P(TOTAL-M+1)/(2.5*10**-2);
536 > DFILM=DAPTOT+DDATUM;
537 > DTIME=TIME(X)*(MASS*981)/(VISC(1)*(RADIUS**2));
538 >
539 > /* PRINTOUT OF NON-DIMENSIONAL PARAMETERS OF TRAJECTORY */
540 > PUT SKIP EDIT(X,DDATUM,DACCEL,DVU,DVL,DPLOAD,DPTOT,DAPTOT,
541 > DFILM,DTIME)(F(4),
542 > E(12,4),E(12,4),E(12,4),E(12,4),E(12,4),E(12,4),
543 > E(12,4),E(12,4));

```

```

> 544
> 545
> 546
> 547
> 548
> 549
> 550
> 551
> 552
> 553
> 554
> 555
> 556
> 557
> 558

/* PRINTOUT OF PRESSURES ALONG FILM */
  PUT SKIP EDIT(P(TOTAL-M+1),P(TOTAL-5*M+1),P(TOTAL-9*M+1),
P(TOTAL-13*M+1),P(TOTAL-17*M+1),P(TOTAL-21*M+1),
P(TOTAL-25*M+1),P(TOTAL-29*M+1))(E(12,4),
E(12,4),E(12,4),E(12,4),E(12,4),E(12,4),E(12,4),E(12,4));
  PUT SKIP EDIT(P(TOTAL-33*M+1),P(TOTAL-37*M+1),P(TOTAL-41*M+1),
P(TOTAL-45*M+1),P(TOTAL-49*M+1),P(TOTAL-53*M+1),
P(TOTAL-57*M+1),P(TOTAL-61*M+1))(E(12,4),
E(12,4),E(12,4),E(12,4),E(12,4),E(12,4),E(12,4),E(12,4));
  DO J=LENGTH BY -4 TO (LENGTH-32);
  PUT EDIT(VISC(J))(E(12,4));
END;
FINN:END;
END RN7;

```

APPENDIX III

A Finite Element Approach to Laminar Fluid Flow

by

R. Norman

SUMMARY

A finite element method for the solution of problems involving laminar isoviscous flow between rigid boundaries is presented using a minimization principle. Results of some simple flow situations are calculated to illustrate convergence of the method to the exact solution. It is shown that knowledge of the downstream boundary condition in the case of a rigid cylinder rotating against a rigid plate is not necessary for the calculation of its pressure distribution.

INTRODUCTION

In both Structural and Fluid Mechanics, traditional methods of solution have relied on the development of general governing differential equations which have then to be solved, usually numerically and often with awkward boundary conditions.

The great success of finite element methods in structural mechanics avoiding such differential equations suggests that similar success may be obtainable in fluid mechanics, reference (1). This paper describes the development of such a method and, it is hoped, points the way to a new approach to other hydrodynamic problems.

DEVELOPMENT OF THE METHOD

In deriving the following equations, three assumptions, all consistent with the simple derivation of Reynolds Equation in one dimension, are made:-

1. The flow is laminar and unidirectional,
2. The fluid is isoviscous,
3. The boundaries of the system are rigid.

An obvious choice for a finite element for thin film flow is shown in fig. (1). The top and bottom of the element are the boundaries of the system, the vertical sides are arbitrary bounds and the element is of unit width (at right angles to the paper). The two boundary velocities are considered parallel to each other and the pressure constant across the thickness of the film.

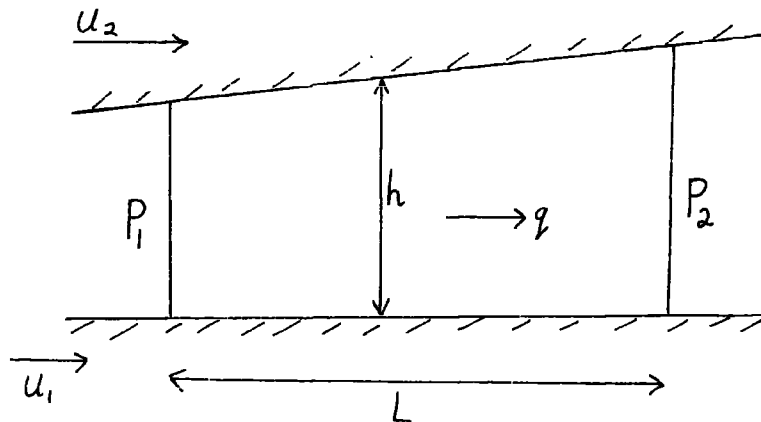


FIG. (1)

The first step is to define a function, minimization of which, over the whole system, with respect to the pressures at interelement faces will

yield the correct pressure distribution, i.e. one that satisfies Reynolds Equation in one dimension.

$$\text{Such a function is } \psi = \int_{\substack{\text{whole} \\ \text{system}}} \left[\frac{h^3}{12\eta} \cdot \left(\frac{dP}{dx} \right)^2 - h \cdot (U_1 + U_2) \cdot \left(\frac{dP}{dx} \right) \right] dx \quad (1)$$

A full justification of this function can be found in Reference (2).

This function can be approximated as:-

$$\psi = \sum_{\substack{\text{over all} \\ \text{the elements}}} \int_0^L \left[\frac{h^3}{12\eta} \left(\frac{dP}{dx} \right)^2 - h \cdot (U_1 + U_2) \cdot \left(\frac{dP}{dx} \right) \right] dx \quad (2)$$

Since $q = \frac{h(U_1 + U_2)}{2} - \frac{h^3}{12\eta} \cdot \left(\frac{dP}{dx} \right)$ we can rewrite (2) as

$$\begin{aligned} \psi &= \sum_{\substack{\text{over all} \\ \text{the elements}}} \int_0^L \left[-\frac{h(U_1 + U_2)}{2} \cdot \left(\frac{dP}{dx} \right) - q \cdot \left(\frac{dP}{dx} \right) \right] dx \\ &= \sum_{\substack{\text{over all} \\ \text{the elements}}} \left\{ \frac{-(U_1 + U_2)}{2} \left[h_1 \cdot (P_2 - P_1) + \alpha \int_0^L x \cdot \left(\frac{dP}{dx} \right) \cdot dx \right] - q(P_2 - P_1) \right\} \end{aligned} \quad (4)$$

where $h = h_1 + \alpha x$ and $\alpha = \frac{h_2 - h_1}{L}$

The integral in (4) can be evaluated by substituting a polynomial in x for the pressure distribution through the element,

$$P = a_1 + a_2 x + a_3 x^2 \quad (5)$$

Since we want to describe the element completely in terms of P_1 and P_2 we must reduce the three unknowns in (5) to two.

This can be done by imposing a continuity condition on the element of zero nett flow into the element,

$$\int_0^{h_1} U \, dx = \int_0^{h_2} U \, dx \quad (6)$$

These integrals are evaluated by using

$$U = \frac{(z^2 - hz)}{2\eta} \cdot \left(\frac{dP}{dx} \right) + \frac{(U_2 - U_1)}{h} \cdot z + U_1$$

$$\text{and } \frac{dP}{dx} = a_2 + 2a_3x \text{ from (5)}$$

Equation (6) gives us the relation

$$a_3 = \frac{h_1^3 - h_2^3}{2L h_2^3} a_2 + \frac{3\eta (U_1 + U_2)(h_2 - h_1)}{L h_2^3} = a_2 F + G \text{ say}$$

Whence

$$\psi = \sum \left\{ \begin{array}{l} -(U_1 + U_2) \\ \frac{2}{\text{over all}} \\ \text{the elements} \end{array} \left[(h_2 P_2 - h_1 P_1) - (h_2 - h_1) \left[a_1 + a_2 \left(\frac{L}{2} + \frac{L^2 F}{3} \right) + \frac{GL^3}{3} \right] - q (P_2 - P_1) \right] \right\}$$

Now since

$$\begin{Bmatrix} a_1 \\ a_2 \end{Bmatrix} = \begin{bmatrix} 1 & 0 \\ \frac{-1}{L + L^2 F} & \frac{1}{L + L^2 F} \end{bmatrix} \begin{Bmatrix} P_1 \\ P_2 \end{Bmatrix} + \begin{Bmatrix} 0 \\ -L^2 G \end{Bmatrix}$$

and $q = \int_0^{h_1} U \, dx$ with little error,

we have ψ explicitly as a function of the pressures at the inter-element faces through the system. Minimization of ψ with respect to these pressures will yield the pressure distribution through the system,

$$\text{i.e. we say } \left\{ \frac{\partial \psi}{\partial P_i} \right\} = 0 \quad (7)$$

$i \rightarrow 1$ to $n + 1$ say for n elements in a system.

$$\text{Now } \left\{ \frac{\partial \psi}{\partial P_i} \right\} = \frac{h_i^3 h_{i+1}^3}{3(h_i^3 + h_{i+1}^3) \eta L_i} \begin{bmatrix} +1, & -1 \end{bmatrix} \begin{Bmatrix} P_i \\ P_{i+1} \end{Bmatrix} + \frac{(U_1 + U_2)}{6(h_i^3 + h_{i+1}^3)}$$

$$\begin{bmatrix} 5 h_i^3 h_{i+1} + h_i^4 + h_{i+1}^4 + 5 h_i h_{i+1}^3 \end{bmatrix} + \frac{h_{i-1}^3 h_i^3}{3(h_{i-1}^3 + h_i^3) \eta L_{i-1}}$$

$$\begin{bmatrix} -1, & +1 \end{bmatrix} \begin{Bmatrix} P_{i-1} \\ P_i \end{Bmatrix} - \frac{(U_1 + U_2)}{6(h_{i-1}^3 + h_i^3)} \begin{bmatrix} 5 h_{i-1}^3 h_i + h_{i-1}^4 \\ + h_i^4 + 5 h_{i-1} h_i^3 \end{bmatrix}$$

$$\left(\text{Note: } \frac{d^2 \psi}{dp^2} \text{ is +ve} \right)$$

since only the $(i - 1)$ th and the (i) th elements contribute terms in P_i to ψ (see fig. (2))

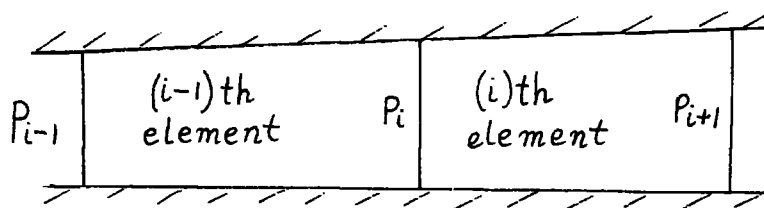
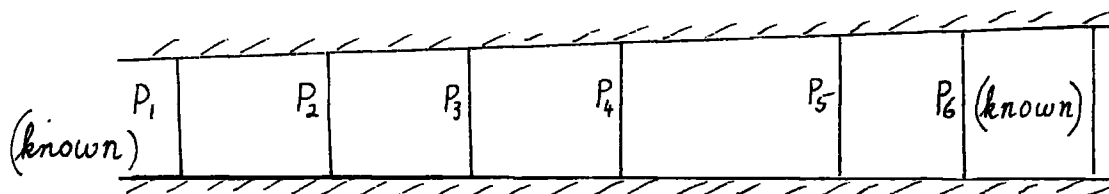


FIG. (2).



In a typical lubrication problem, say with 5 elements, equation (7) takes the form

$$\left\{ \frac{\partial \psi}{\partial P_i} \right\} = 0 = \begin{bmatrix} * & * & & & & & \\ * & * & * & & & & \\ & * & * & * & & & \\ & & * & * & * & & \\ & & & * & * & * & \\ & & & & * & * & * \\ & & & & & * & * \end{bmatrix} \begin{Bmatrix} P_1 \\ P_2 \\ P_3 \\ P_4 \\ P_5 \\ P_6 \end{Bmatrix} + \begin{Bmatrix} * \\ * \\ * \\ * \\ * \\ * \end{Bmatrix} \quad (8)$$

$i \rightarrow 1 \text{ to } 6$

where * indicates a term independent of P_i (a constant). Normally the first and last pressures ($P_{(1)}$ and $P_{(6)}$ in equation (8)) are known and so equation (8) would be solved from line (2) to line (5) inclusive to yield $P_{(2)}$ to $P_{(5)}$.

Once assembled, this matrix equation is easily solved by digital computer and, in itself, should present few computational problems. With the narrowness of its band (note that the matrix is

symmetric), a large number of elements can be used if desired. The diagonal term is not dominant however and the speed of convergence of iterative solutions to matrix equations is dependent on this dominance.

CONVERGENCE OF THE METHOD

Three simple situations were solved by Gauss-Seidel iterative procedures for their pressure distributions and convergence of the method with increasing number of elements used is presented in tabular form.

CASE 1. LAMINAR FLOW THROUGH A NOZZLE

Using Reynold's Equation in its one-dimensional form, the pressure mid-way through the nozzle, P_M was found to be 1.741 units.

<u>Number of Elements Used</u>	<u>Error as % of $P_M - P_{OUT}$</u>
1	- 6.25
2	+ 1.89
4	+ 0.57
8	+ 0.15

Dimensions

length	=	5 cms
h_1	=	0.5 cms
h_2	=	0.25 cms
P_{IN}	=	2 units
P_{OUT}	=	1 unit

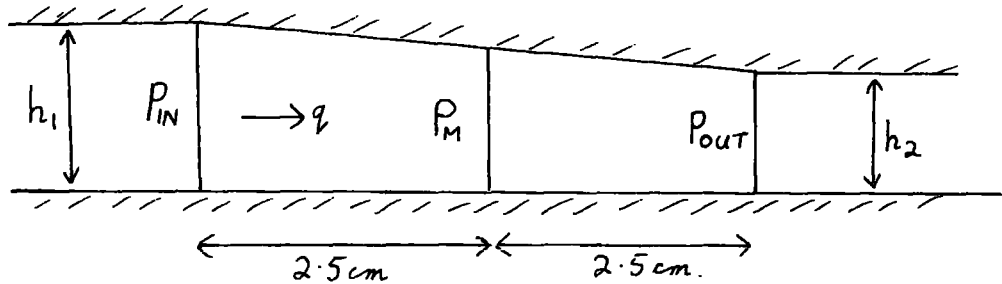


FIG. (3), CASE 1.

CASE 2. A SIMPLE TILTING-PAD BEARING

Reynolds Equation gave the maximum pressure as 2.5×10^7 dynes/cm² at 3.33 cms from the inlet.

<u>Number of Elements Used</u>	<u>% Error in Max^m Press.</u>	<u>% Error in Posⁿ of Max^m Pressure</u>
1	-33.33	-25.00
2	+10.68	- 7.05
4	+ 3.25	- 0.34
8	+ 1.08	- 0.21
16	+ 0.26	- 0.03
32	+ 0.05	- 0.01

Dimensions

length	=	5 cms
h_1	=	0.01 cms
h_2	=	0.005 cms
viscosity	=	1 poise
P_{IN}	=	0
P_{OUT}	=	0
velocity U_1	=	500 cms/sec
U_2	=	0

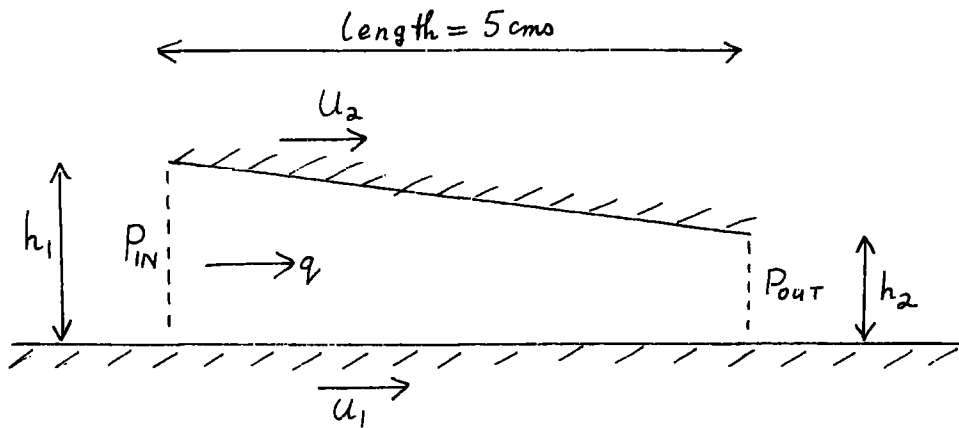


FIG. (4). CASE 2.

CASE 3. A RIGID CYLINDER ROTATING AGAINST A RIGID PLANE

For this case, the element shape no longer conforms to the bearing geometry and to compensate for this, the number of elements used must be somewhat larger than in the previous examples.

Element lengths (as a fraction of the radius of the cylinder) were chosen as $1/1000$, $2/1000$ and $4/1000$. The length of the system was taken equal to the cylinder diameter.

<u>Element Length/ Radius</u>	<u>% Error in Max^m Pressure</u>	<u>% Variation in Flowrate From X = -0.05 to 0.0</u>
$4/1000$	1.03	5.69
$2/1000$	0.32	1.39
$1/1000$	0.13	0.31

Note: Error is +ve if $\frac{dP}{dx}$ is +ve, -ve if $\frac{dP}{dx}$ is -ve

Dimensions

Radius	=	5.71 cms
Clearance h_0	=	5.71×10^{-4} cms
viscosity	=	1.11 poise

ω = 300 r.p.m.
 Pressure = 0 at $x = \pm 1$
 and Pressure $\nless 0$

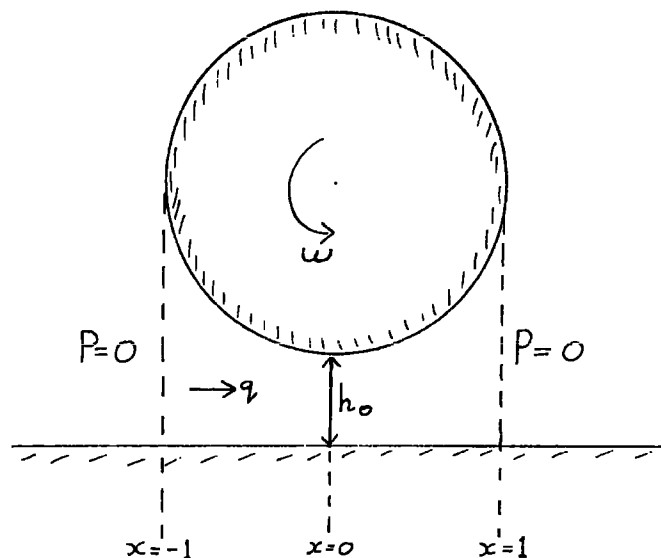


FIG. (5) , CASE 3.

The physical condition that the fluid cannot sustain a negative pressure was included in the computer programme by equating to zero, any pressures that were calculated as negative in the Gauss-Seidel procedure. This was done immediately after the calculations on each line in the matrix had been performed, not at the end of a complete iteration. The resulting pressure distribution was found to terminate at the same exit point as used for the computation of the exact curve from Reynolds Equation (in which the exit point satisfied the condition $P = \frac{dP}{dx} = 0$).

This is a most useful feature of this method since it removes the need for knowledge of the position of this exit point prior to calculation of the pressure distribution. Christopherson has shown theoretically the dependence of the position of the exit point on the Principle of Minimum Energy Dissipation (3). (A physical description of ψ in terms of energy dissipation and work done on the system can

be made if so desired, reference (4)).

Failure to impose this condition on the fluid results in the Full-Sommerfeld Solution to the problem. Although interelement continuity is not enforced over the system, no solution of the pressure curve can be correct unless it satisfies the continuity condition to a high degree of accuracy. We can see that this is so in the above table.

It should be pointed out that in this method, flowrate is calculated from the pressure gradient at entry to an element and this gradient can be somewhat in error without affecting nearby pressures (compare % flowrate variation with % pressure error in the above table).

CONCLUDING REMARKS

The three worked examples above show that the element developed is quite powerful in that halving element length reduces errors by a factor of about three. Whilst not as powerful as some structural finite elements that have been devised, this is more than compensated for in its simplicity, its almost total lack of matrix algebra involved in computation of results and in its very low storage requirements. Once assembled, the matrix needs only three quantities for each of its rows. This allows the use of a large number of elements, 2000 in example 3 above.

ACKNOWLEDGEMENTS

My thanks to Mr. P. Bettess for his unstinting help in the development of the theory of the method and to Mr. A. Bennett for providing the analytical solution of example (3).

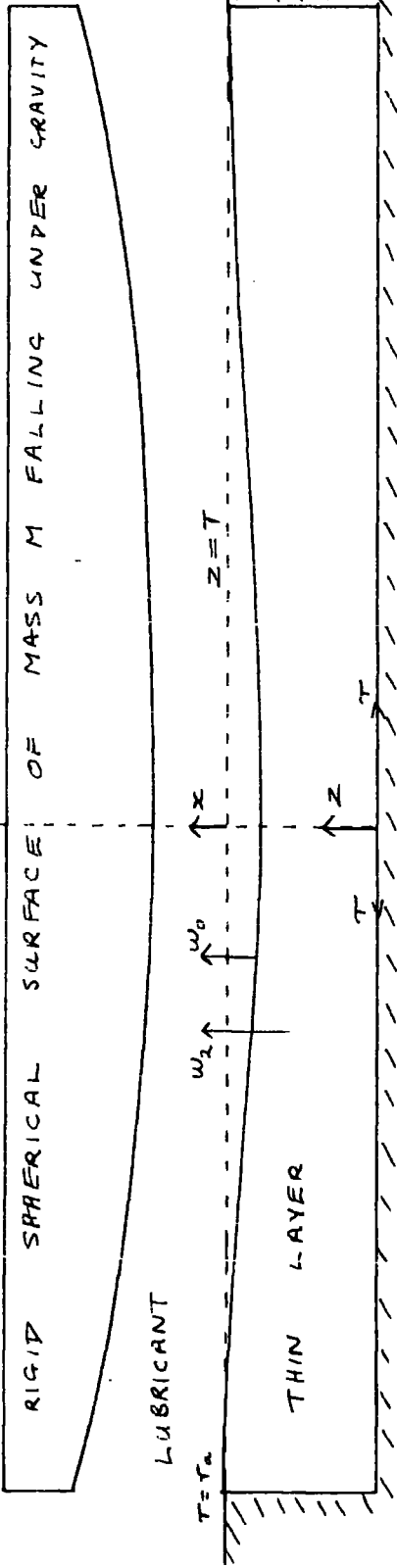
REFERENCES

1. Zienkiewicz. The Finite Element Method in Structural and Continuum Mechanics (McGraw-Hill) p.227.
2. M.M. Reddi. Finite Element Solution of the Incompressible Lubrication Problem, Trans. A.S.M.E., July 1969, p.524.
3. Christopherson, D.G. The Engineer, Jan 18 1957, p.100.
4. D.F. Hays. A variational approach to Lubrication Problems and the solution of the finite Journal Bearing, Journal of Basic Engineering, March 1959, p.13.

NOMENCLATURE

$a_1, 2, 3$	disposable constants used for the description of the pressure distribution.
F, G,	constants involving geometry, viscosity and bearing speeds.
h	film thickness.
i	subscript for a typical element.
n	number of elements used in a system.
L	element length
P	pressure at some point
1, 2	subscripts referring to inlet and outlet of element when applied to P and h.
q	flowrate through a cross section of an element.
U	velocity of fluid at any point
$U_1, 2$	velocity of lower and upper bearing surfaces.
α	$\frac{dh}{dx}$
η	viscosity of the fluid.
ψ	A function whose minimum value yields the pressure distribution.

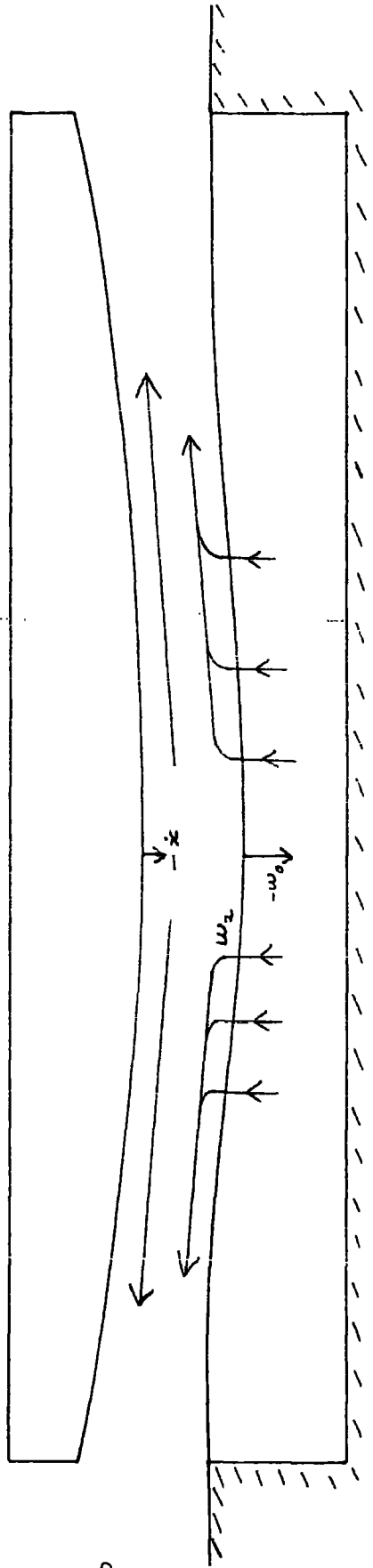




1
NOT TO SCALE

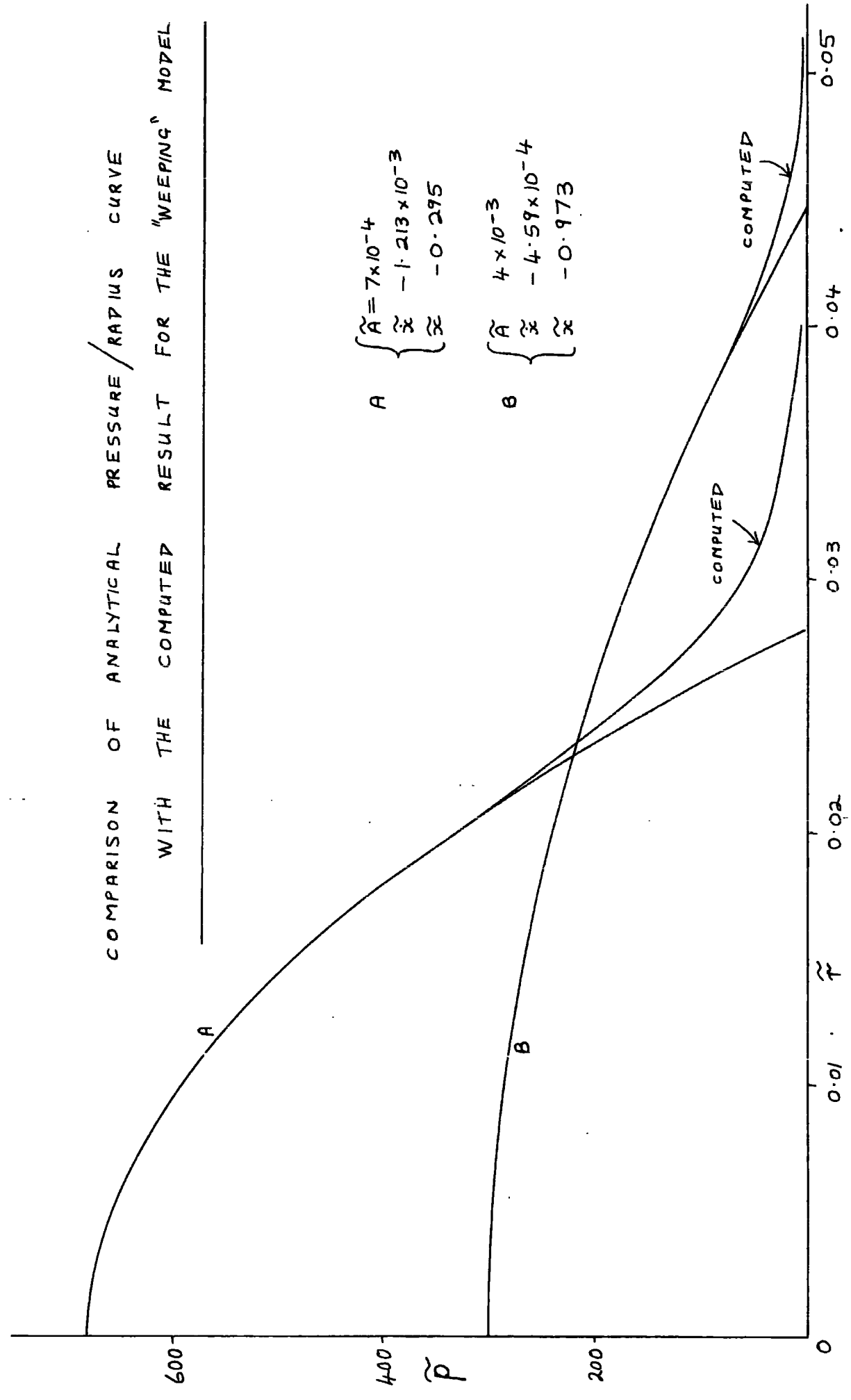
ORIENTATION OF THE CO-ORDINATE SYSTEM FOR ALL THE MODELS.

SKETCH SHOWING THE FLOW OF FLUID AND THE MOTION OF THE SURFACES OF THE "WEEPING" MODEL



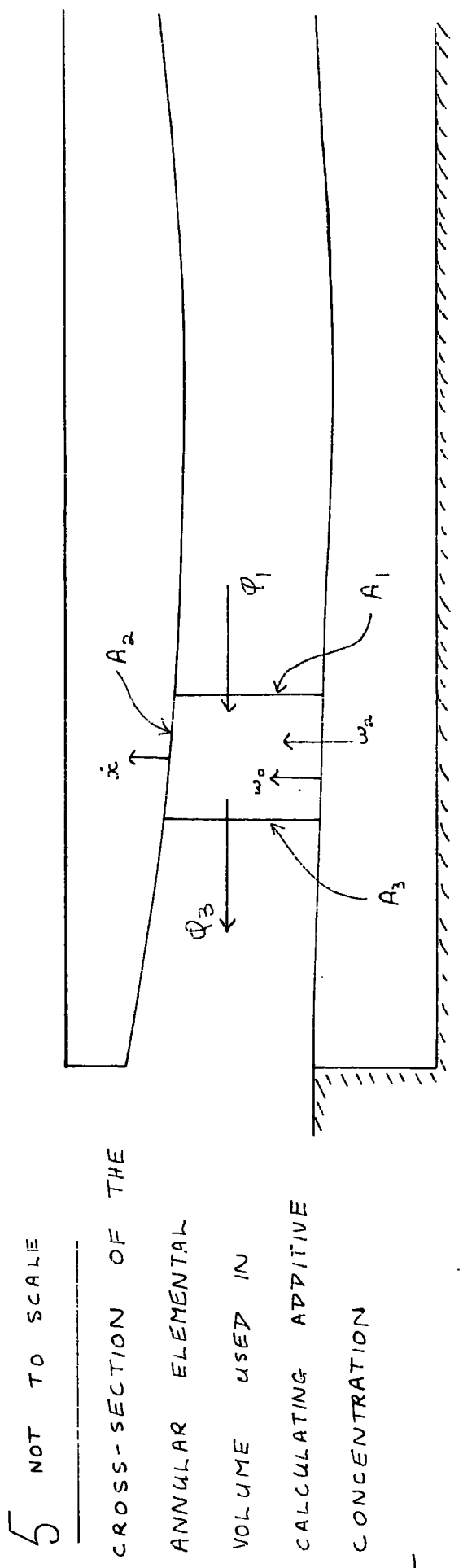
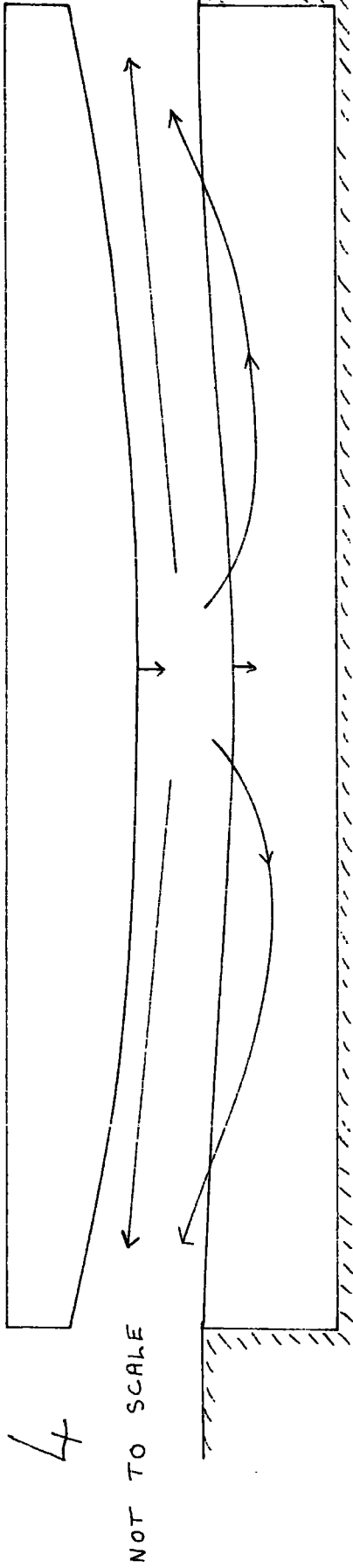
2
NOT TO SCALE

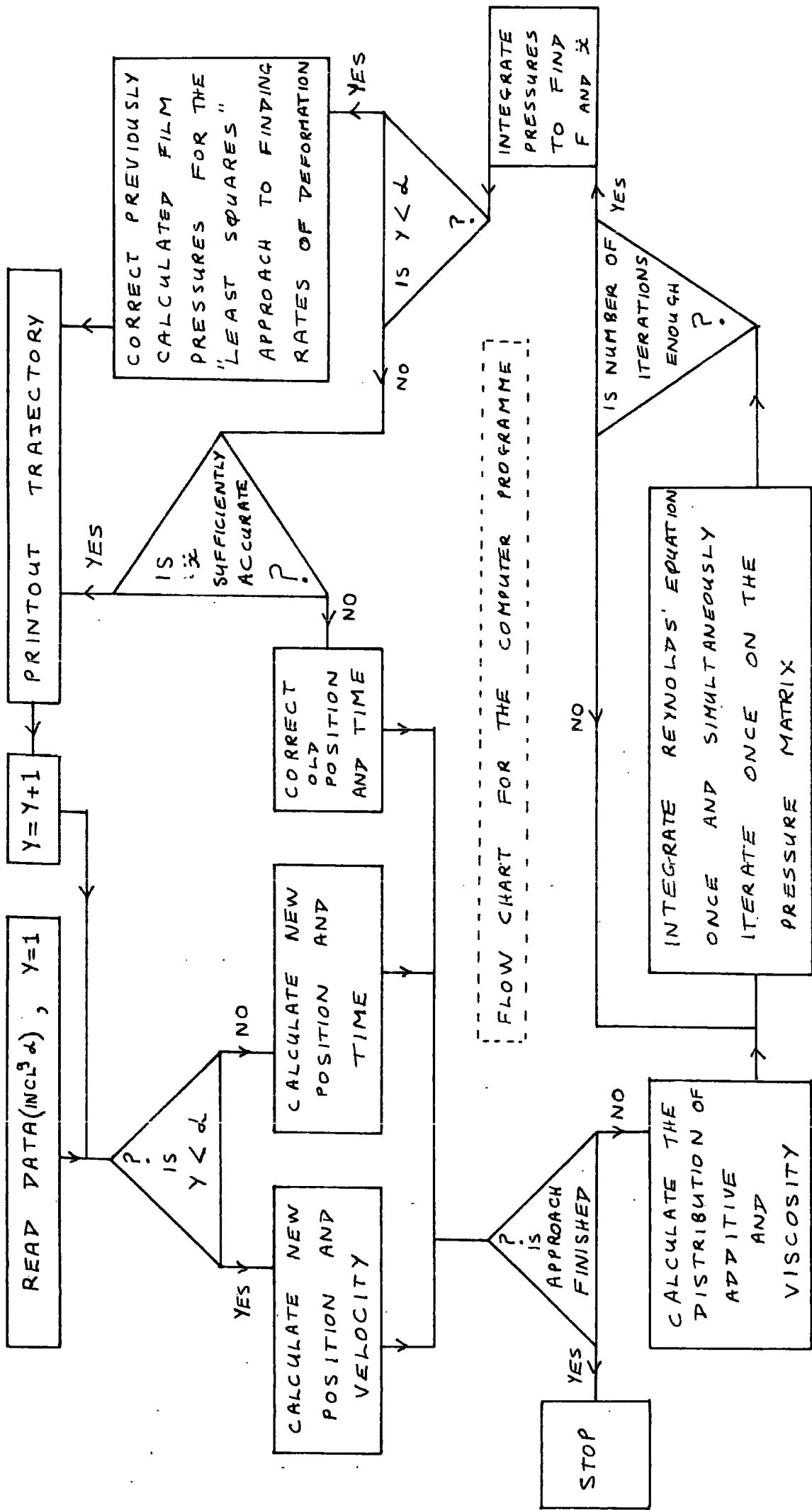
COMPARISON OF ANALYTICAL PRESSURE / RADIUS CURVE
 WITH THE COMPUTED RESULT FOR THE "WEEPING" MODEL



$$A \begin{cases} \tilde{A} = 7 \times 10^{-4} \\ \tilde{x} = -1.213 \times 10^{-3} \\ \tilde{z} = -0.295 \end{cases}$$

$$B \begin{cases} \tilde{A} = 4 \times 10^{-3} \\ \tilde{x} = -4.59 \times 10^{-4} \\ \tilde{z} = -0.973 \end{cases}$$

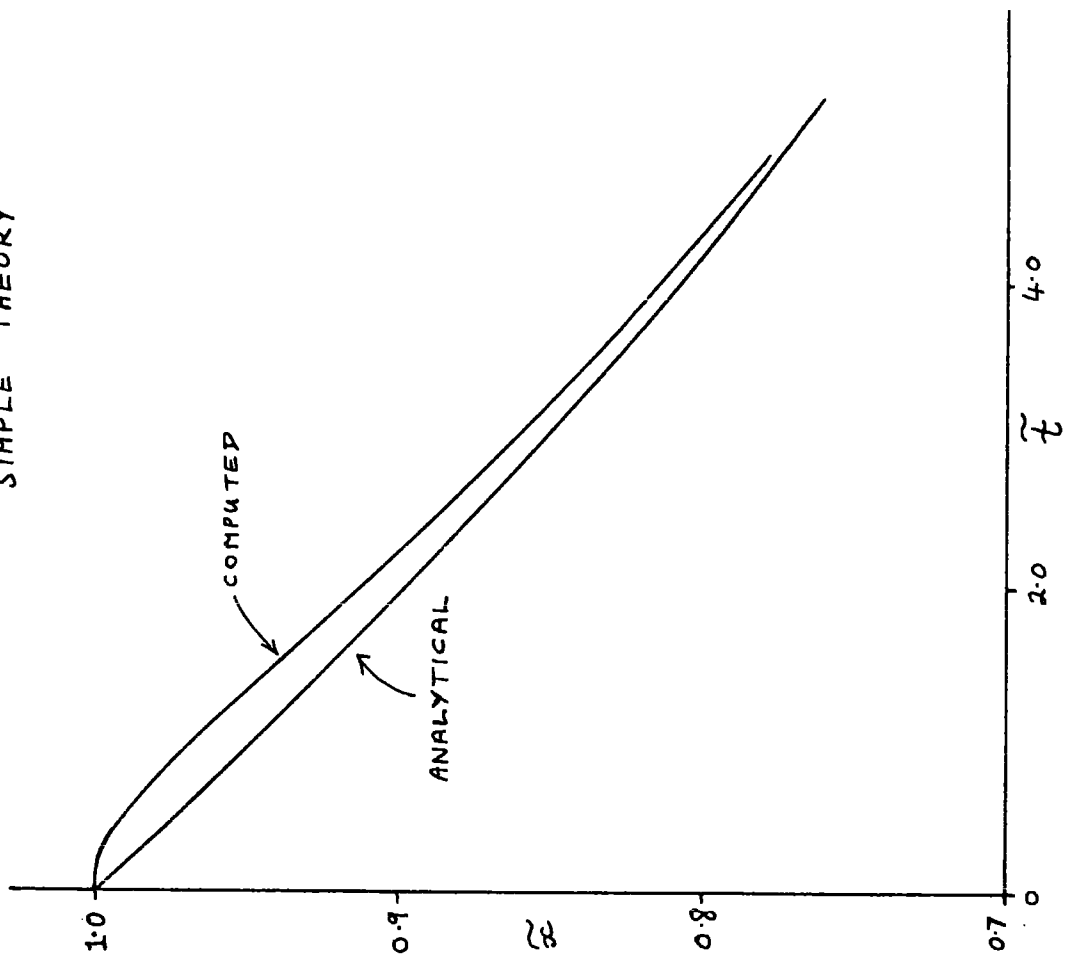
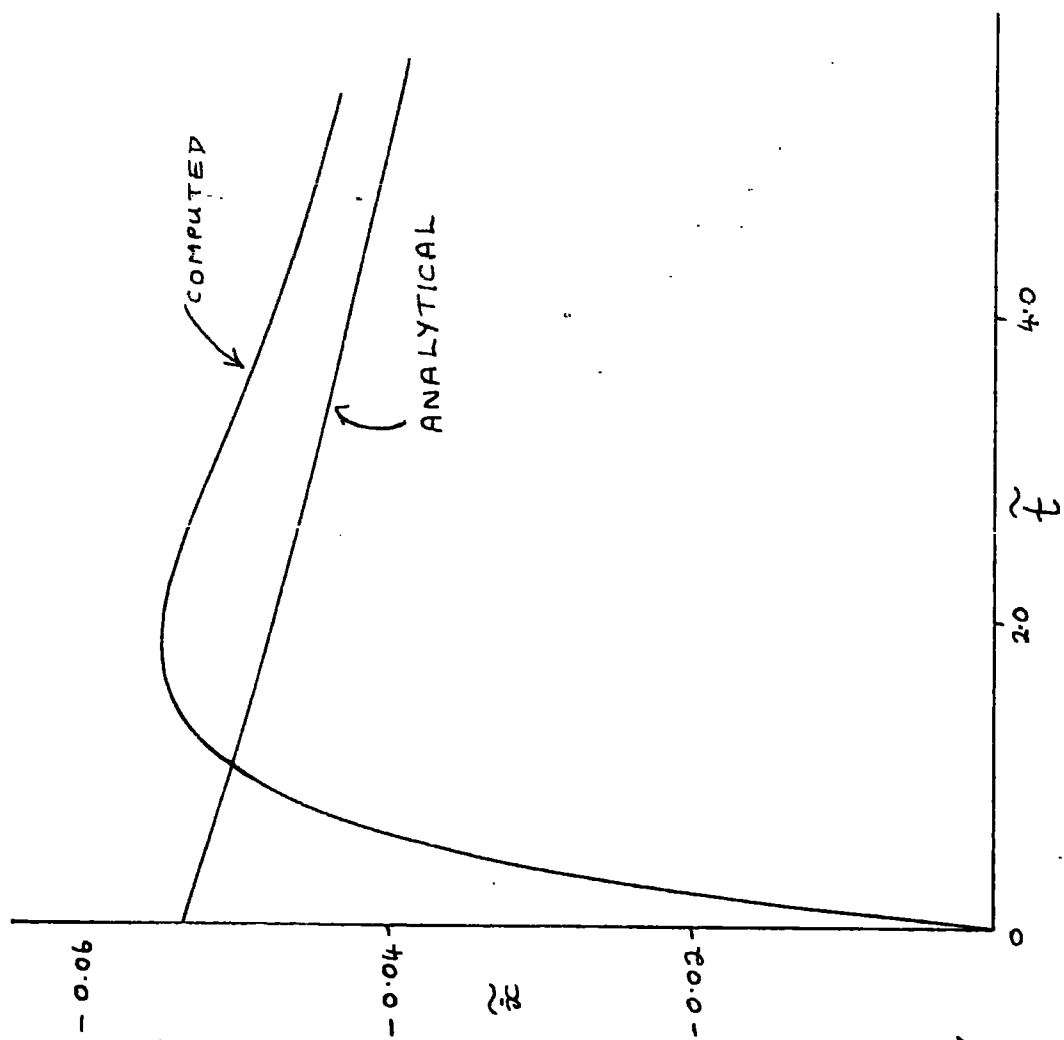




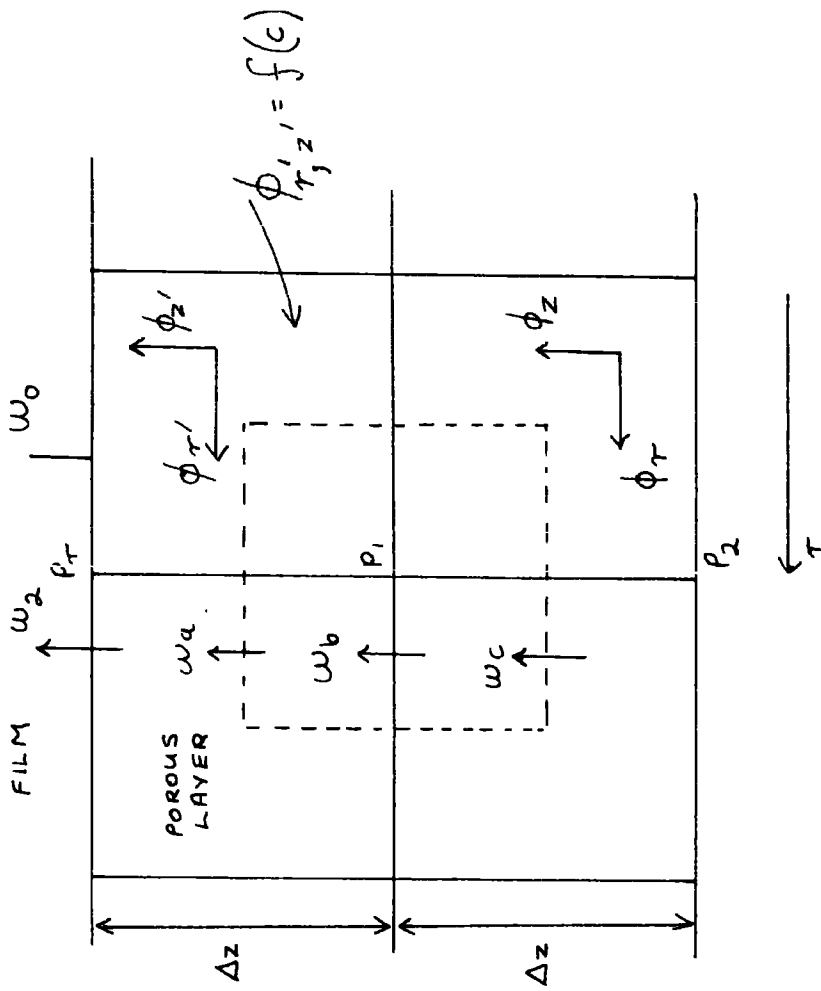
FLOW CHART FOR THE COMPUTER PROGRAMME

(IF $Y = \alpha$ THEN THE CALCULATION CHANGES FROM EQUAL INCREMENTS OF TIME TO EQUAL INCREMENTS OF VELOCITY)

INITIAL VELOCITY / TIME AND INITIAL DISPLACEMENT / TIME FOR THE RIGID IMPERMEABLE MODEL. COMPUTED TRAJECTORY COMPARED WITH SIMPLE THEORY



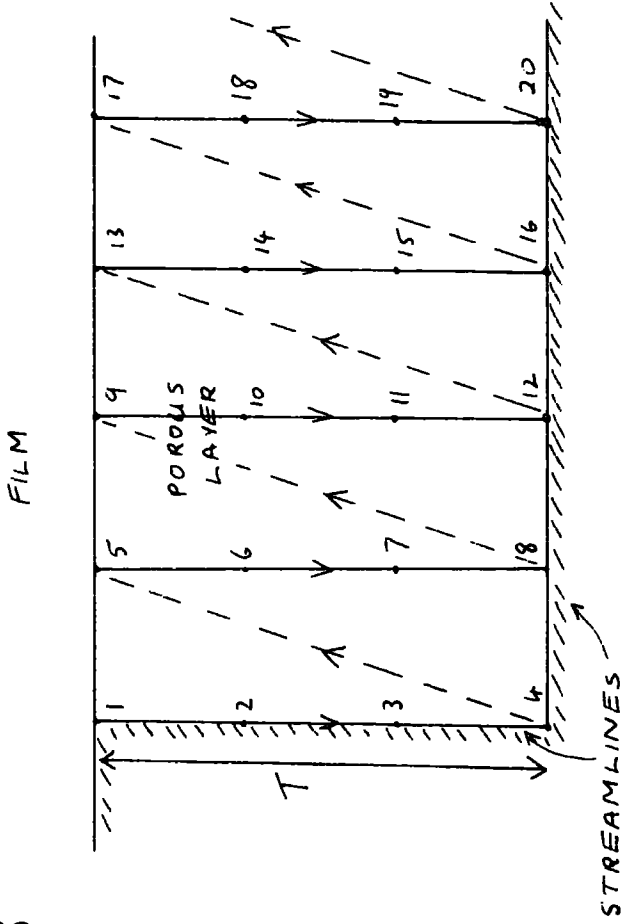
9



THE FINITE DIFFERENCE GRID FOR THE
CALCULATION OF P_1 WHEN THE FILM
IS ENRICHED.

8 AND 9

8



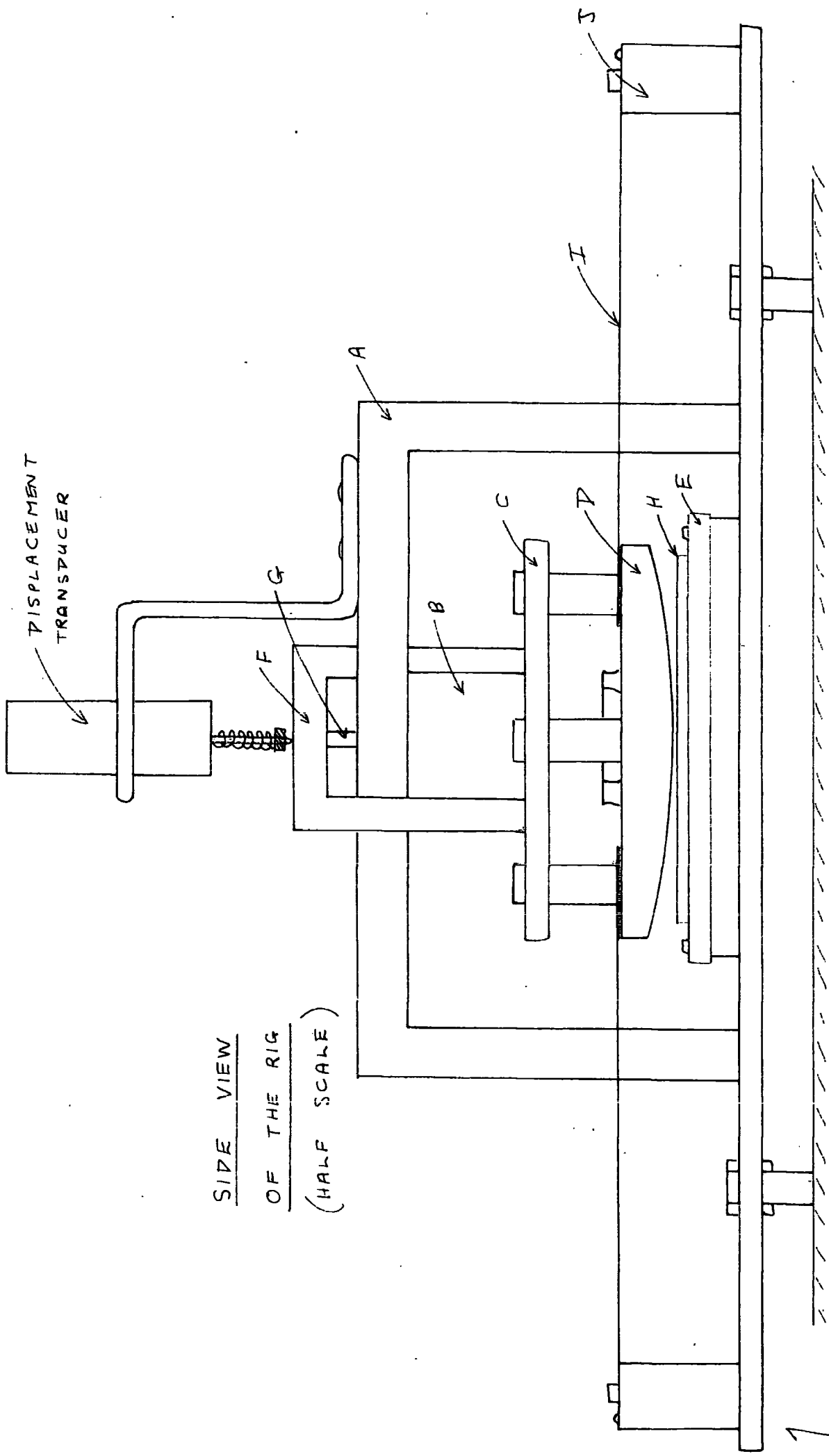
SKETCH SHOWING ORDER OF
CALCULATION OF NODAL
PRESSURES IN THE POROUS LAYER

8 AND 9

DIAGRAM 10

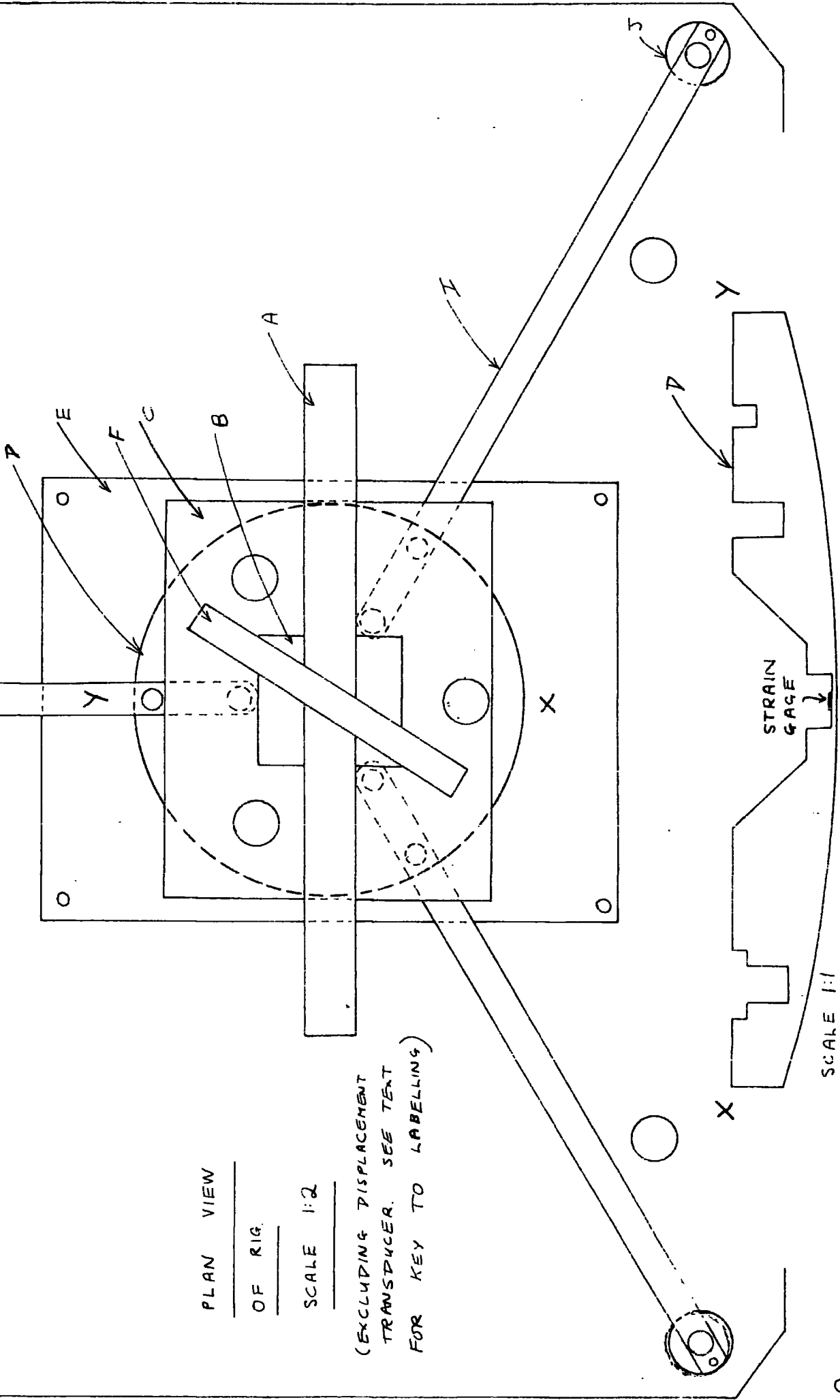
A COMPARISON OF THE RELEVANT PARAMETERS FOR ANIMAL JOINTS AND THE EXAMINED MODELS.

PARAMETER	REGIME	ANIMAL JOINT (TYPICAL VALUES)	MODEL THEORY	MODEL EXPERIMENTS
LOAD (N)		1000 N	78.4	42.5 - 78.0
INITIAL VISCOSITY Ns/m^2		0.02 - 0.03	1.5	0.2 - 10.0
RADIUS OF CURVATURE mm		300	300	300
INITIAL SEPARATION mm		10^{-2}	0.25	0.25
\tilde{A}		0.5	$0 - 10^{-3}$	$0 - 1.84 \times 10^{-3}$
$\tilde{\phi}_z$		$4 \times 10^{-8} - 2 \times 10^{-7}$	$0 - 10^{-2}$	$4.6 \times 10^{-4}, 3.3 \times 10^{-5}$
$\tilde{\phi}_z / \tilde{\phi}_r$?	1, 100, 1000	2.26, 2.31
c		3.5×10^{-3}	$3.5 \times 10^{-3} - 0.35$	-
V		0.7 - 0.8	0.25	0.29, 0.12
n_i / n_i		278	278, 28.5, 2.86	-
\tilde{T}		500	20	20
$\tilde{\tau}_e$		0.05	0.167	0.16



DISPLACEMENT
TRANSDUCER

SIDE VIEW
OF THE RIG
(HALF SCALE)



PLAN VIEW
 OF RIG.
 SCALE 1:2

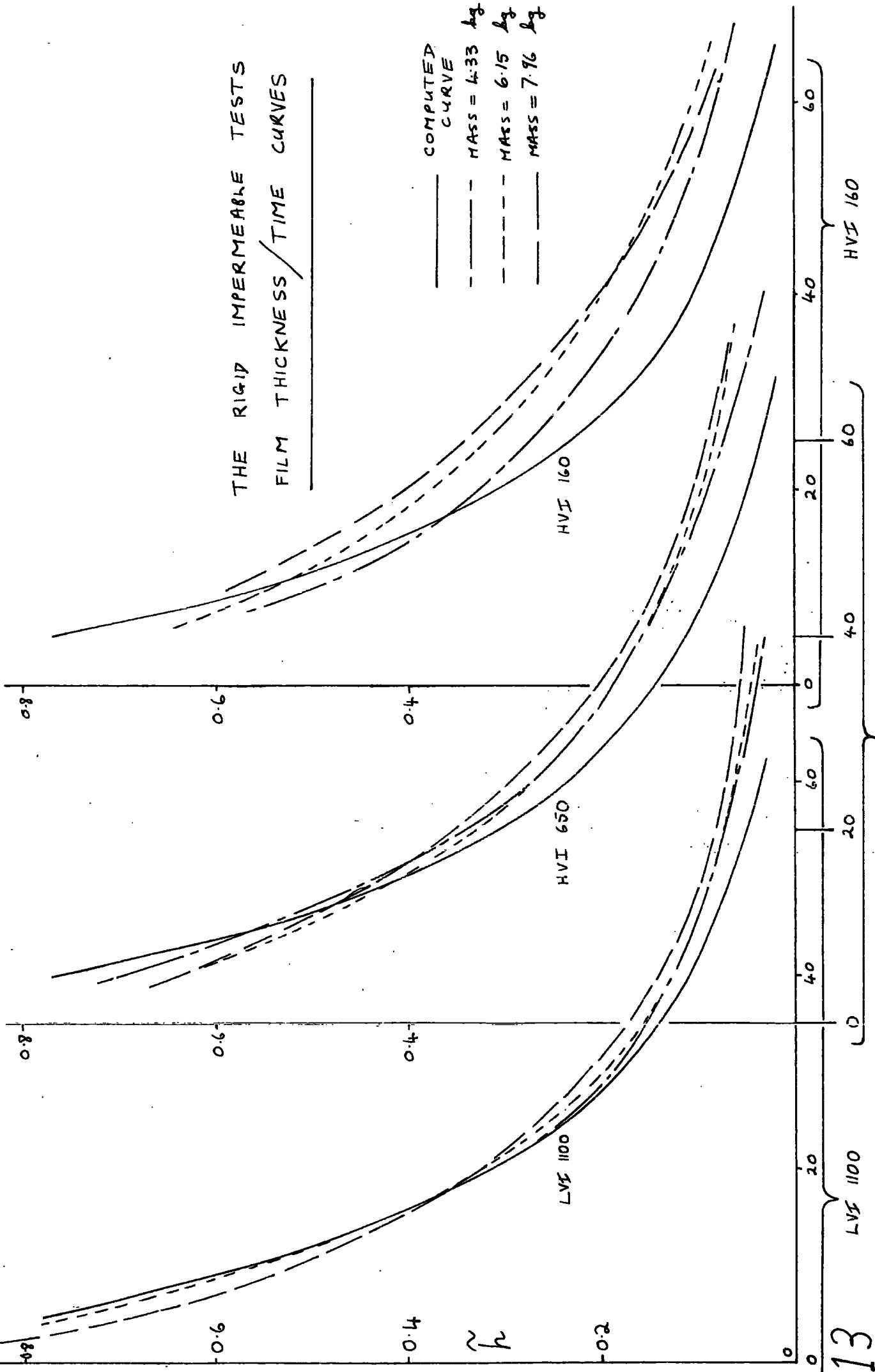
(EXCLUDING DISPLACEMENT
 TRANSDUCER. SEE TEXT
 FOR KEY TO LABELLING)

SCALE 1:1

CROSS-SECTION OF SPHERICAL SURFACE

THE RIGID IMPERMEABLE TESTS
FILM THICKNESS / TIME CURVES

COMPUTED
CURVE
--- MASS = 4.33 Ag
--- MASS = 6.15 Ag
--- MASS = 7.96 Ag



2000

THE RIGID IMPERMEABLE
TESTS. PRESSURE
TIME CURVES

1500

P

1000

500

LVI 1100

HVI 650

HVI 650

HVI 160

0

20

40

20

40

20

40

60

LVI 1100

t

HVI 160

— COMPUTED
CURVE

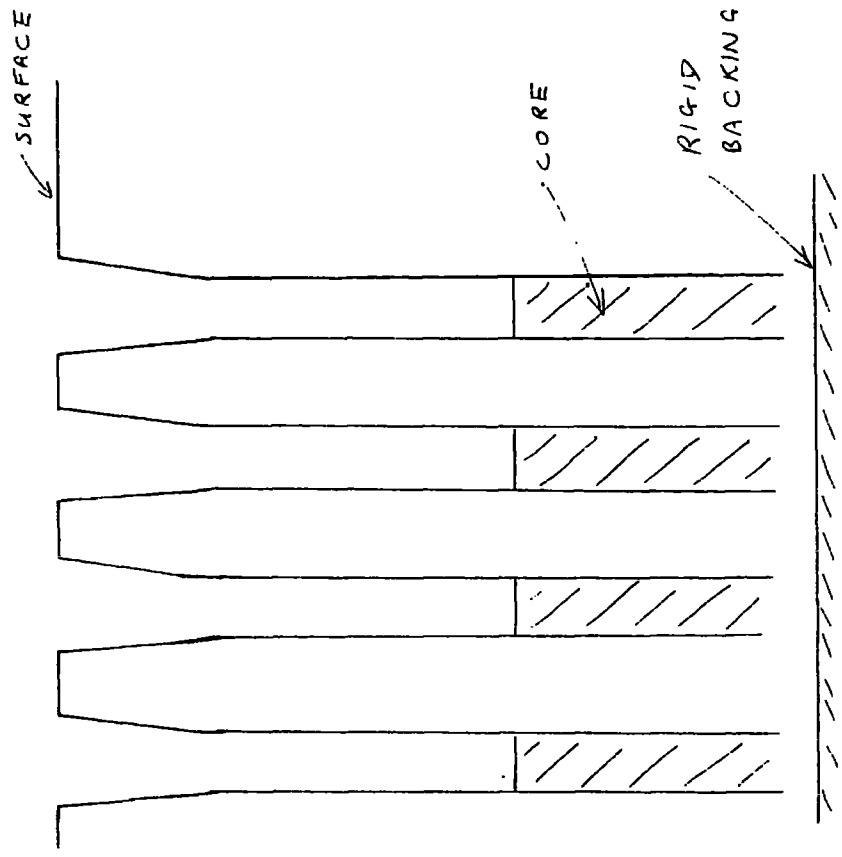
- - - MASS = 4.33 kg

- - - MASS = 6.15 kg

- - - MASS = 7.96 kg

TYPICAL CROSS-SECTION
OF A "WEEPING" LAYER

OF RUBBER

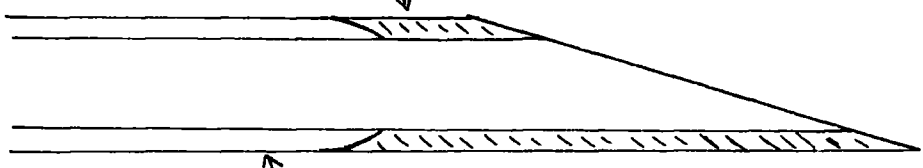


NEEDLE MACHINED FOR

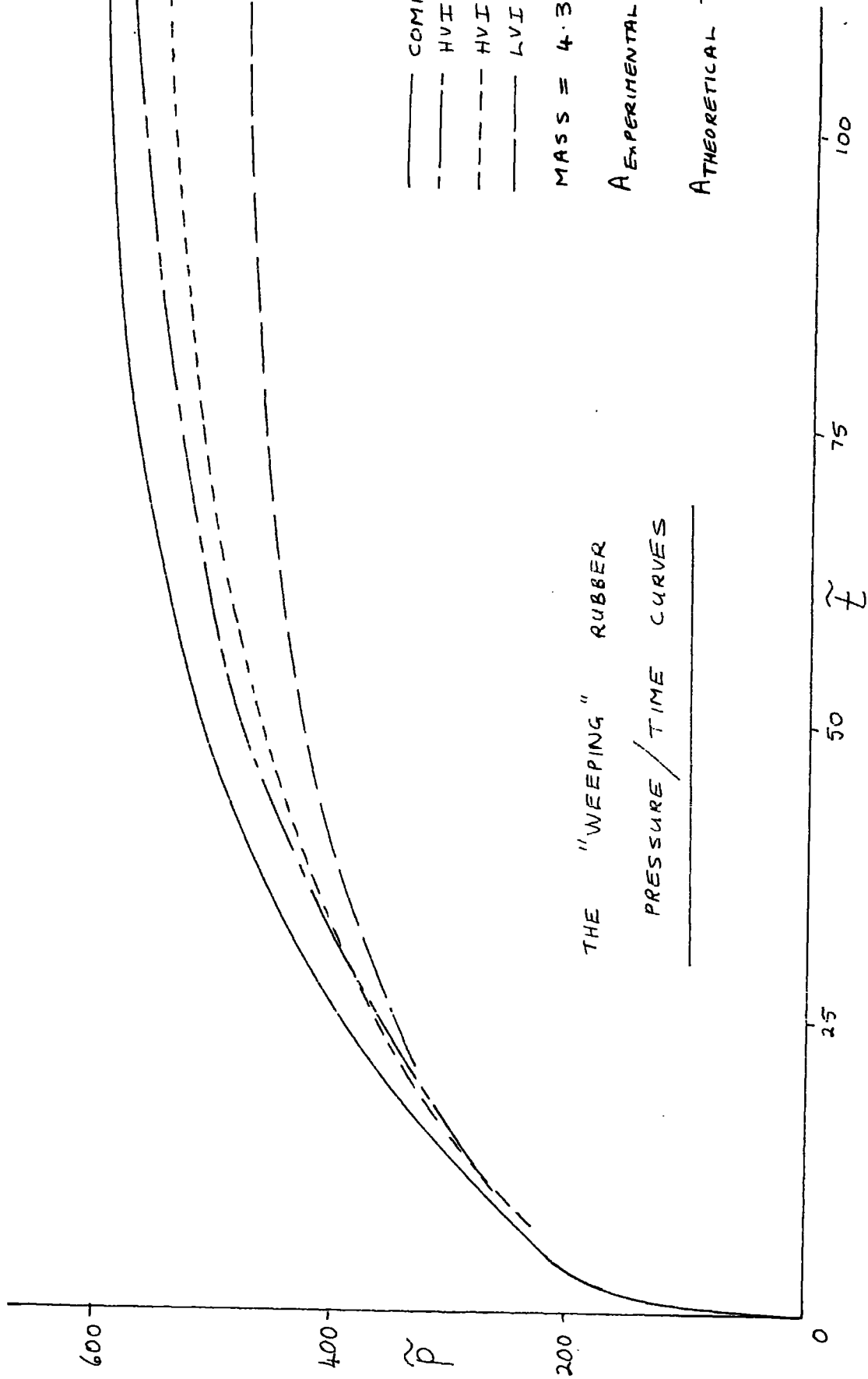
PRODUCING HOLES.

REMOVED BY
GRINDING.

SCALES 20:1



FINAL
FORM



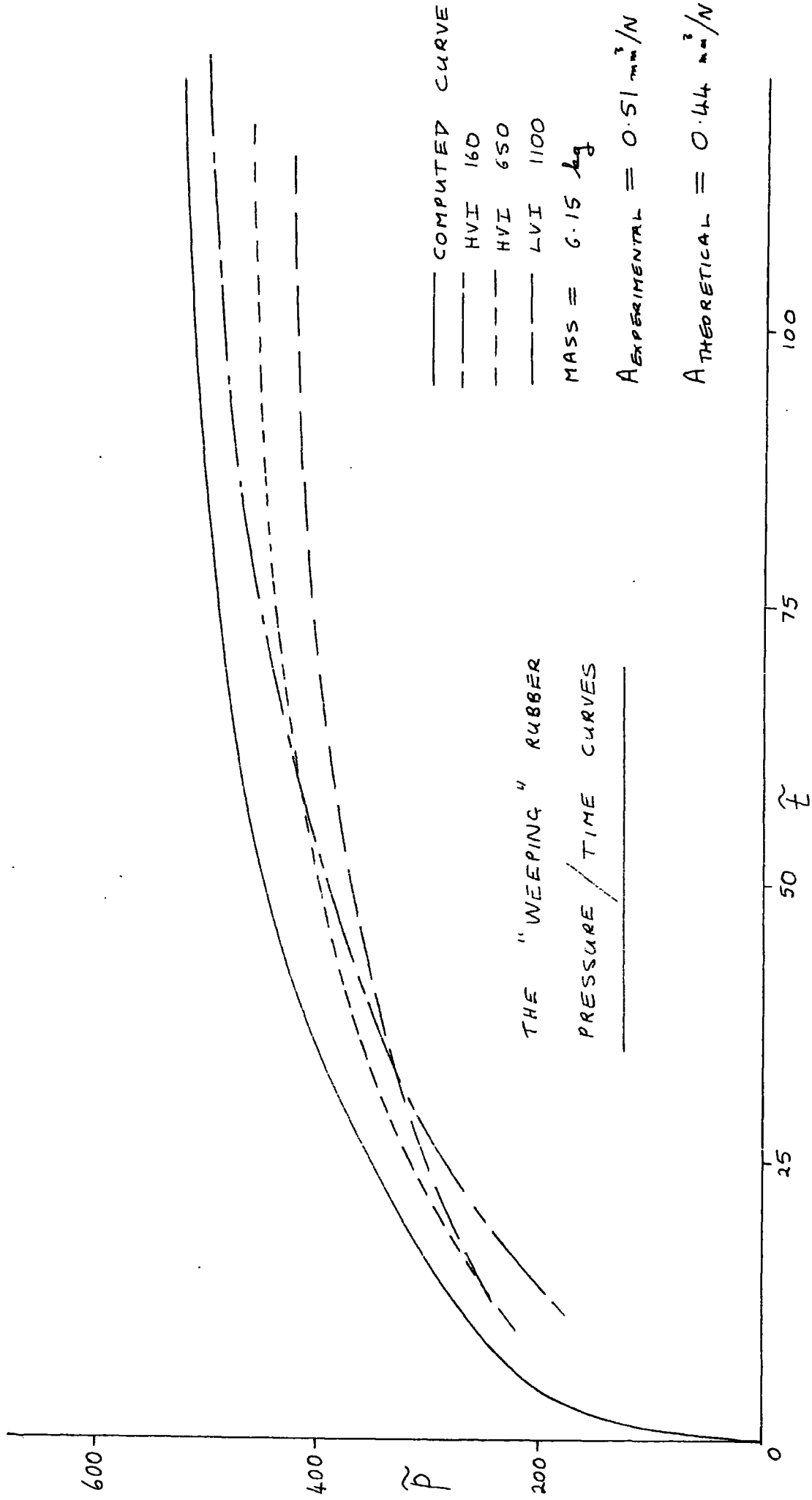
COMPUTED CURVE
 HVI 160
 HVI 650
 LVI 1100

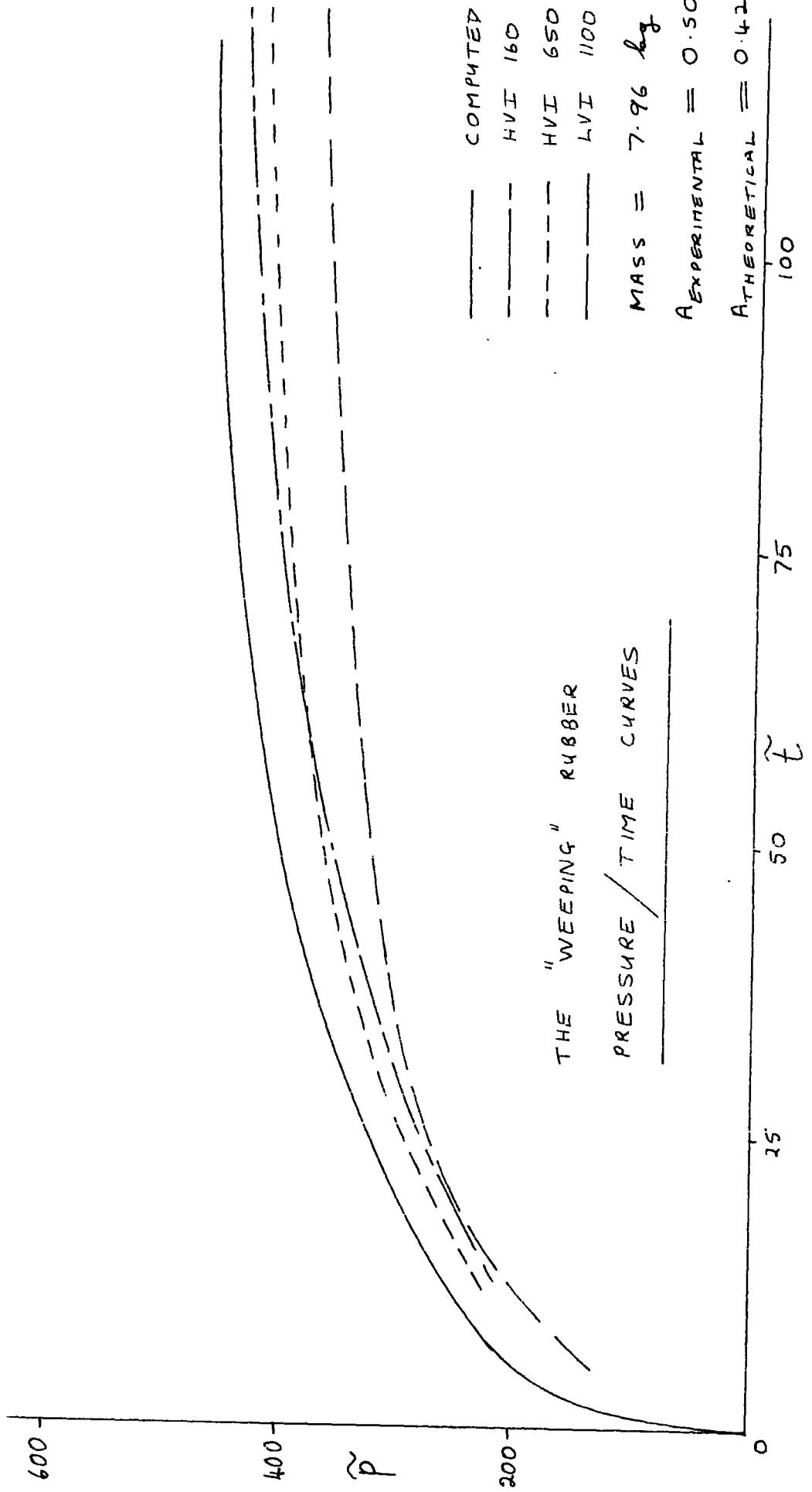
MASS = 4.33 kg

$A_{\text{EXPERIMENTAL}} = 0.53 \text{ mm}^3/\text{N}$

$A_{\text{THEORETICAL}} = 0.45 \text{ mm}^3/\text{N}$

THE "WEEPING" RUBBER
 PRESSURE / TIME CURVES





THE "WEEPING" RUBBER
PRESSURE / TIME CURVES

_____ COMPUTED CURVE
 _____ HVI 160
 - - - - - HVI 650
 - . - . - LVI 1100

MASS = 7.96 *log*
 A_{EXPERIMENTAL} = 0.50 *mm*³/*N*
 A_{THEORETICAL} = 0.42 *mm*²/*N*

THE "WEEPING" RUBBER

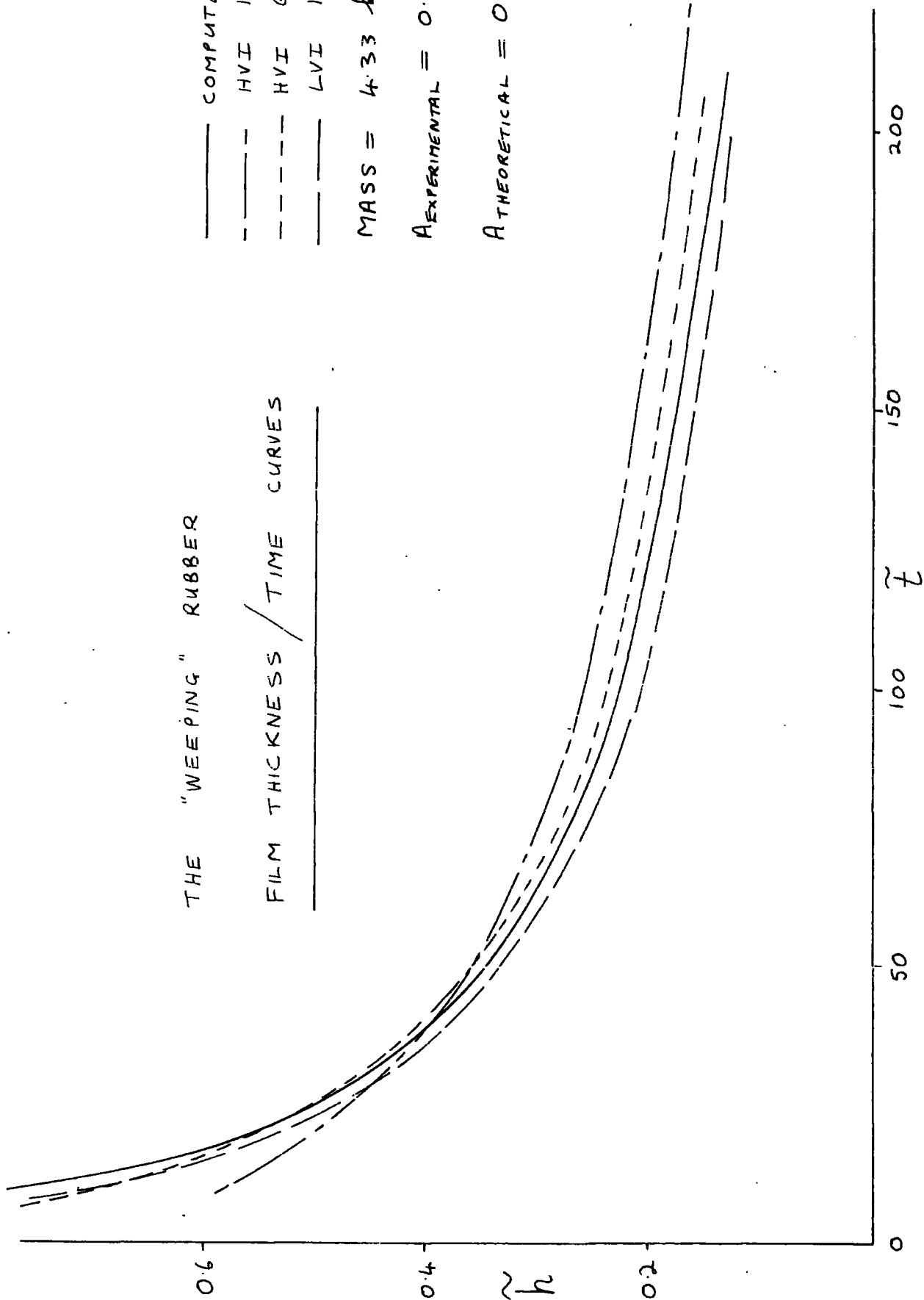
FILM THICKNESS / TIME CURVES

_____ COMPUTED CURVE
 - - - - - HVI 160
 - - - - - HVI 650
 _____ LVI 1100

MASS = 4.33 *log*

$A_{\text{EXPERIMENTAL}} = 0.53 \text{ mm}^3/N$

$A_{\text{THEORETICAL}} = 0.45 \text{ mm}^3/N$



THE "WEEPING" RUBBER

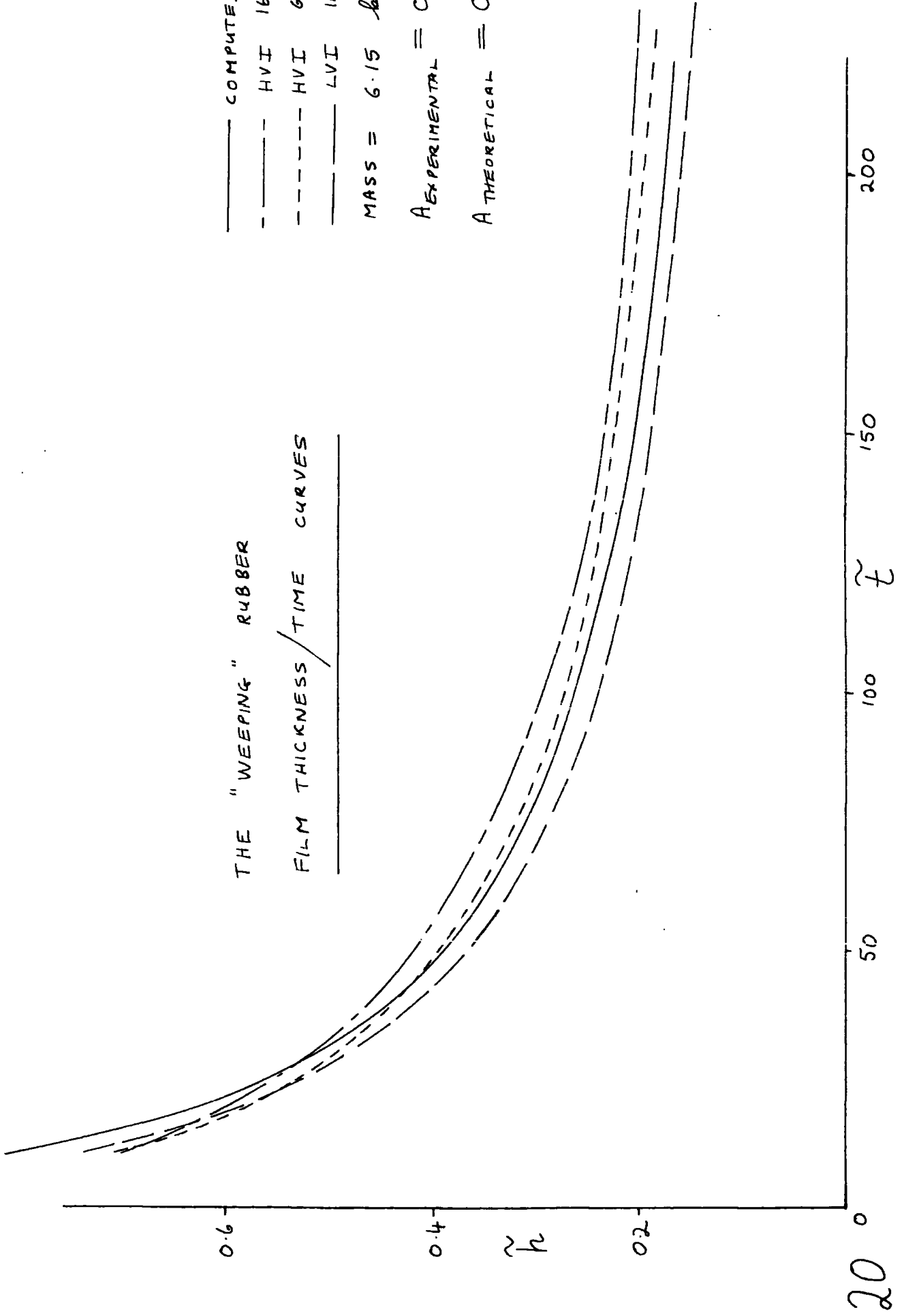
FILM THICKNESS / TIME CURVES

_____ COMPUTED CURVE
 - - - - - HVI 160
 - - - - - HVI 650
 _____ LVI 1100

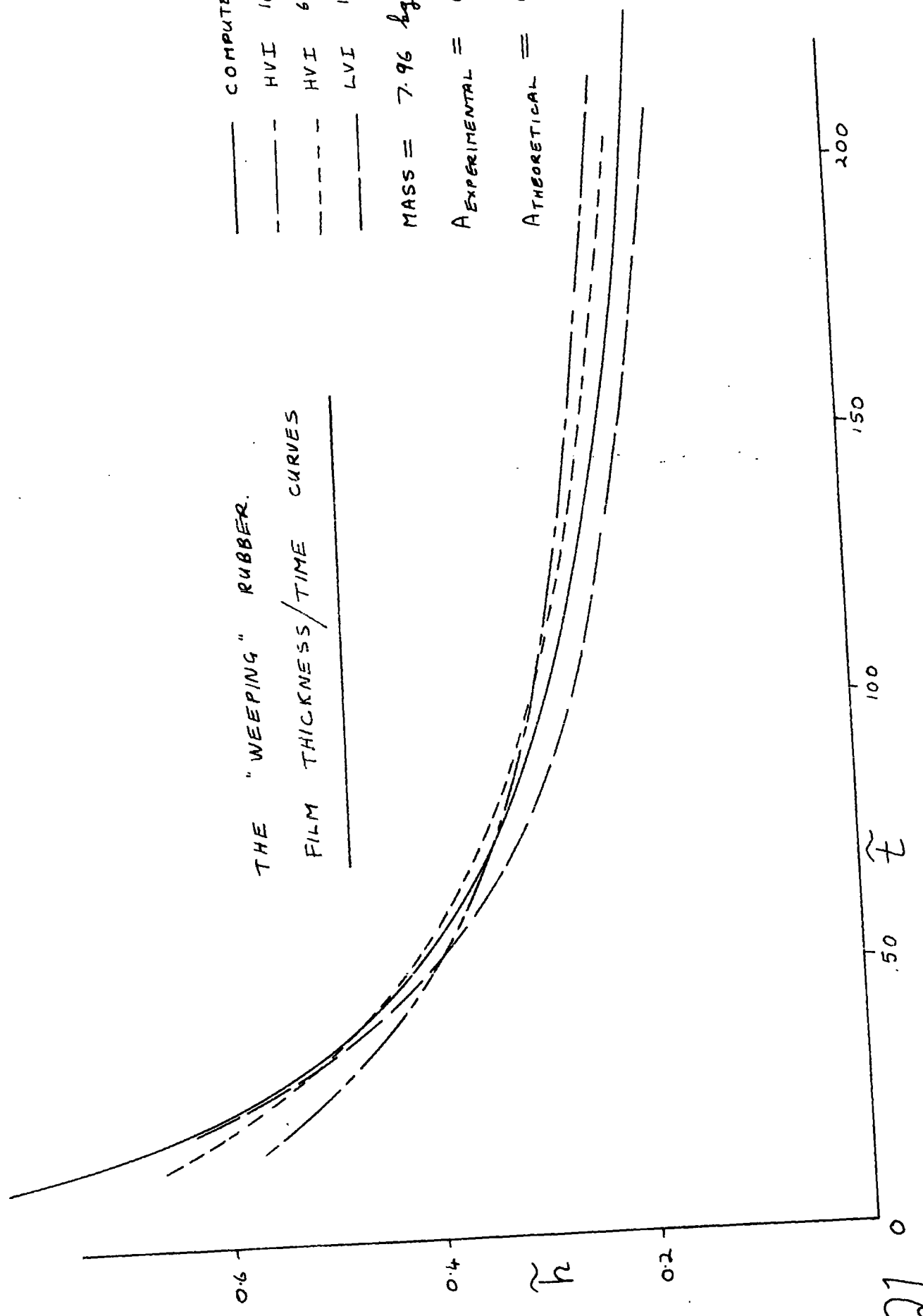
MASS = 6.15 *g*

$A_{EXPERIMENTAL} = 0.51 \text{ mm}^3 / N$

$A_{THEORETICAL} = 0.44 \text{ mm}^3 / N$



THE "WEEPING" RUBBER.
 FILM THICKNESS/TIME CURVES



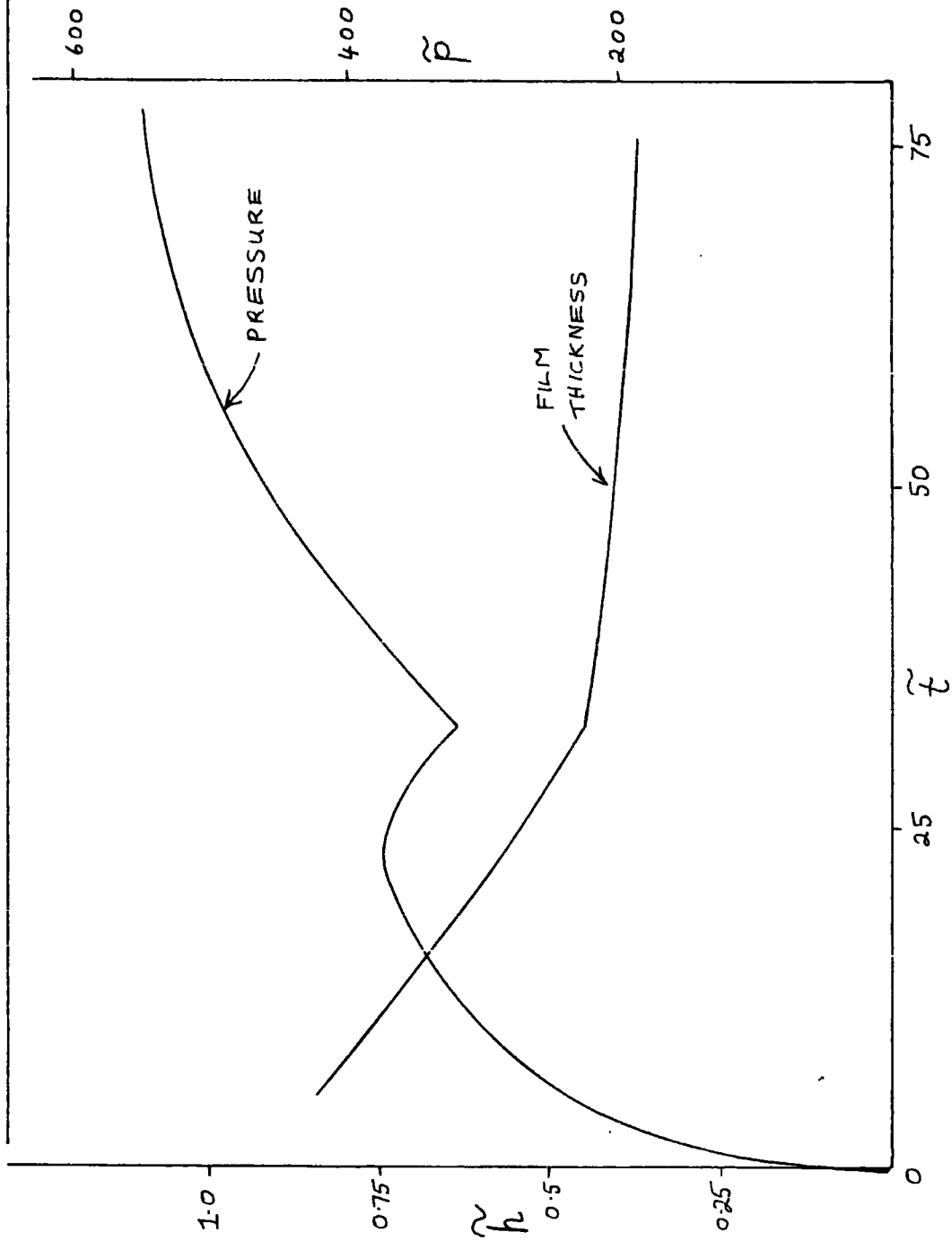
COMPUTED CURVE
 HVI 160
 HVI 650
 LVI 1100

MASS = 7.96 μg

A_{EXPERIMENTAL} = 0.50 mm^2/N

A_{THEORETICAL} = 0.42 mm^2/N

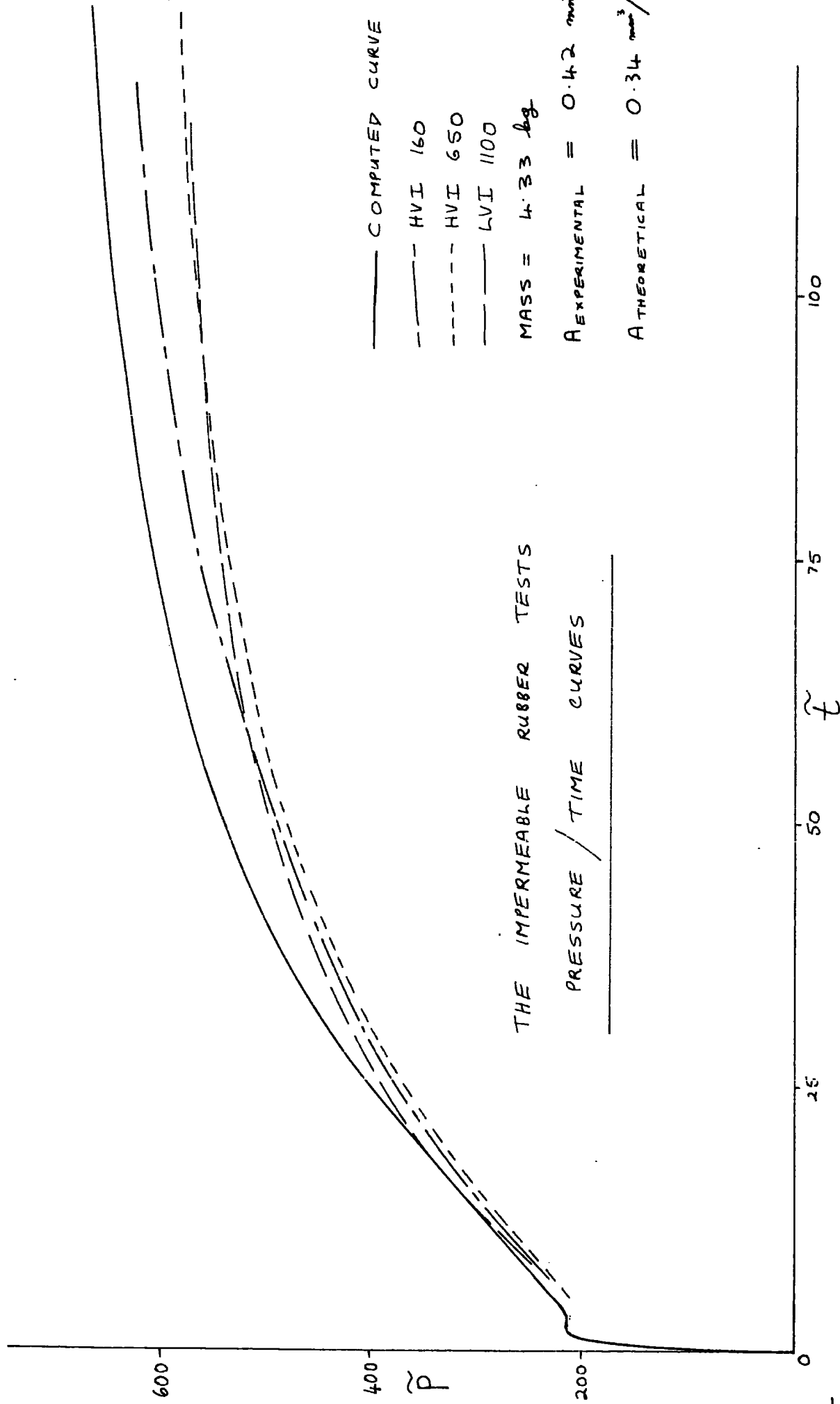
SKETCHES OF TYPICAL FILM THICKNESS AND PRESSURE TRACES FOR THE IMPERMEABLE RUBBER TESTS USING A CAVITATED FLUID





23 11/10/51
11323

PHOTOGRAPH OF AN OIL FILM WITH AN AIR BUBBLE APPEARING AT ITS CENTRE



— COMPUTED CURVE

- - - HVI 160

- - - HVI 650

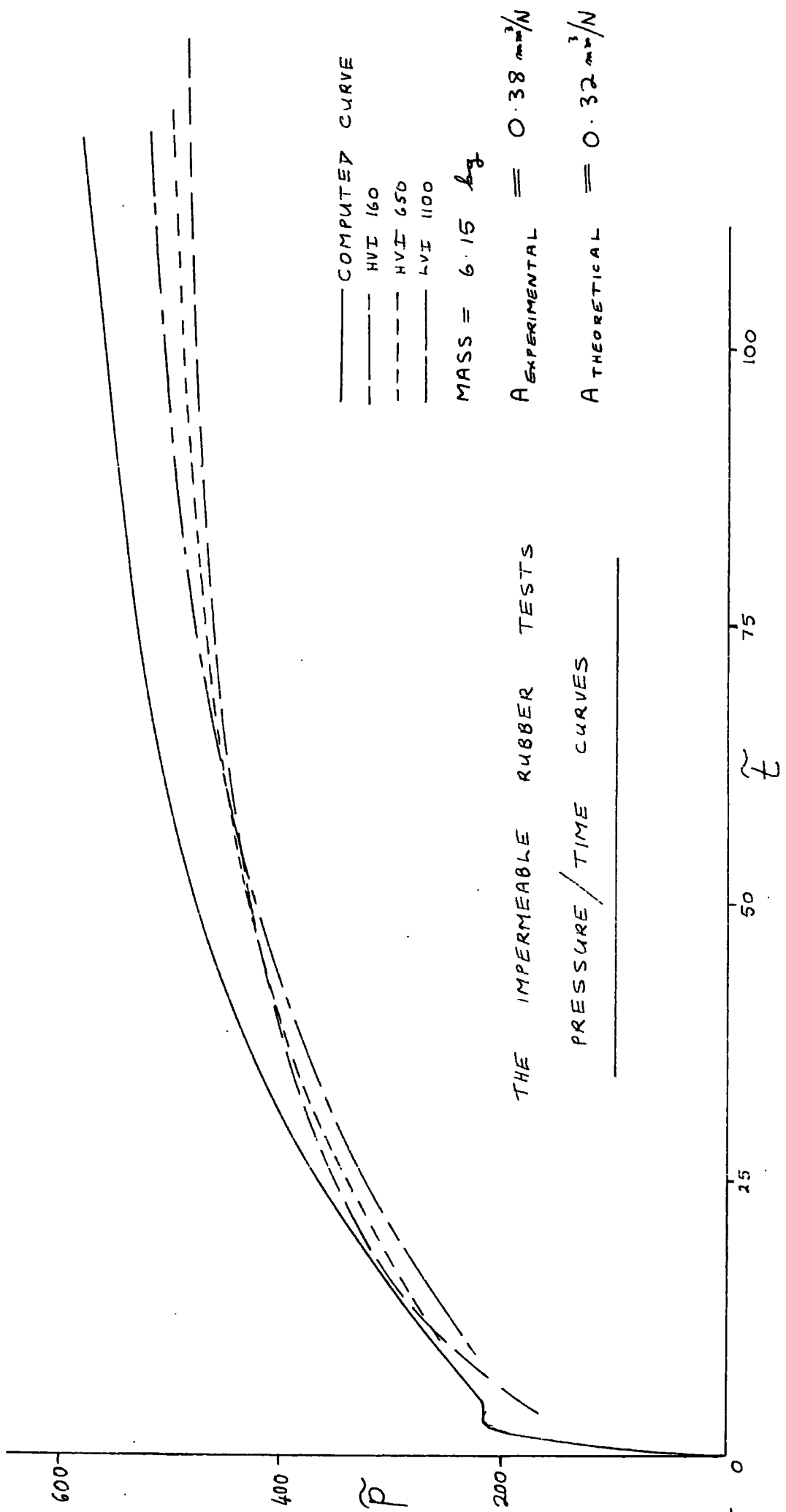
- · - LVI 1100

MASS = 4.33 g

$A_{EXPERIMENTAL} = 0.42 \text{ mm}^3/N$

$A_{THEORETICAL} = 0.34 \text{ mm}^3/N$

THE IMPERMEABLE RUBBER TESTS
PRESSURE / TIME CURVES



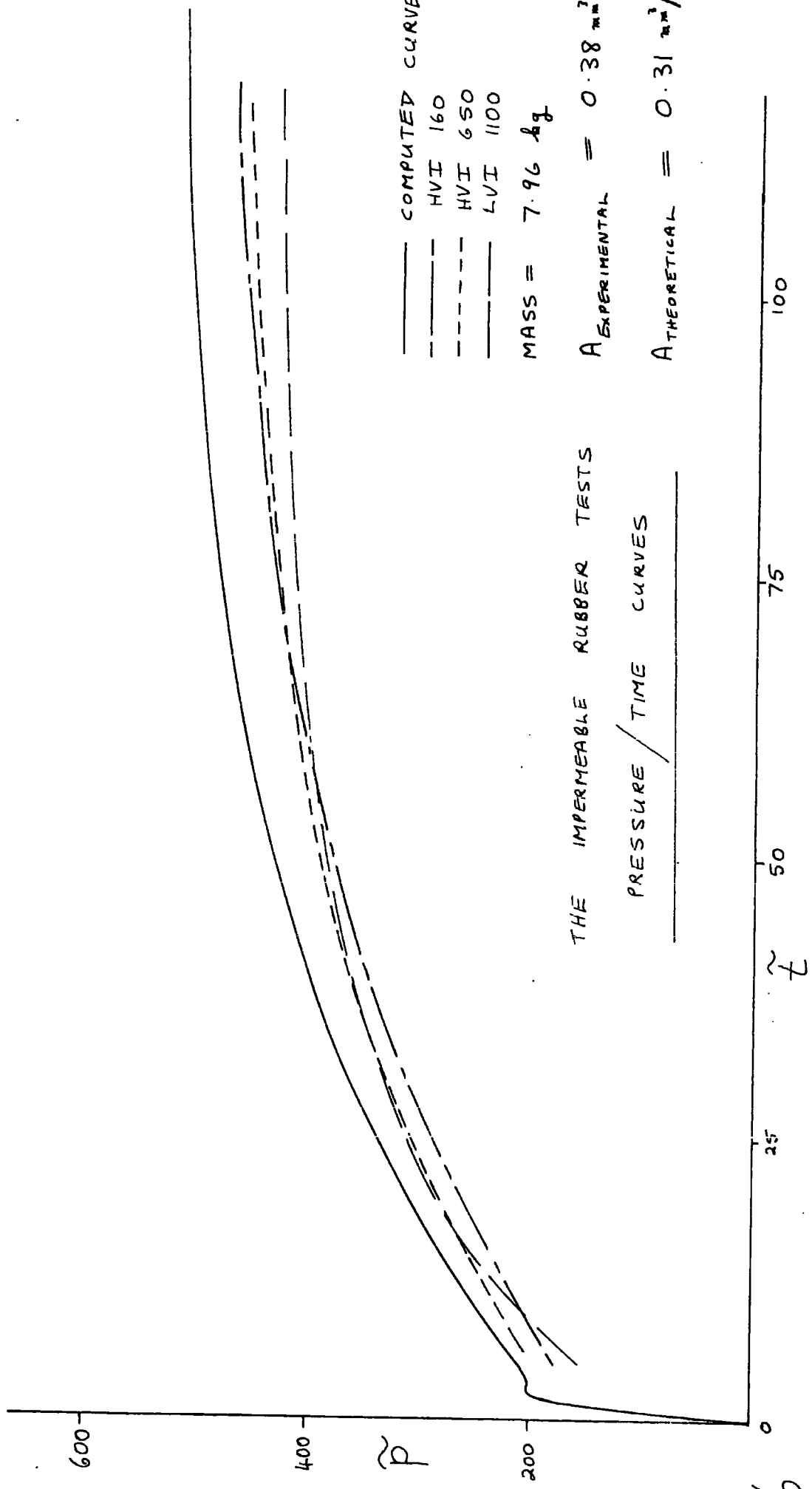
——— COMPUTED CURVE
 - - - HVI 160
 - - - HVI 650
 - · - HVI 1100

MASS = 6.15 kg

$A_{EXPERIMENTAL} = 0.38 \frac{mm^3}{N}$

$A_{THEORETICAL} = 0.32 \frac{mm^3}{N}$

THE IMPERMEABLE RUBBER TESTS
PRESSURE / TIME CURVES



COMPUTED CURVE

HVI 160

HVI 650

LVI 1100

MASS = 7.96 g

THE IMPERMEABLE RUBBER TESTS

PRESSURE / TIME CURVES

$A_{\text{EXPERIMENTAL}} = 0.38 \text{ mm}^3/\text{N}$

$A_{\text{THEORETICAL}} = 0.31 \text{ mm}^3/\text{N}$

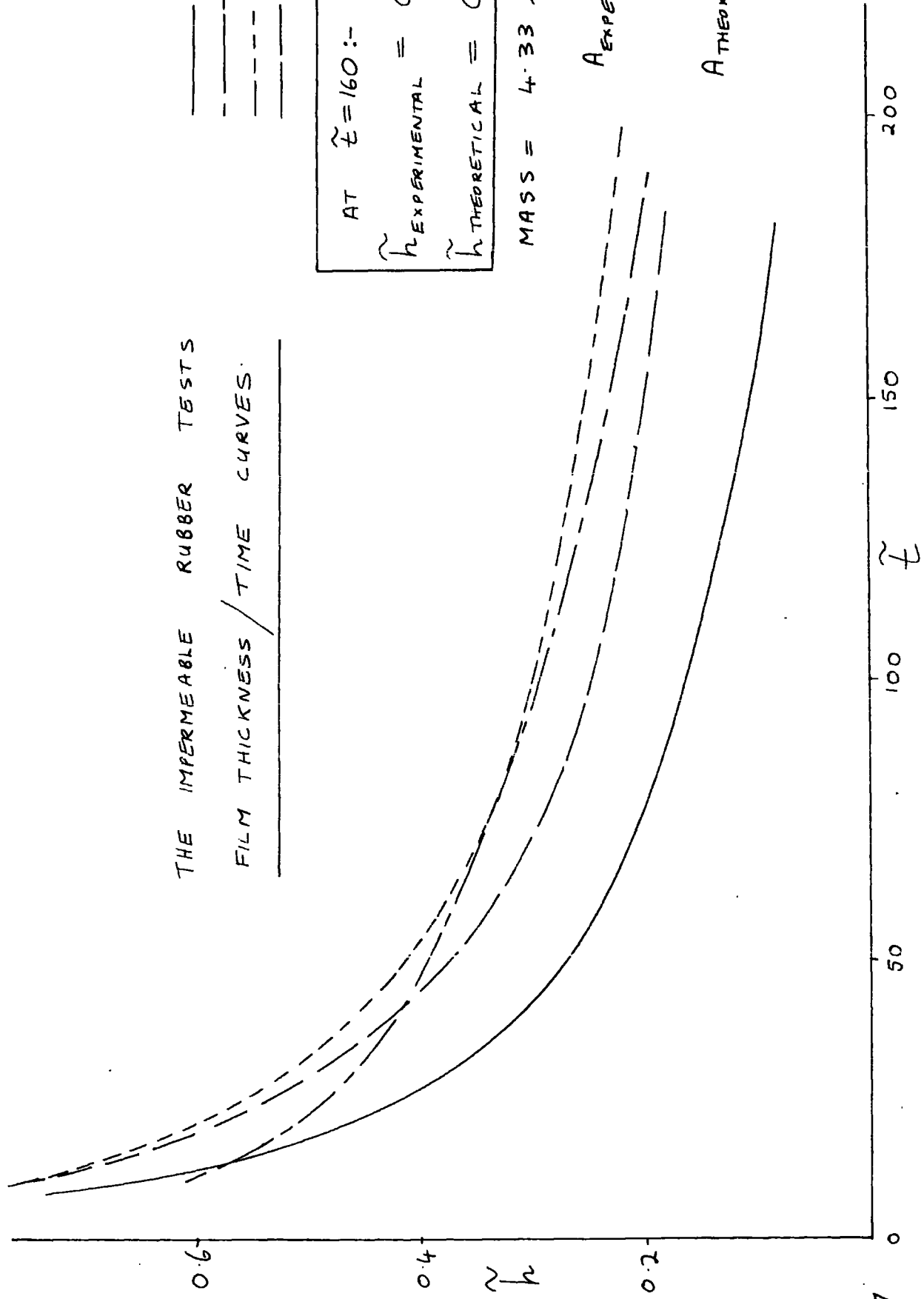
THE IMPERMEABLE RUBBER TESTS
 FILM THICKNESS / TIME CURVES.

— COMPUTED CURVE
 - - - HVI 160
 - - - HVI 650
 - - - LVI 1100

AT $\tilde{E} = 160$:-
 $\tilde{h}_{\text{EXPERIMENTAL}} = 0.220 \pm 0.021$
 $\tilde{h}_{\text{THEORETICAL}} = 0.098$

MASS = 4.33 g

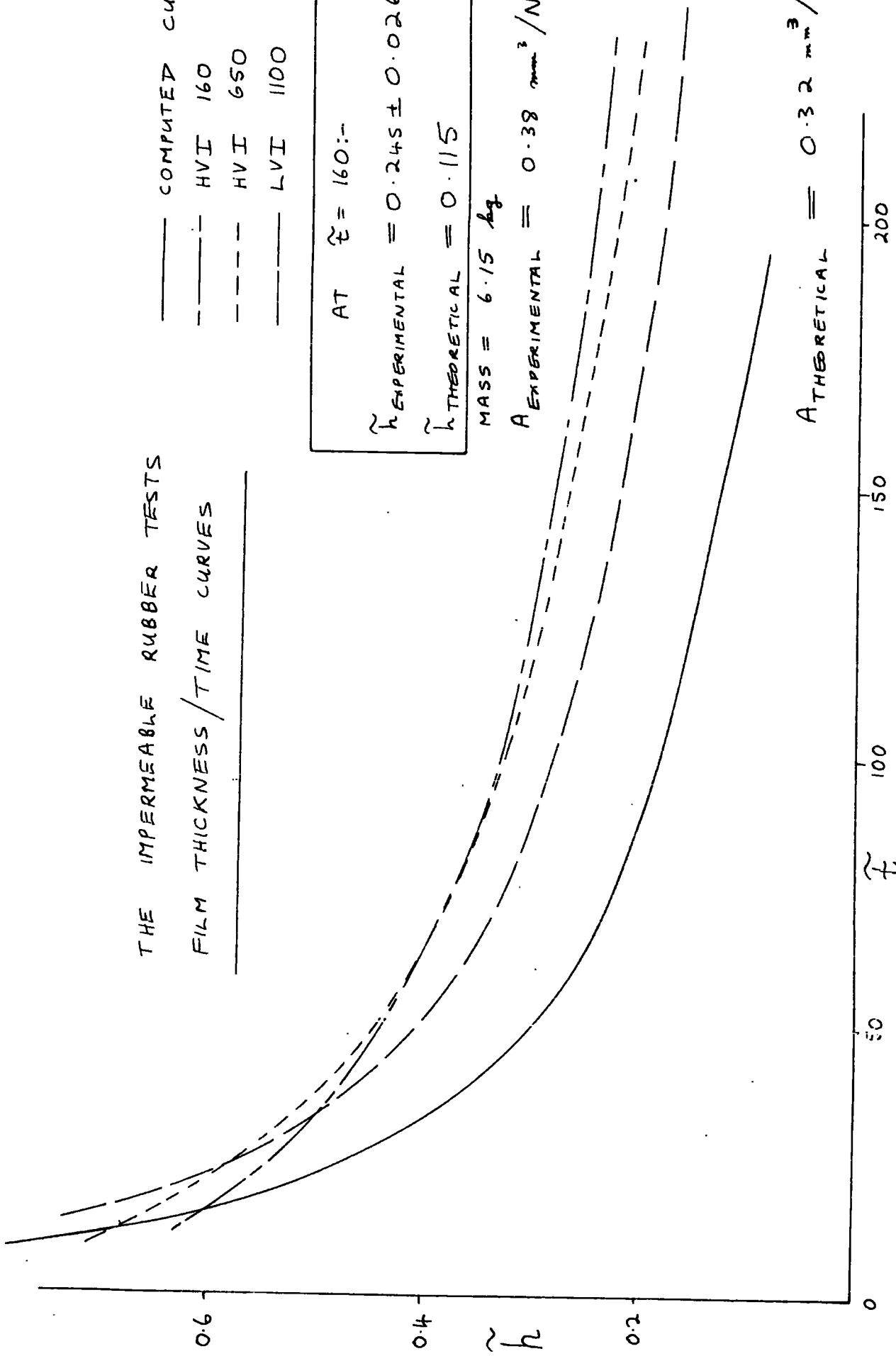
$A_{\text{EXPERIMENTAL}} = 0.42 \text{ mm}^2/\text{N}$
 $A_{\text{THEORETICAL}} = 0.34 \text{ mm}^2/\text{N}$



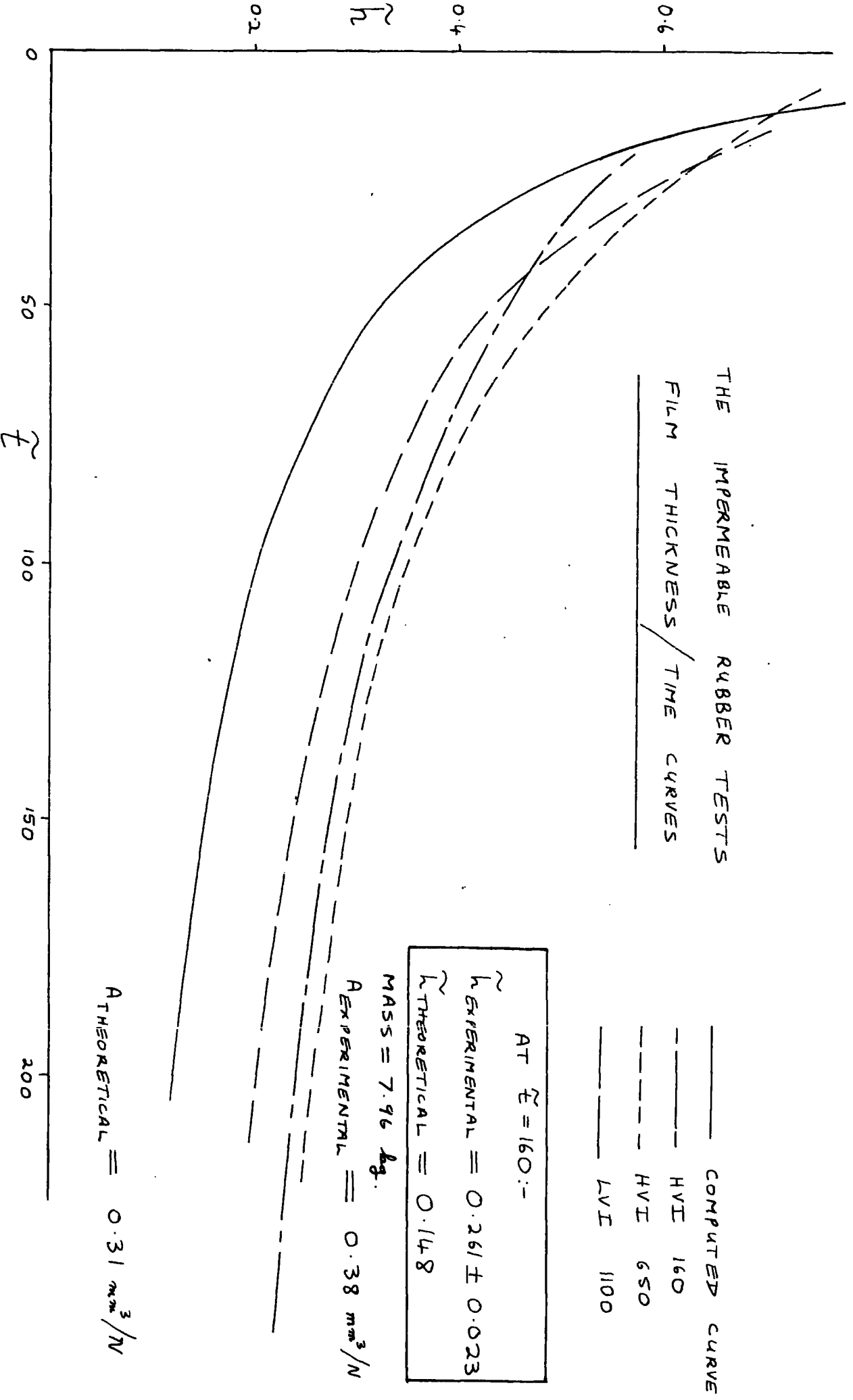
THE IMPERMEABLE RUBBER TESTS
 FILM THICKNESS / TIME CURVES

_____ COMPUTED CURVE
 - - - - - HVI 160
 - - - - - HVI 650
 - - - - - LVI 1100

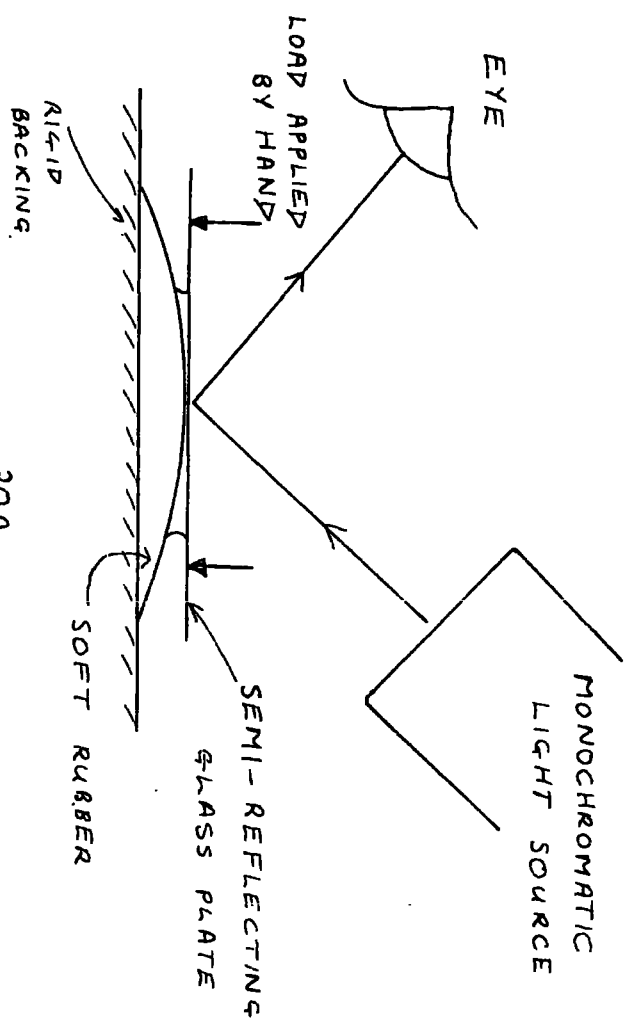
AT $\bar{t} = 160$:-
 $\bar{h}_{\text{EXPERIMENTAL}} = 0.245 \pm 0.026$
 $\bar{h}_{\text{THEORETICAL}} = 0.115$
 MASS = 6.15 kg
 $A_{\text{EXPERIMENTAL}} = 0.38 \text{ mm}^2/\text{N}$



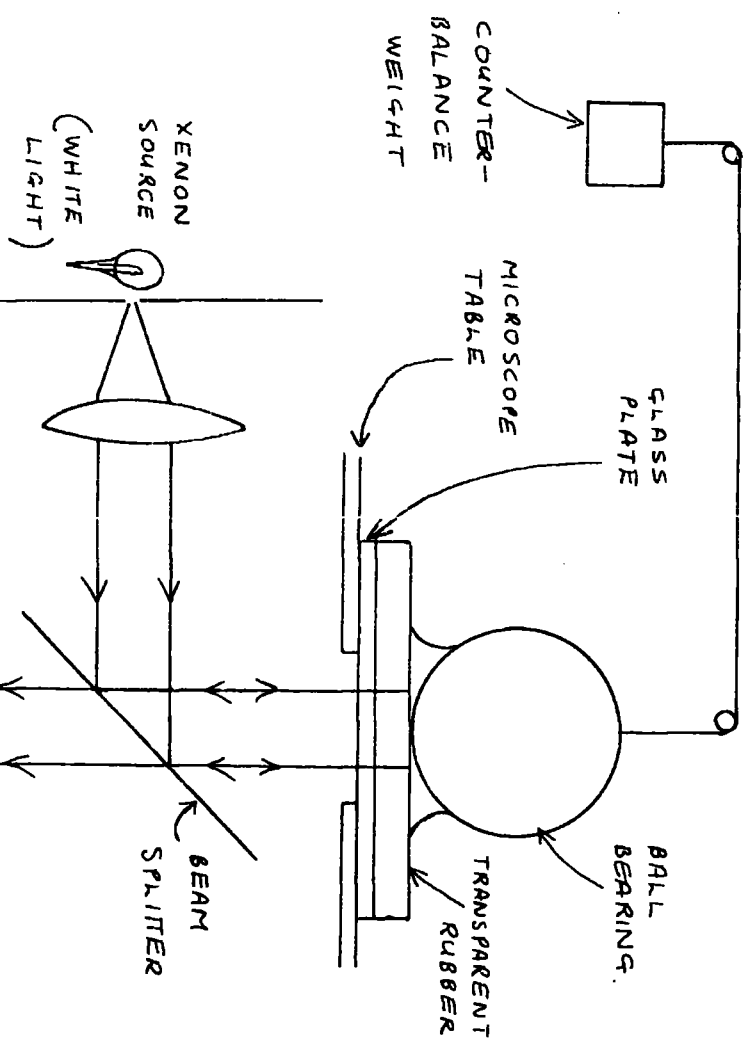
$A_{\text{THEORETICAL}} = 0.32 \text{ mm}^2/\text{N}$



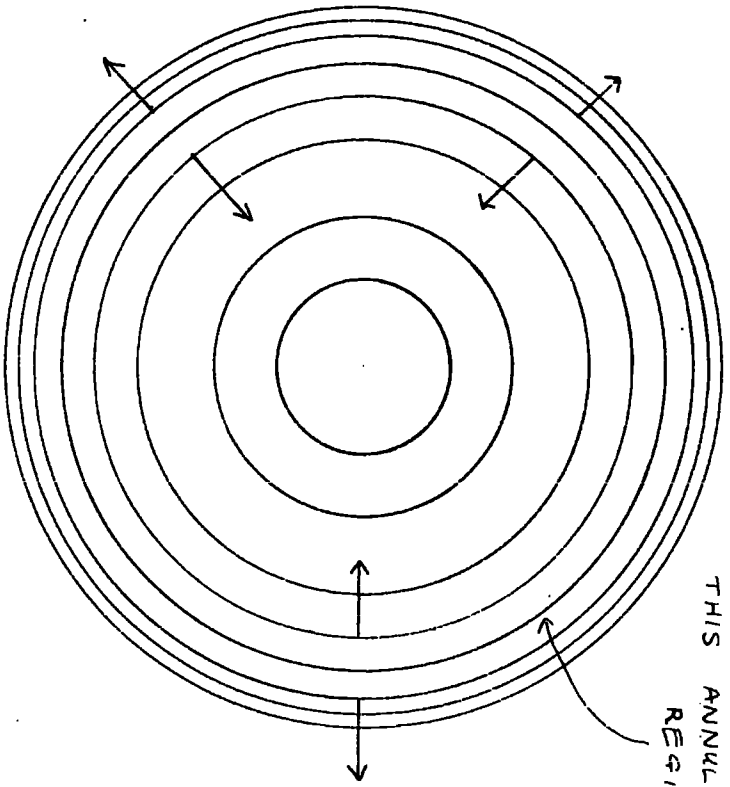
SKETCHES OF THE OPTICAL SYSTEMS
USED TO STUDY ENTRAPMENT.



30A

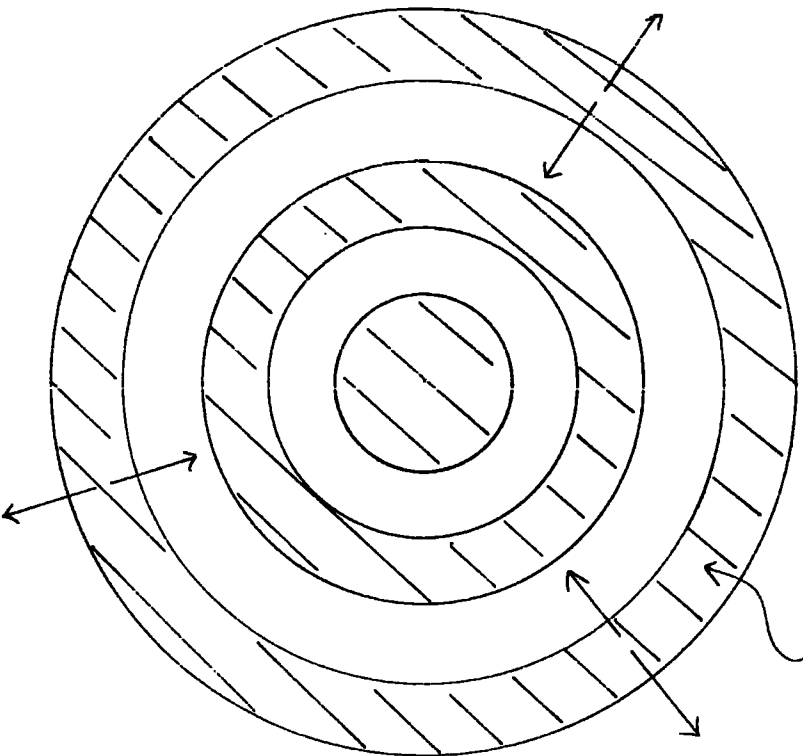


30B



DARK INTERFERENCE
FRINGES APPEAR IN
THIS ANNULAR
REGION

THE SIMPLE ARRANGEMENT



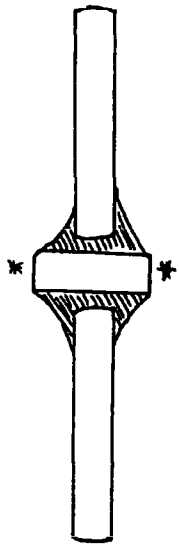
BANDS OF COLOUR MOVE IN
AND OUT FROM THIS RADIUS

THE MICROSCOPE ARRANGEMENT

31A

TYPICAL ENTRAPMENT
FRINGE PATTERNS

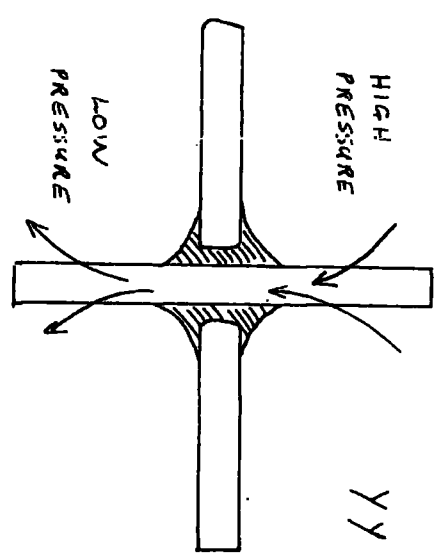
31B



YY

SURFACES DAMAGED
DUE TO CUTTING
MARKED: *

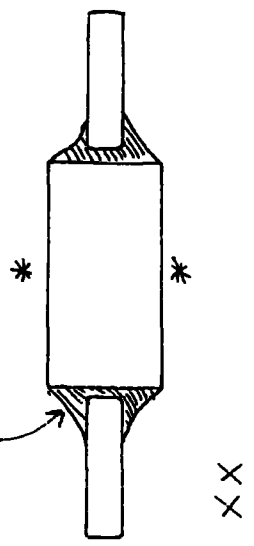
SCALE 1:1



HIGH
PRESSURE

LOW
PRESSURE

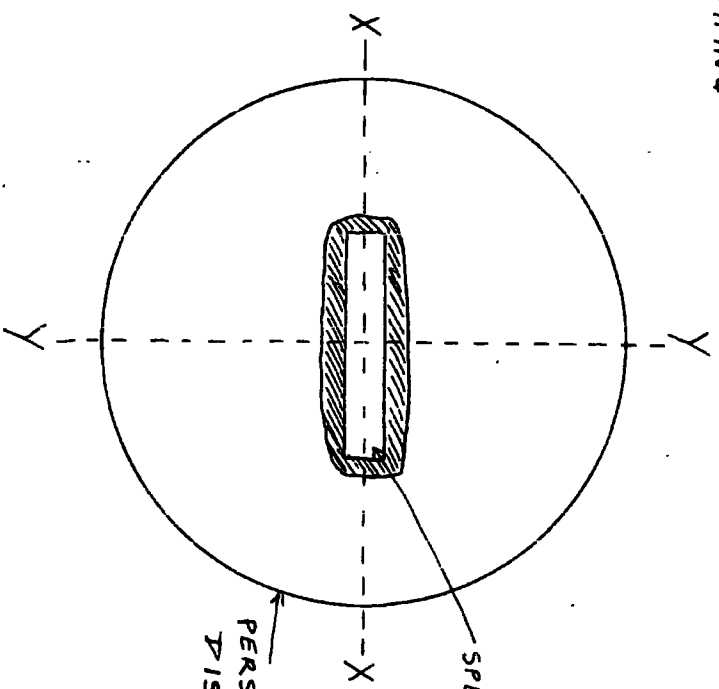
YY



XX

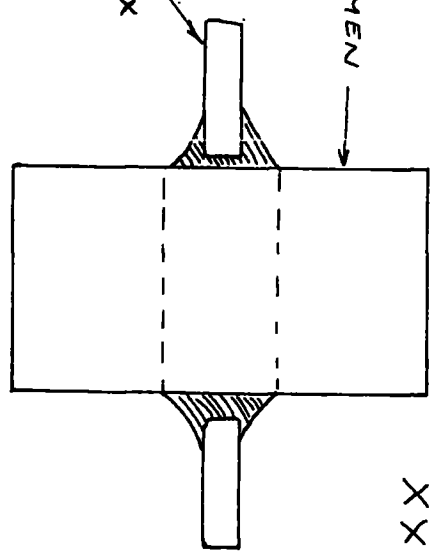
ARALDITE
SEALING

32A



SPECIMEN

PERSPEX
DISC

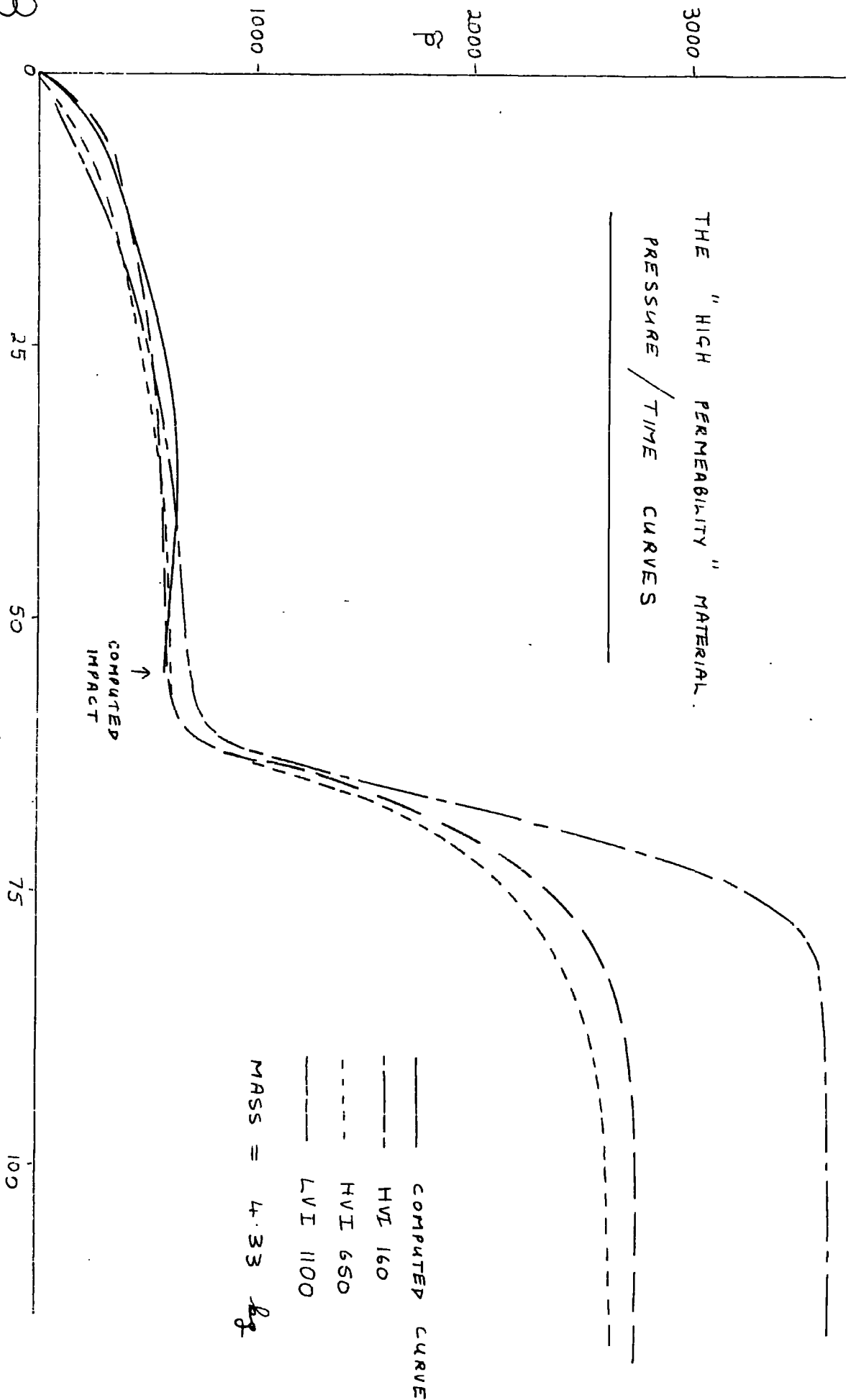


XX

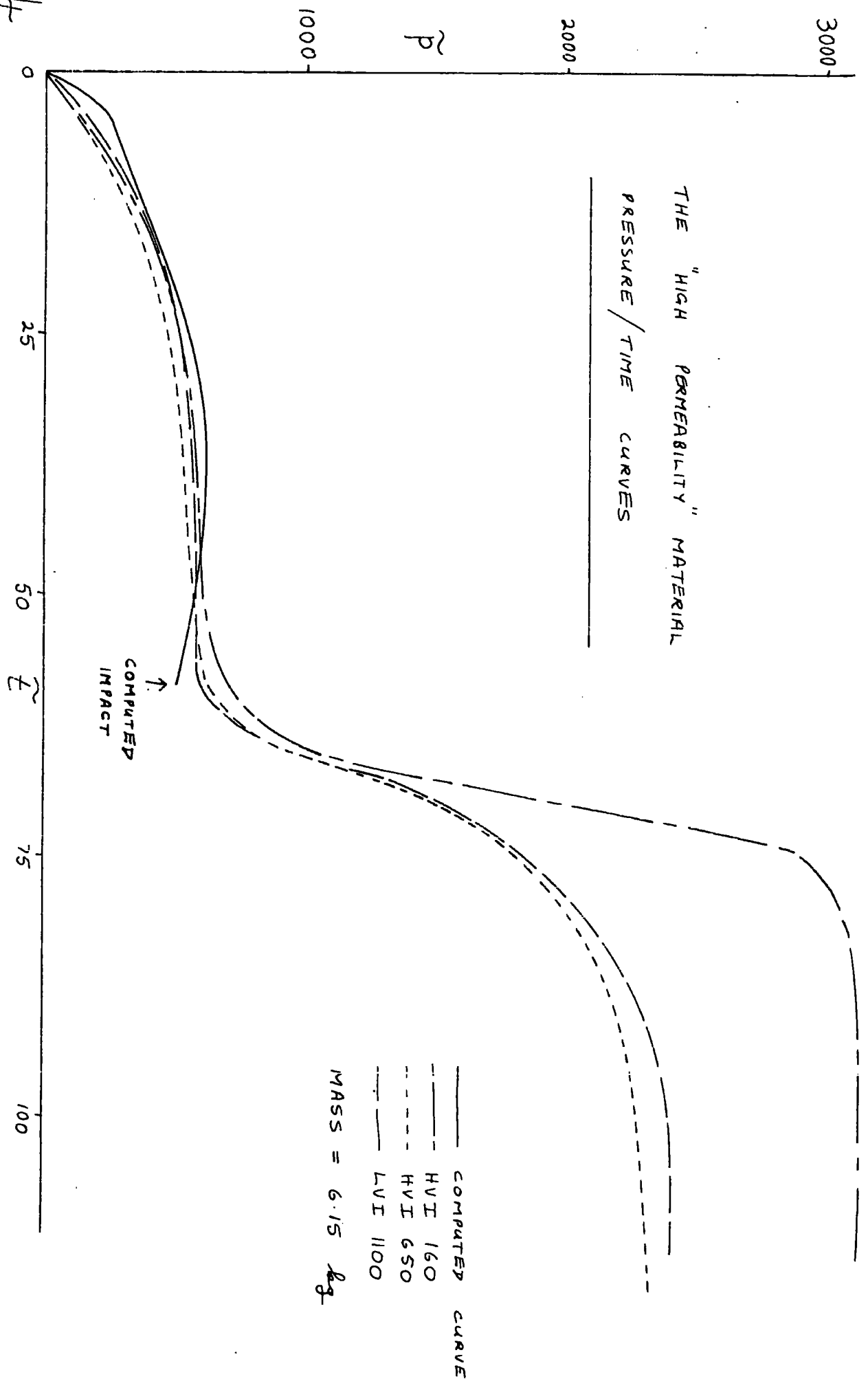
32B

MEASUREMENT OF RADIAL PERMEABILITY

THE "HIGH PERMEABILITY" MATERIAL.
 PRESSURE / TIME CURVES

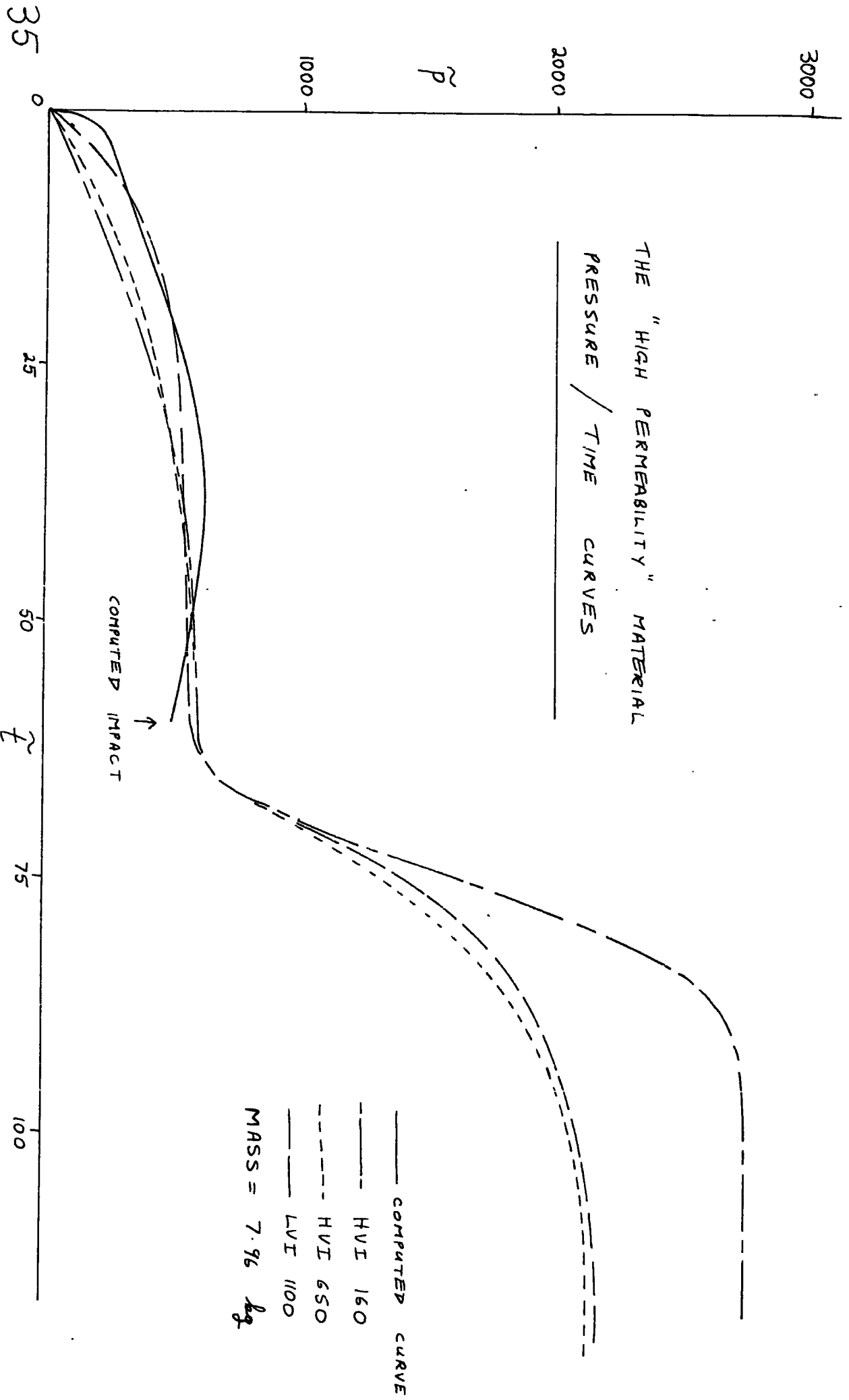


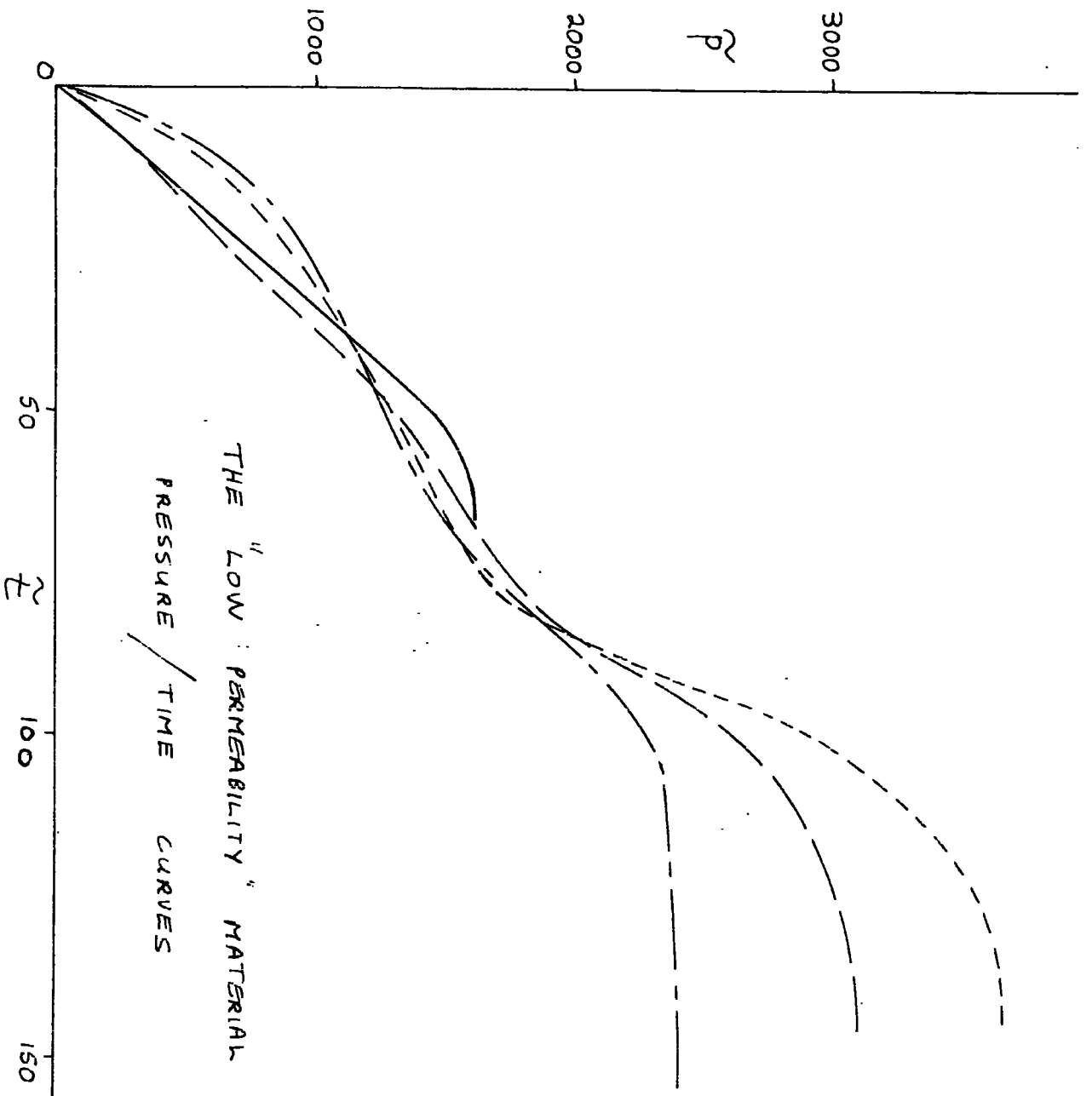
THE "HIGH PERMEABILITY" MATERIAL
PRESSURE / TIME CURVES



——— COMPUTED CURVE
 - - - HVI 160
 - · - HVI 650
 - - - LVI 1100
 MASS = 6.15 kg

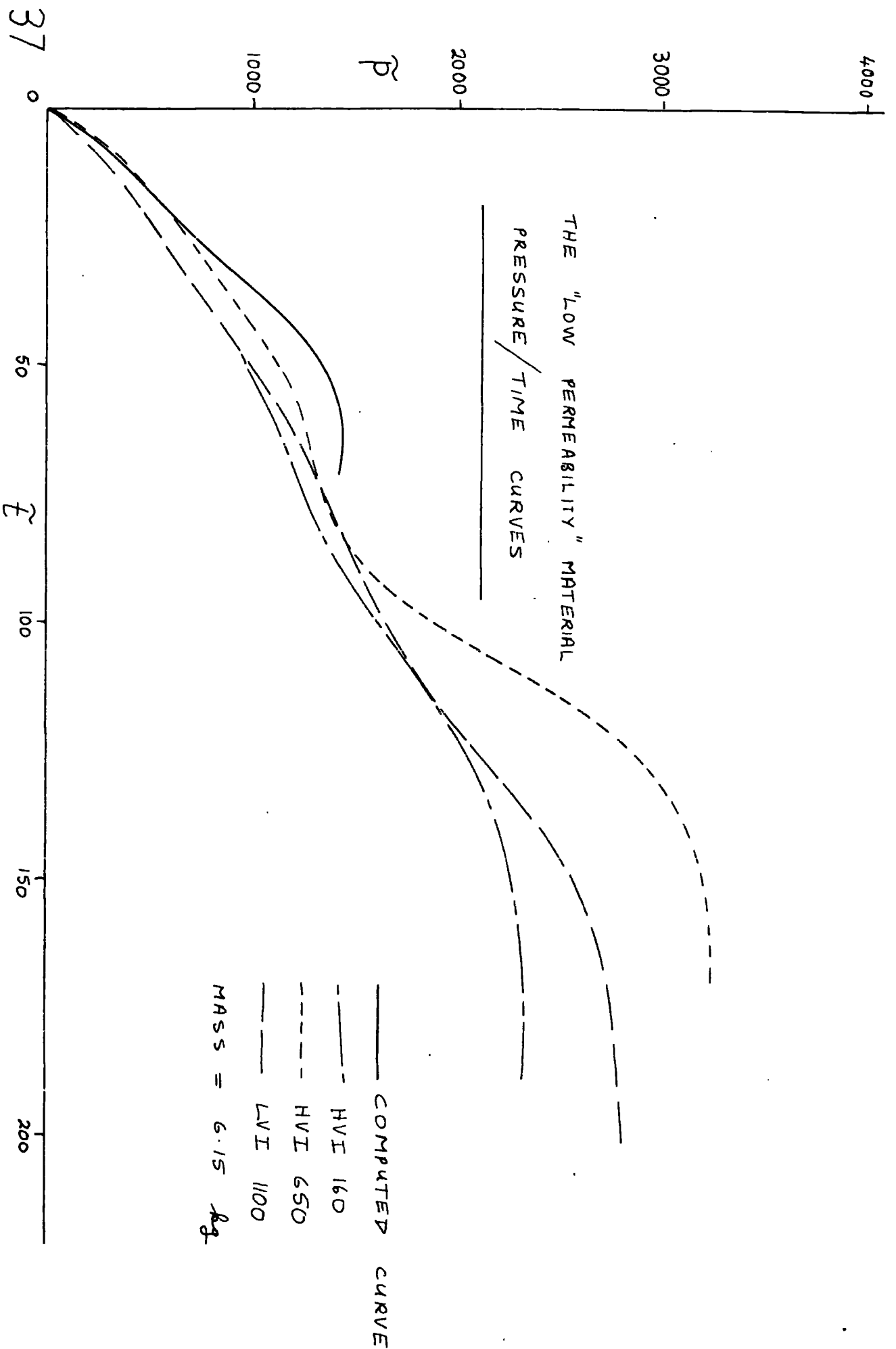
THE "HIGH PERMEABILITY" MATERIAL
PRESSURE / TIME CURVES



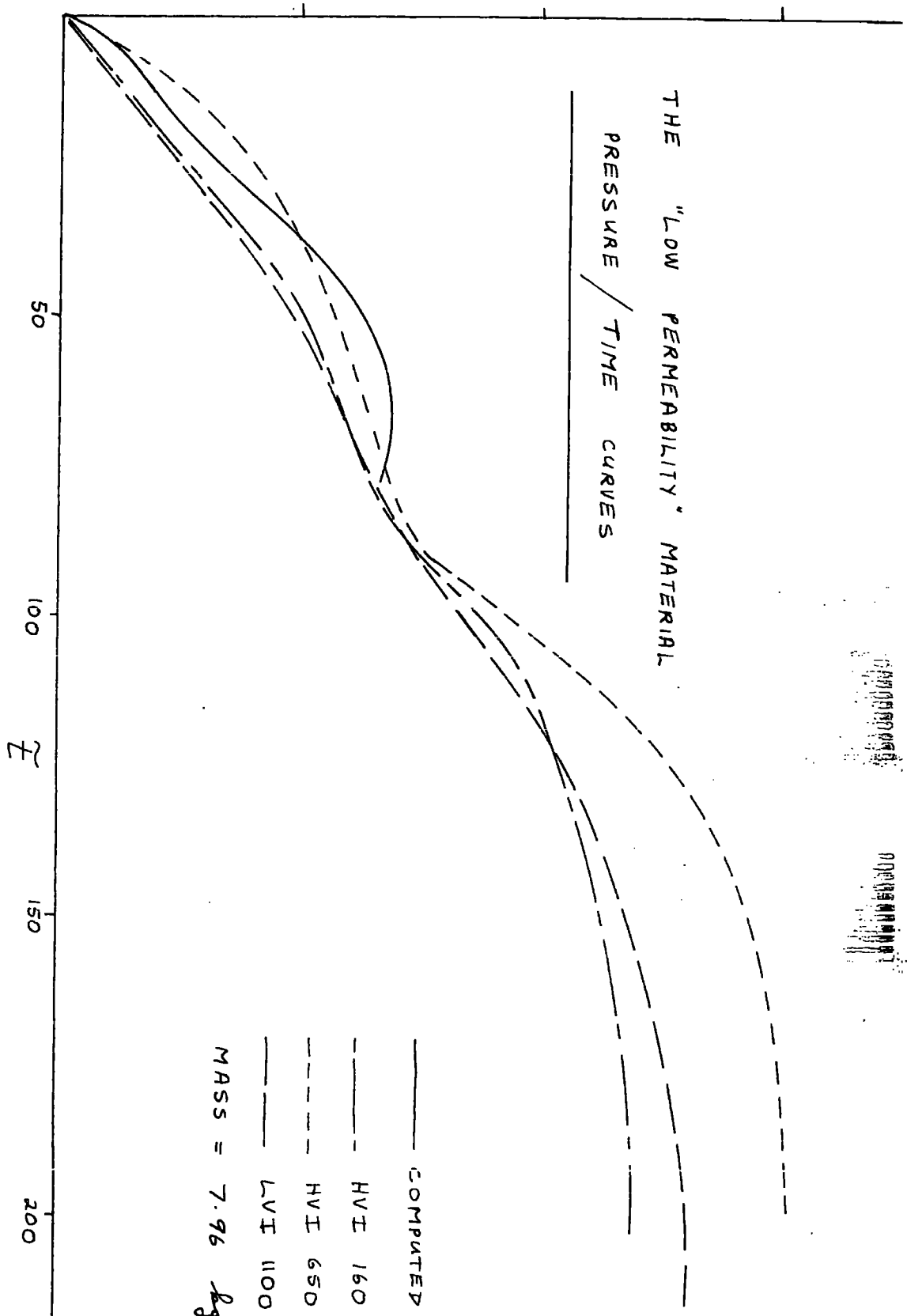


THE "LOW PERMEABILITY" MATERIAL
 PRESSURE / TIME CURVES

- COMPUTED CURVE
 - - - HVI 160
 - · - · - HVI 650
 - LVI 1100
- MASS = 4.33 g



38 °



THE "LOW PERMEABILITY" MATERIAL
 PRESSURE / TIME CURVES

— COMPUTED CURVE
 - - - HVI 160
 - · - HVI 650
 - - - LVI 1100
 MASS = 7.96 g

t

200

150

100

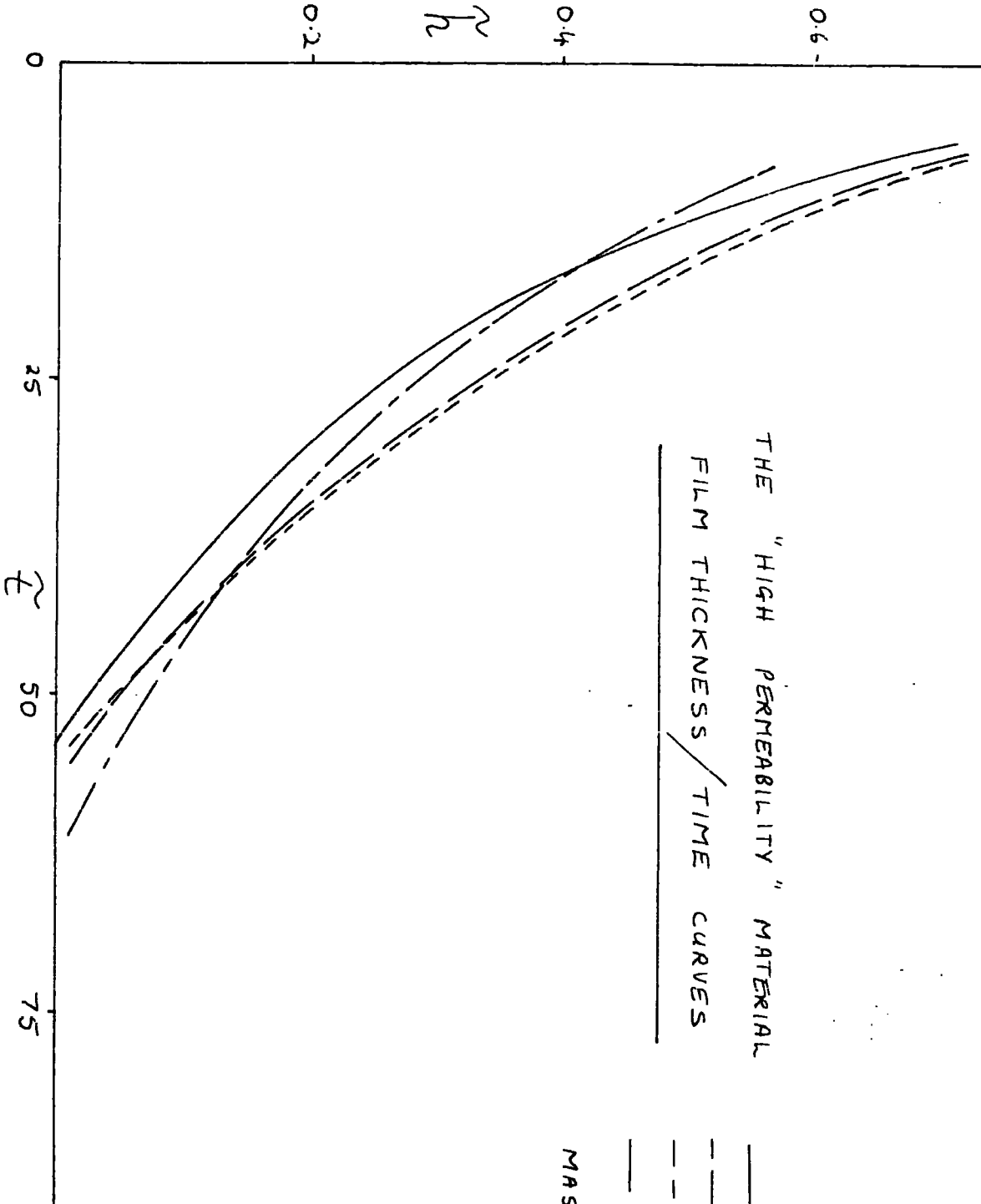
50

2000

3000

1000

p

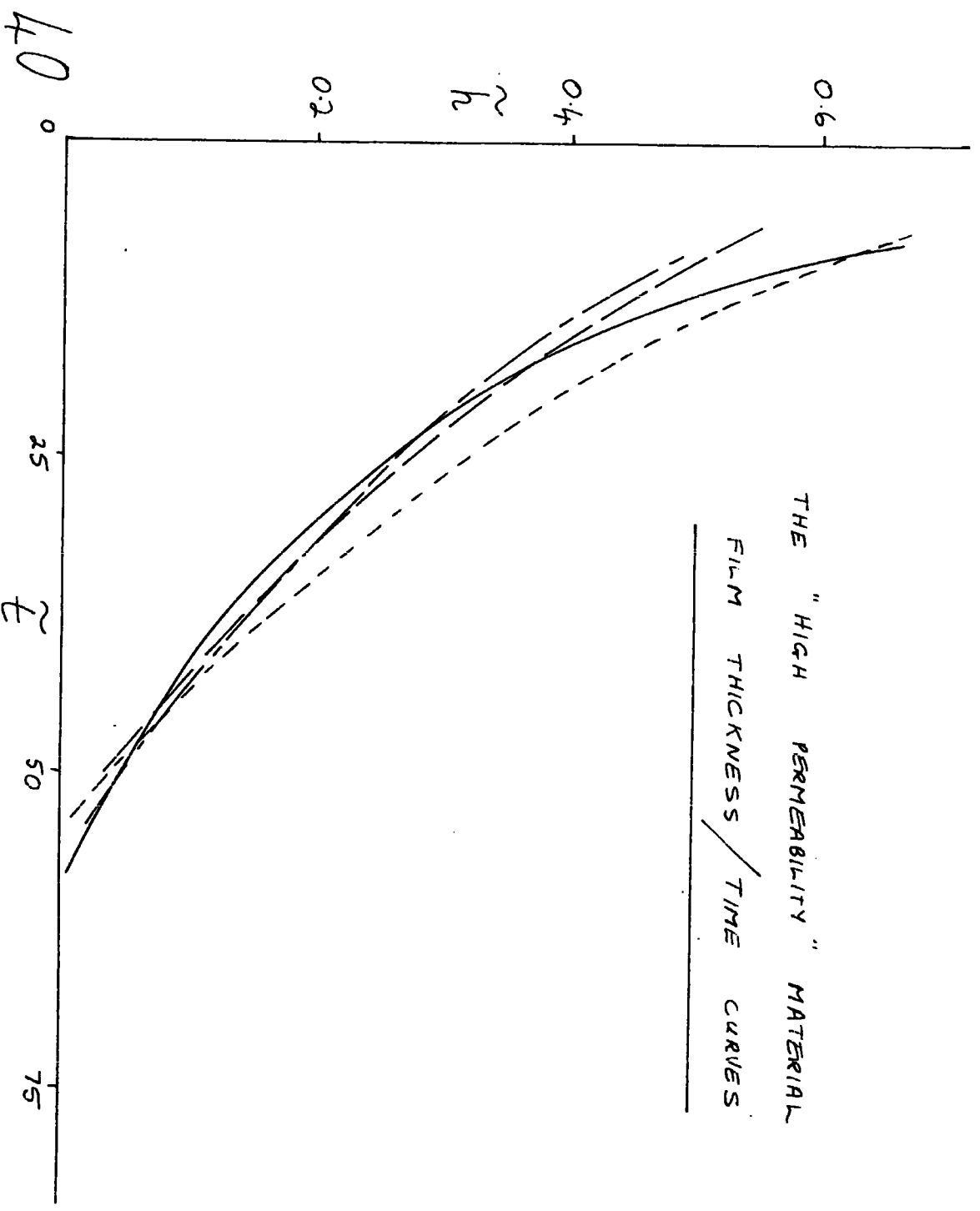


THE "HIGH PERMEABILITY" MATERIAL
 FILM THICKNESS / TIME CURVES

COMPUTED IMPACT

_____	HVI 160
-----	HVI 650
- . - . -	LVI 1100

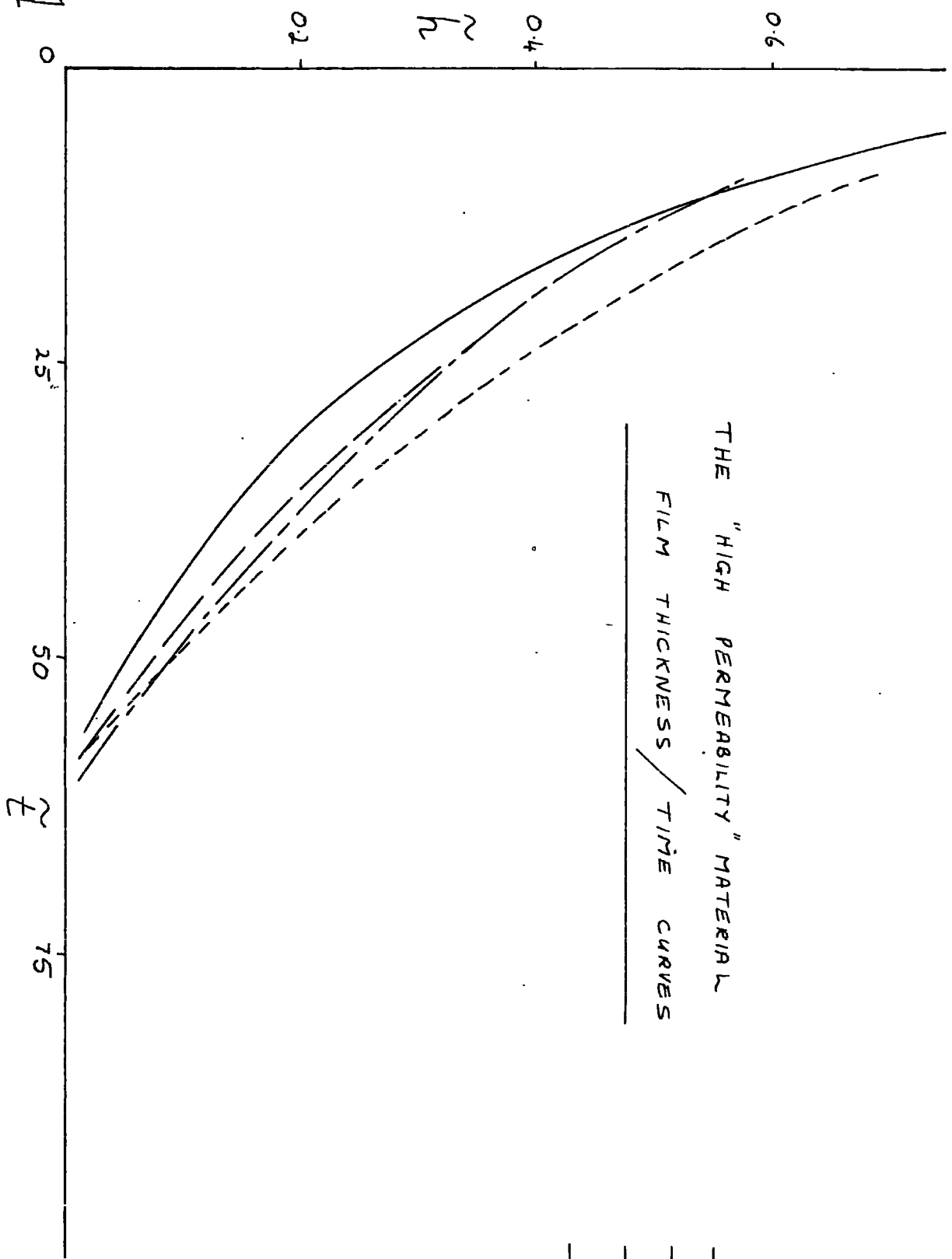
MASS = 4.33 *kg*



THE "HIGH PERMEABILITY" MATERIAL
 FILM THICKNESS / TIME CURVES

_____ COMPUTED CURVE
 _____ HVI 160
 - - - - - HVI 650
 _____ LVI 1100
 MASS = 6.15 *kg*

41

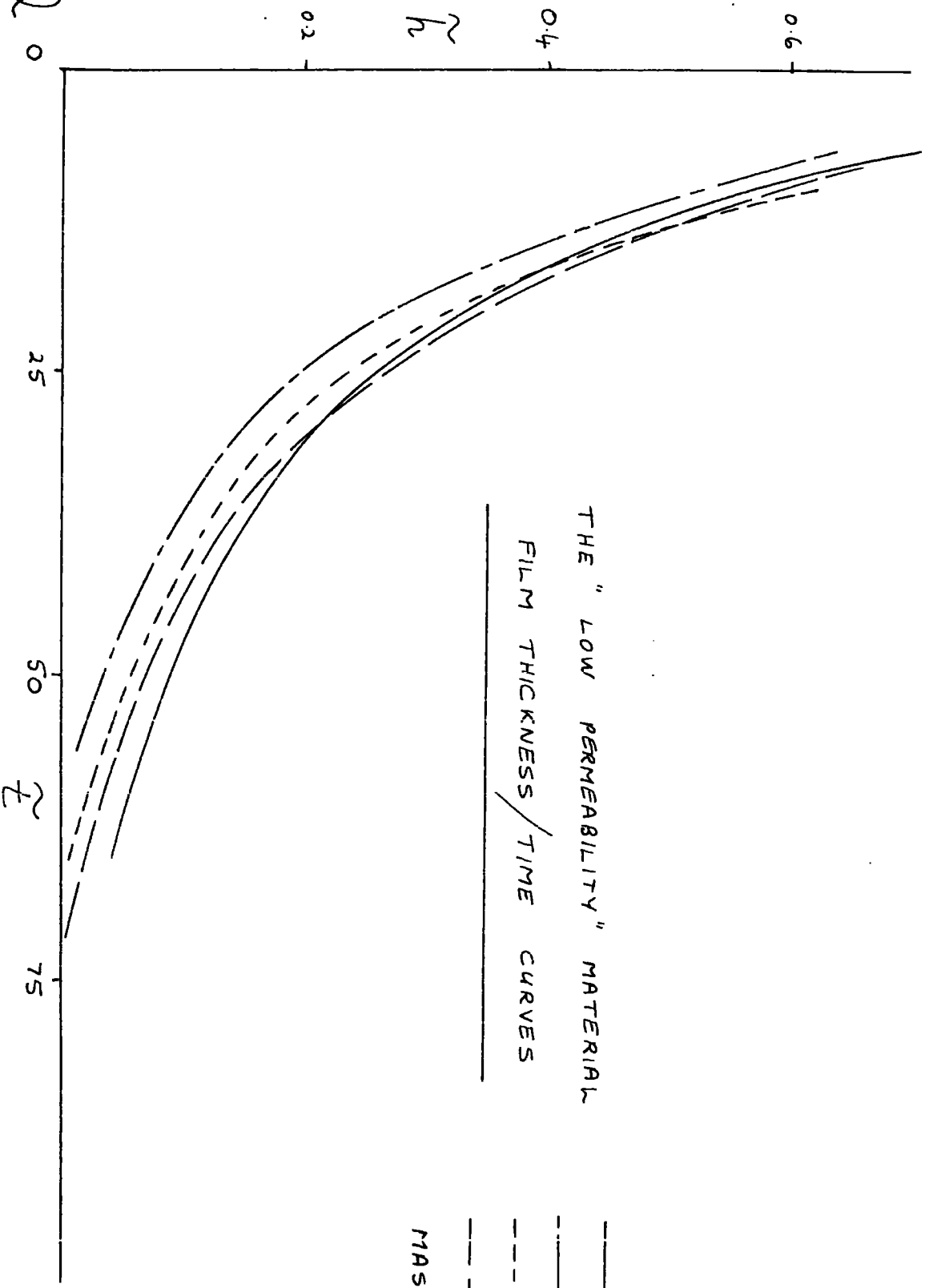


THE "HIGH PERMEABILITY" MATERIAL
 FILM THICKNESS / TIME CURVES

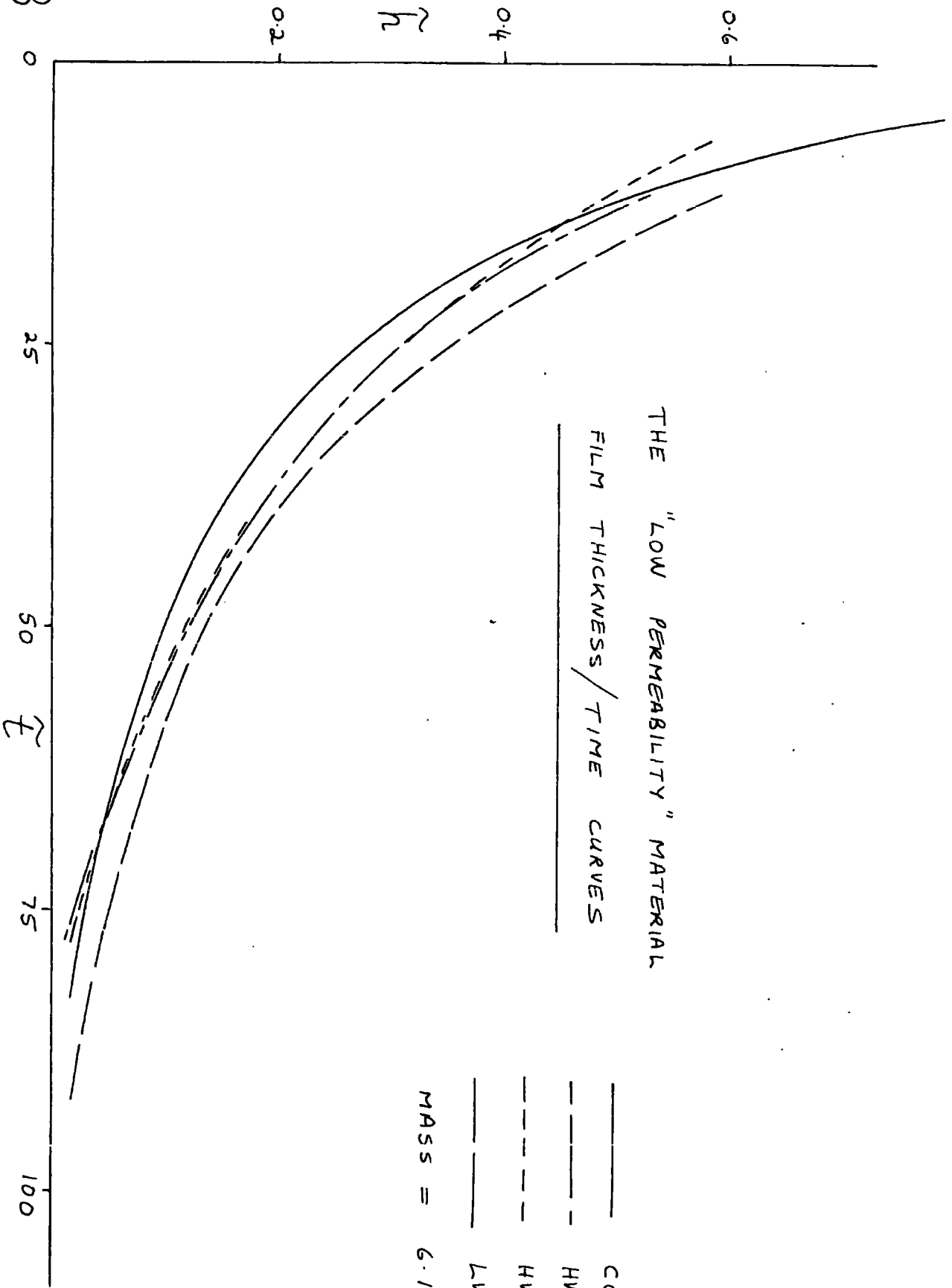
————— COMPUTED CURVE
 - - - - - HVI 160
 - · - · - HVI 650
 _____ LVI 1100

MASS = 7.96 g

4.2



43

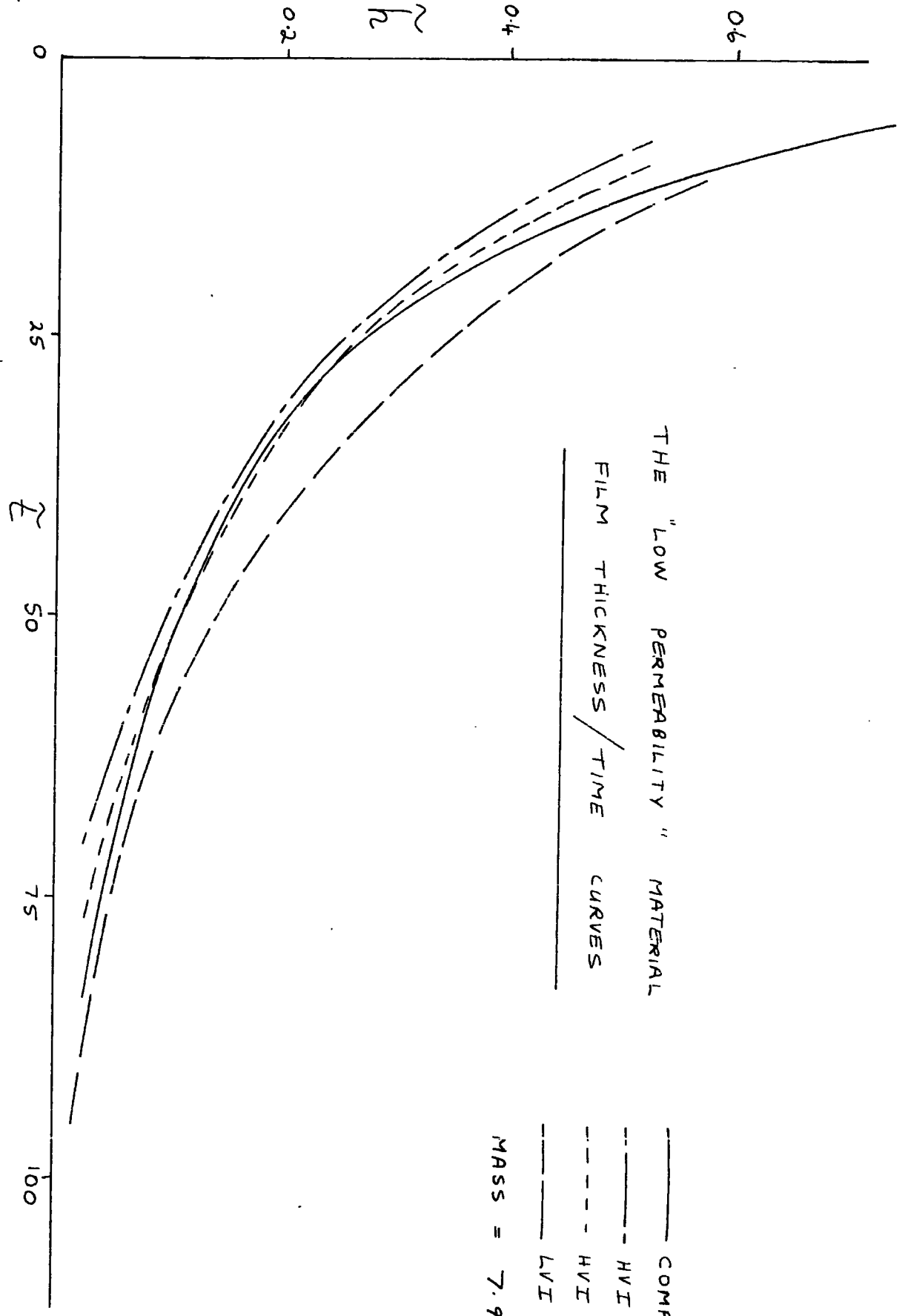


THE "LOW PERMEABILITY" MATERIAL

FILM THICKNESS / TIME CURVES

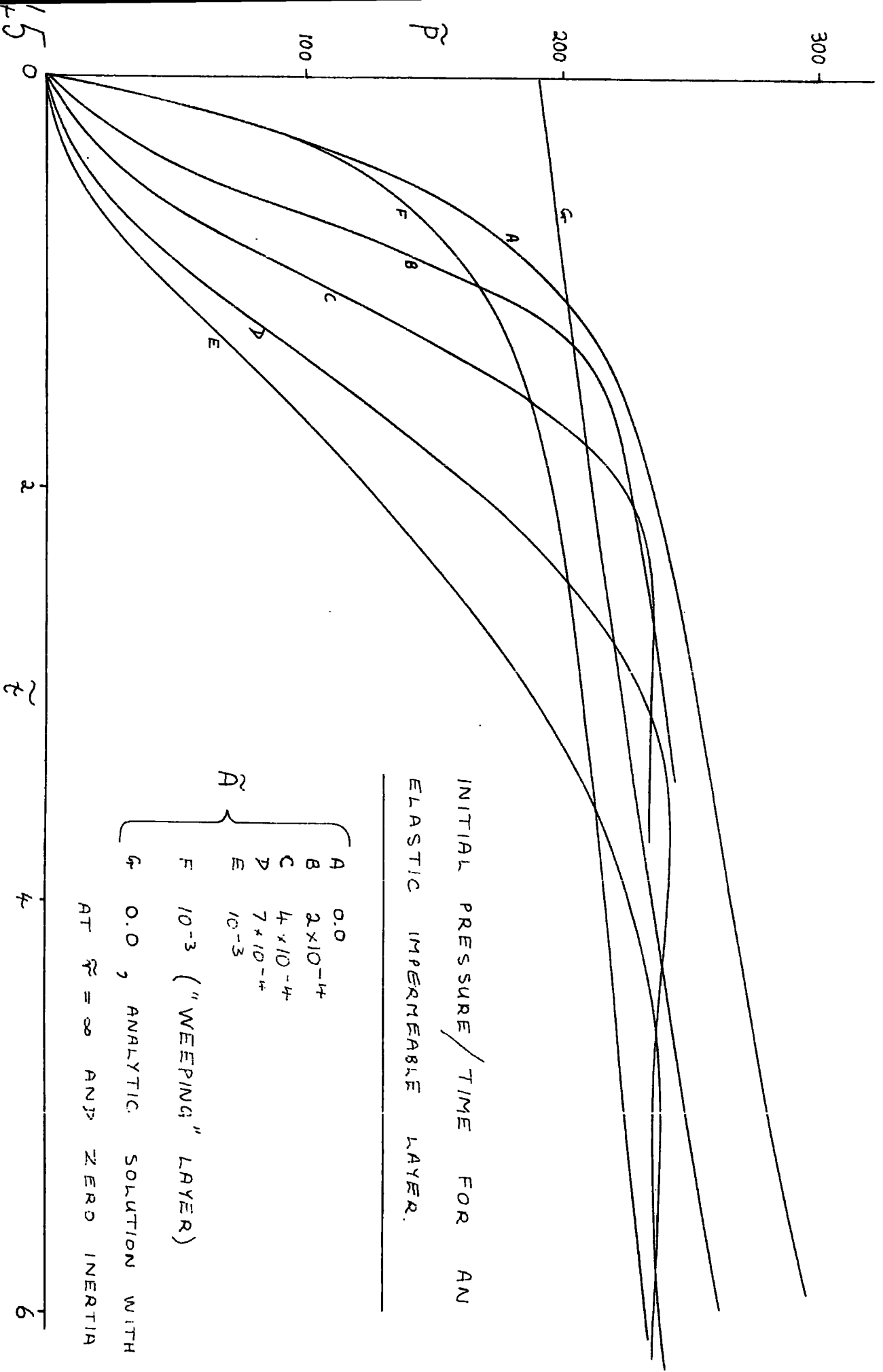
- _____ COMPUTED CURVE
 - HVI 160
 - - - - - HVI 650
 - _____ LVI 1100
- MASS = 6.15 kg

44



THE "LOW PERMEABILITY" MATERIAL
 FILM THICKNESS / TIME CURVES

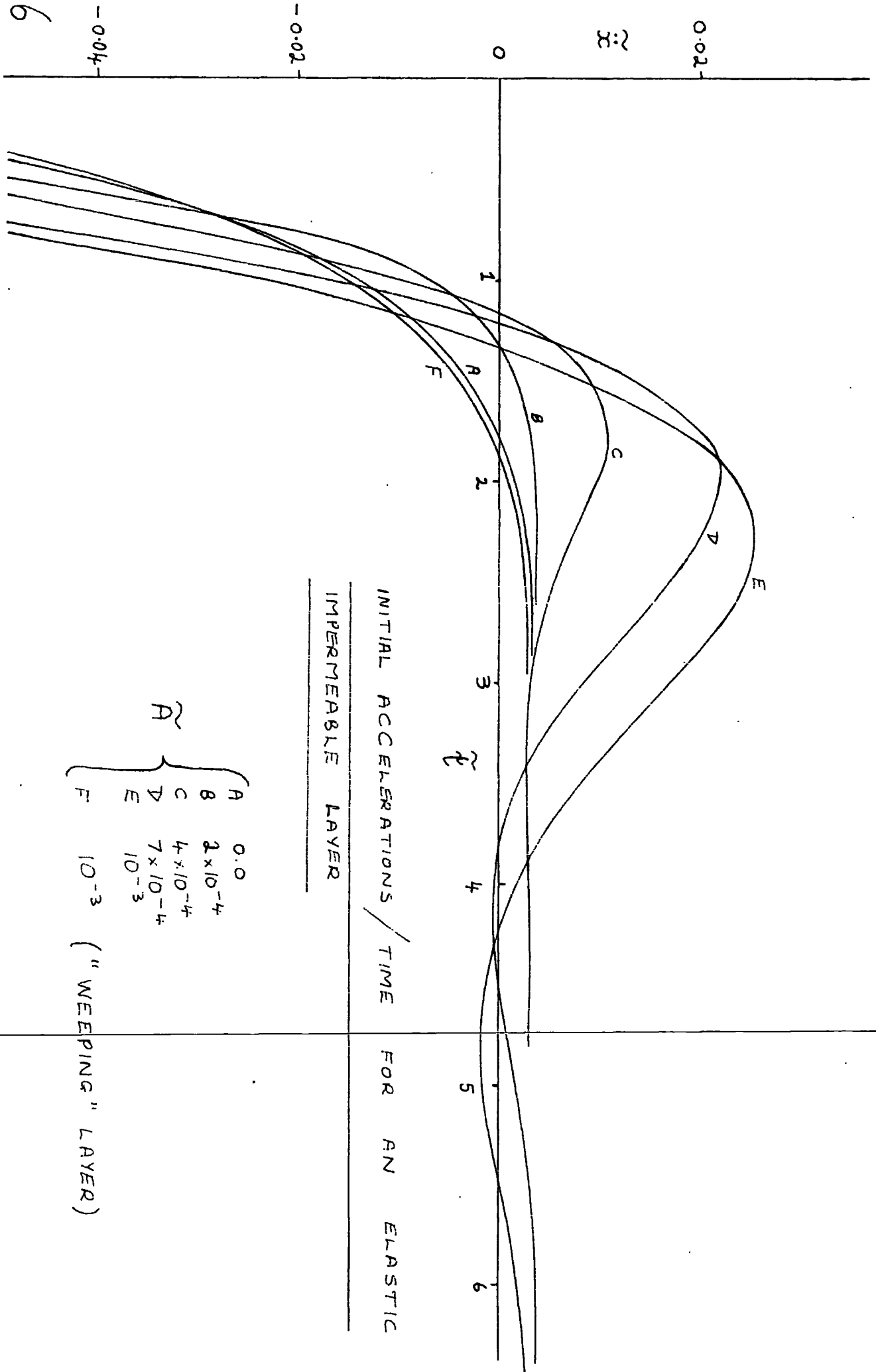
_____ COMPUTED CURVE
 - - - - - HVI 160
 - - - - - HVI 650
 - . - . - LVI 1100
 MASS = 7.96 g



INITIAL PRESSURE / TIME FOR AN
ELASTIC IMPERMEABLE LAYER.

Curve	Initial Pressure
A	0.0
B	2×10^{-4}
C	4×10^{-4}
D	7×10^{-4}
E	10^{-3}
F	10^{-3} ("weeping" layer)
G	0.0, analytic solution with $\bar{r}_2=0$

AT $\bar{r}_2 = \infty$ AND ZERO INERTIA

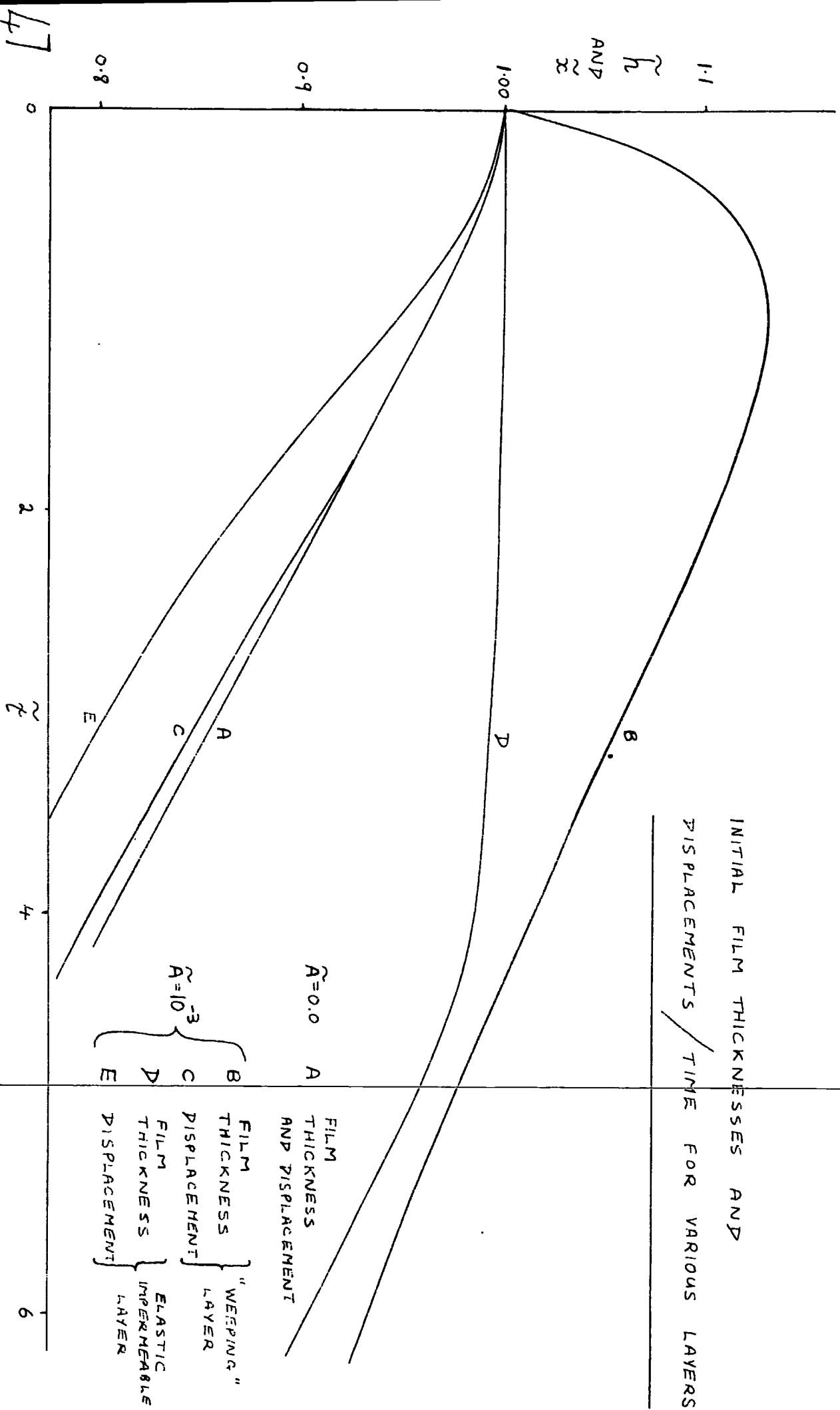


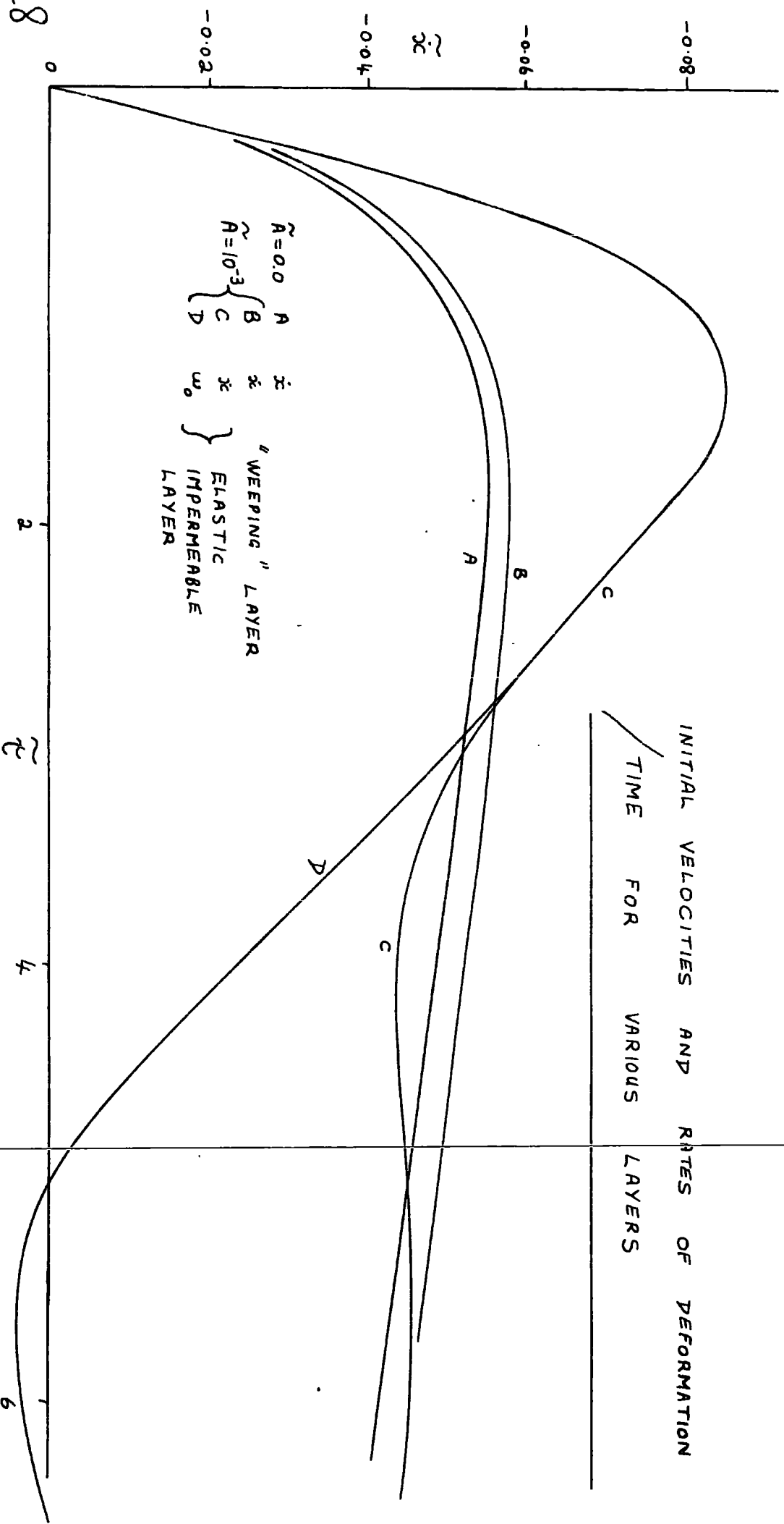
INITIAL ACCELERATIONS / TIME FOR AN ELASTIC
IMPERMEABLE LAYER

A	0.0
B	2×10^{-4}
C	4×10^{-4}
D	7×10^{-4}
E	10^{-3}
F	10^{-3}

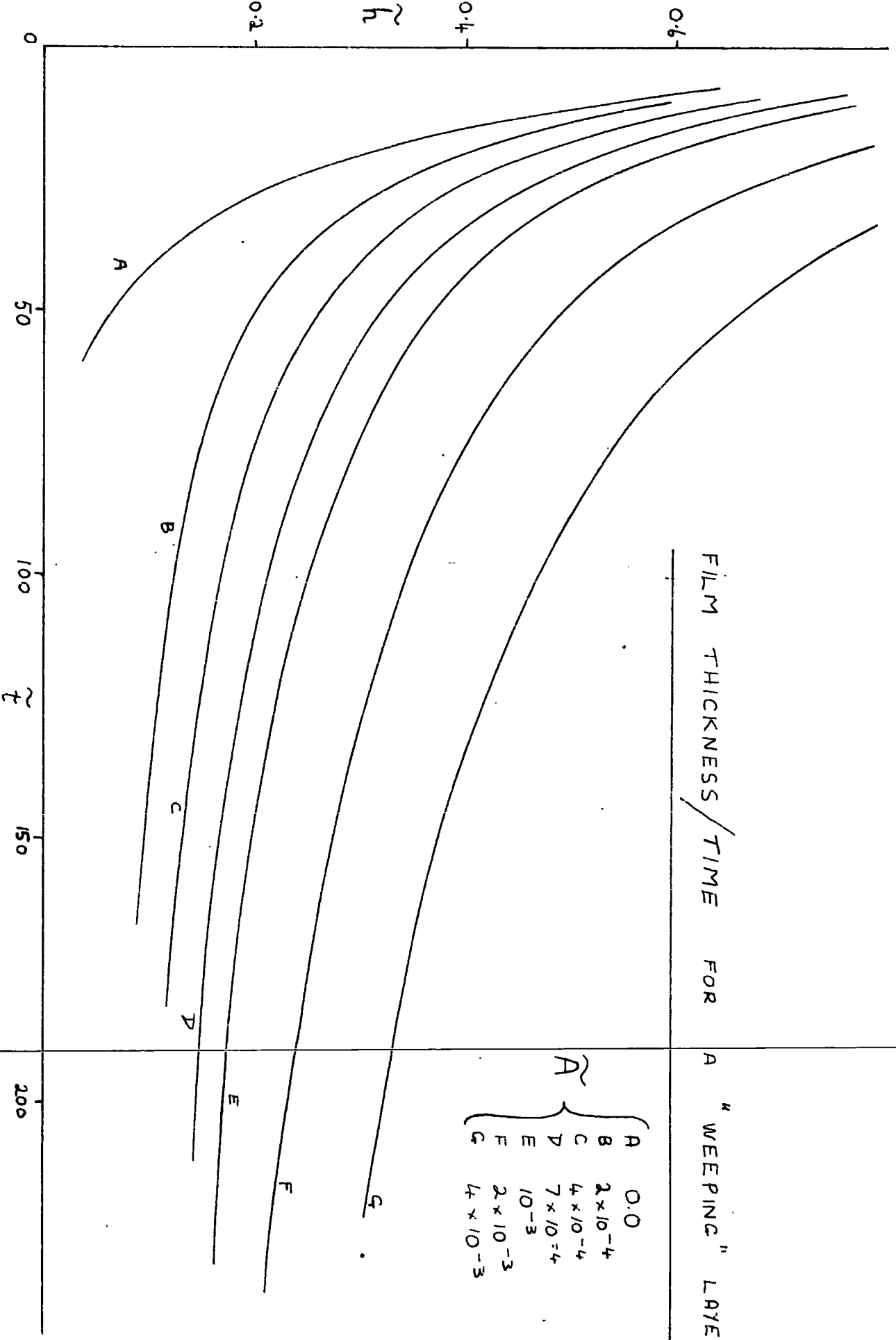
(" WEEPING " LAYER)

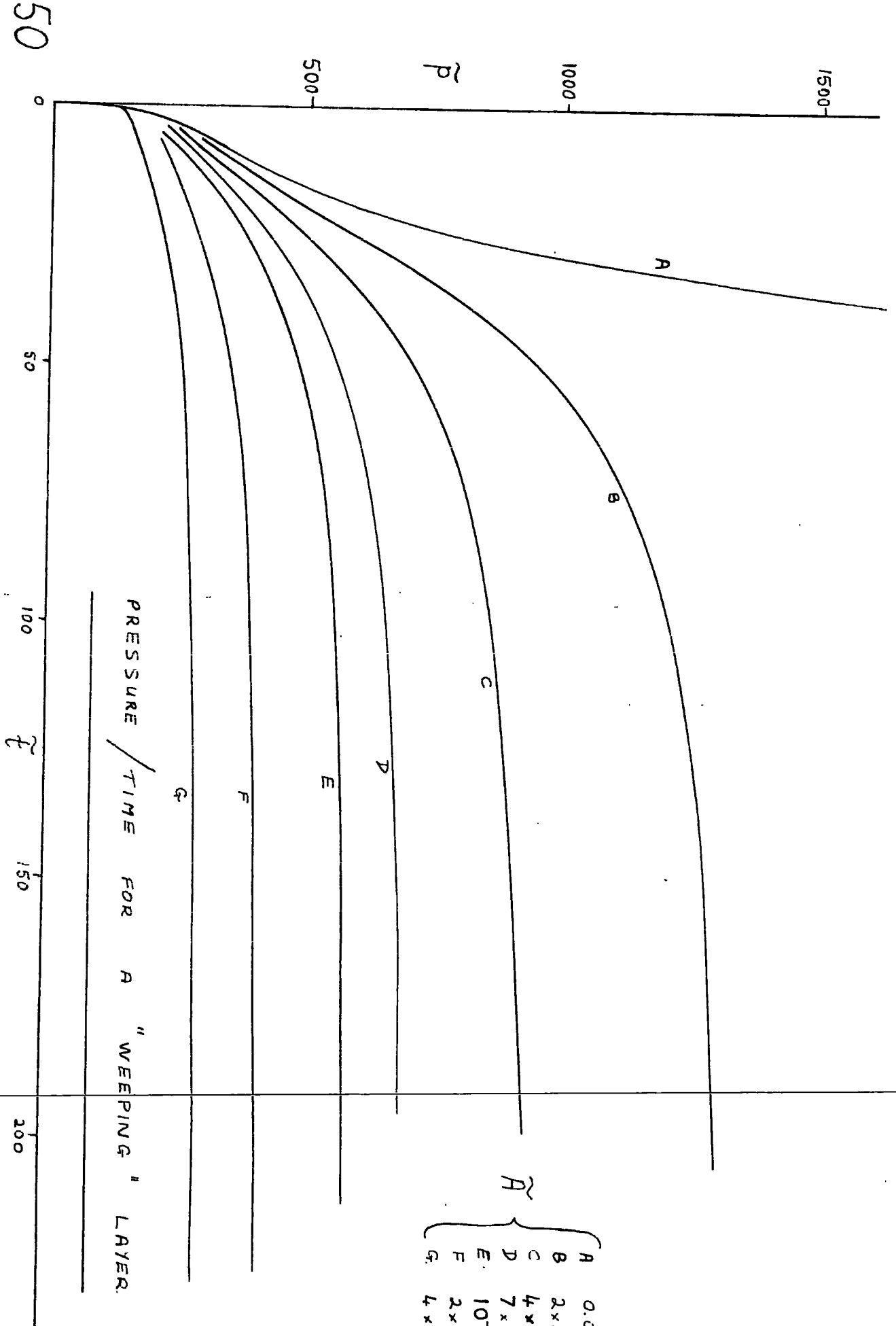
INITIAL FILM THICKNESSES AND
DISPLACEMENTS / TIME FOR VARIOUS LAYERS



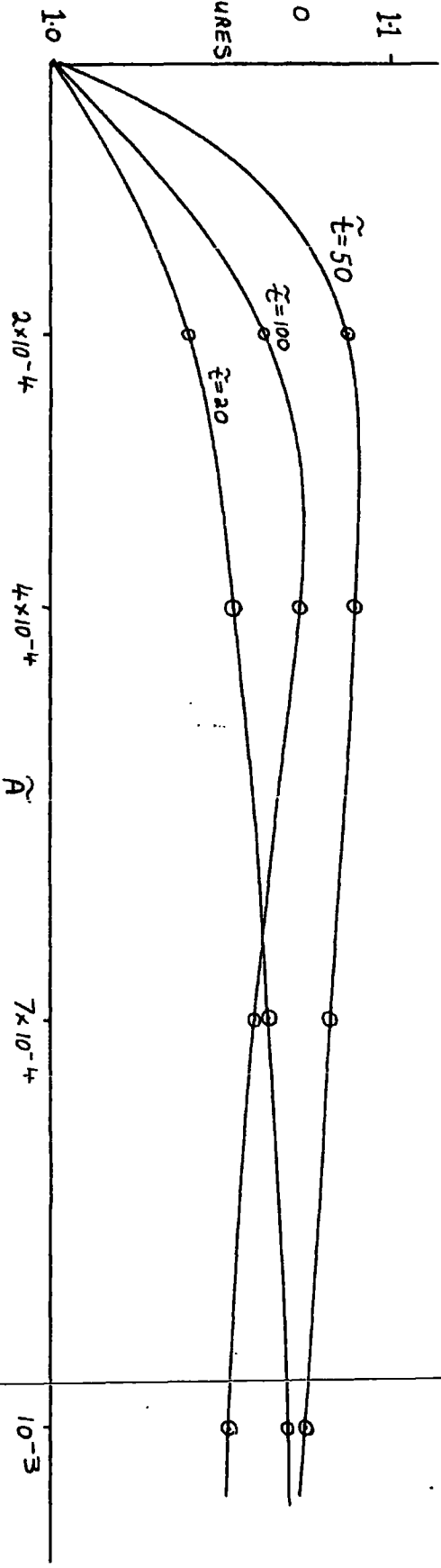


49



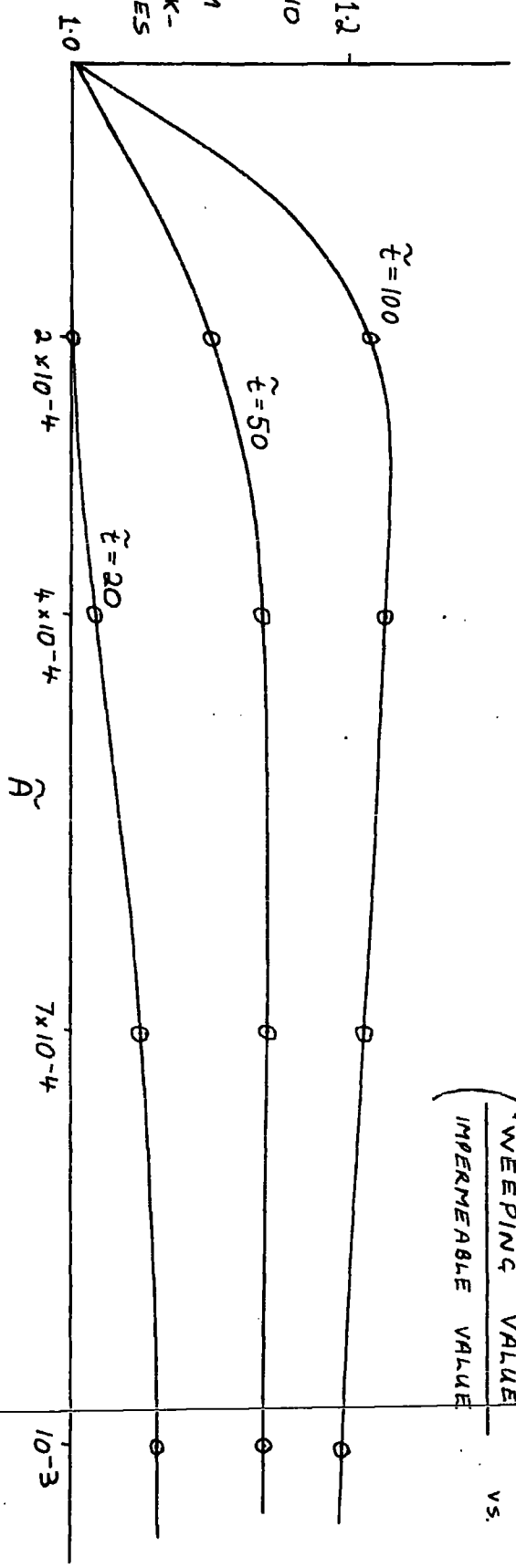


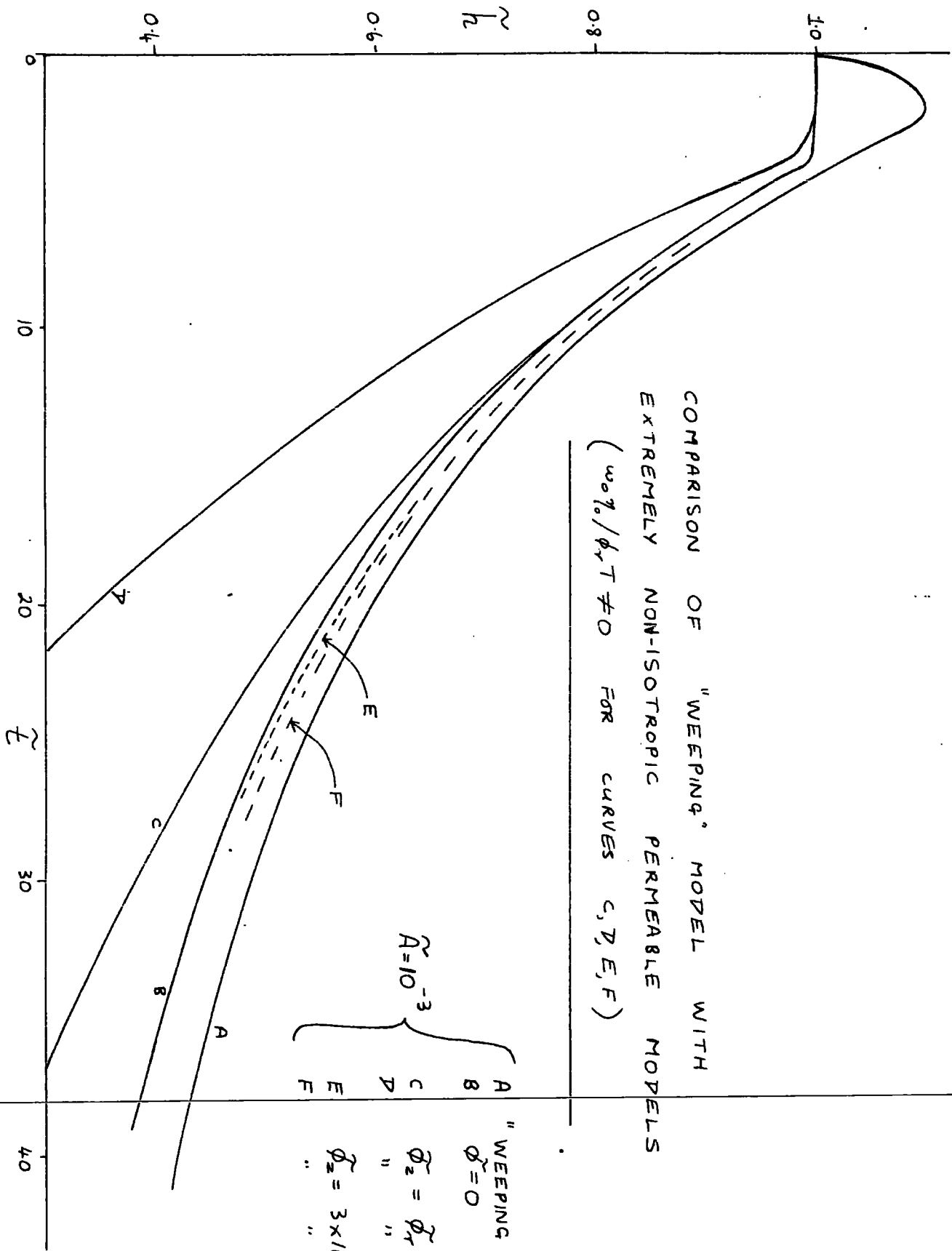
\tilde{A}	Value
A	0.0
B	2×10^{-4}
C	4×10^{-4}
D	7×10^{-4}
E	10^{-3}
F	2×10^{-3}
G	4×10^{-3}



COMPARISON OF THE "WEEPING" MODEL WITH THE IMPERMEABLE MODEL

("WEEPING" VALUE
 IMPERMEABLE VALUE
 vs. \tilde{A})

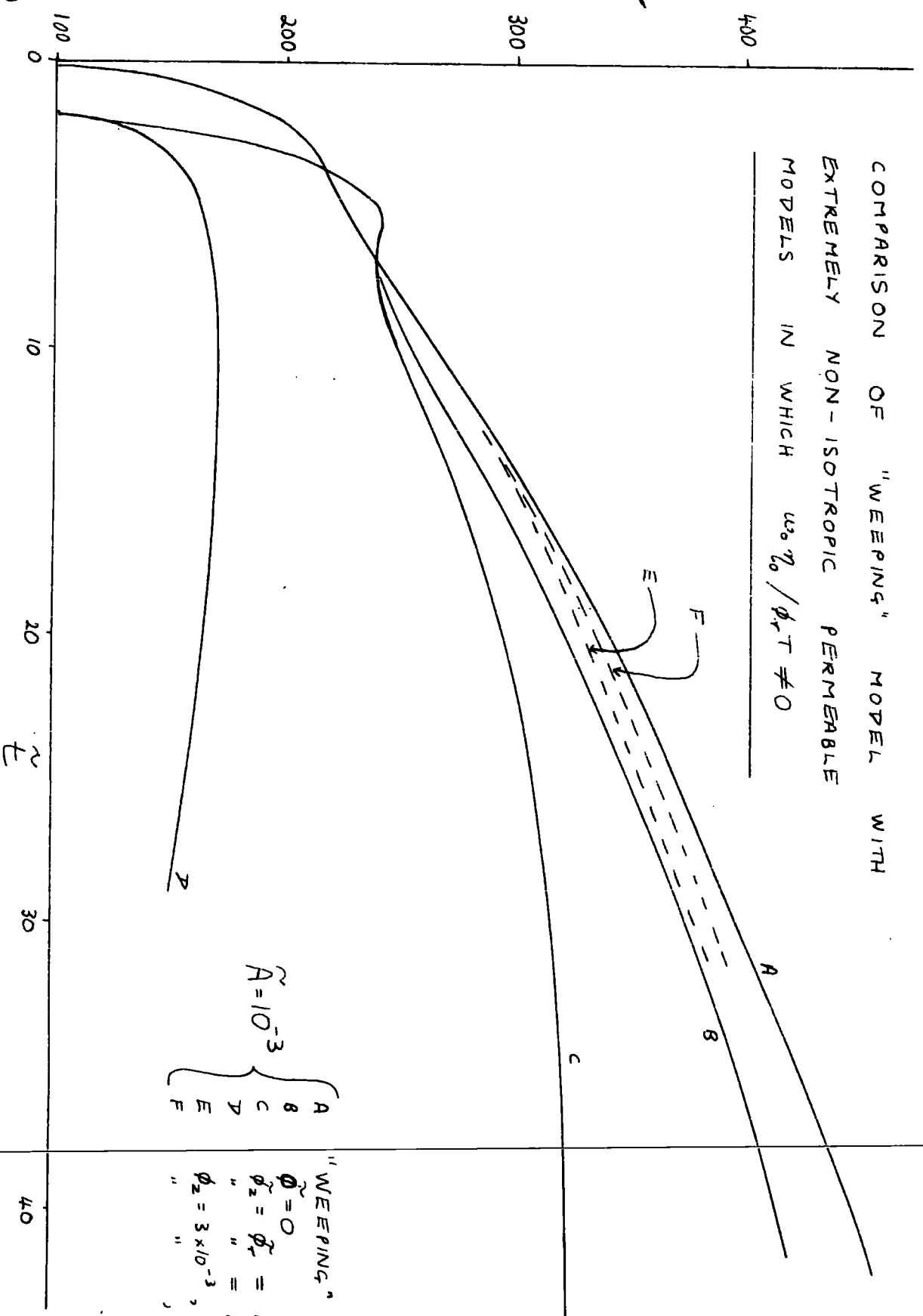




COMPARISON OF "WEEPING" MODEL WITH
EXTREMELY NON-ISOTROPIC PERMEABLE MODELS
($w_0\%/\phi_r T \neq 0$ FOR CURVES C, D, E, F)

$\tilde{A} = 10^{-3}$	}	A	" WEEPING " MODEL		
		B	$\phi_r = 0$		
		C	$\phi_z = \phi_r = 10^{-3}$		
		D	" " " " " " " " " " " "	10^{-2}	
		E	$\phi_z = 3 \times 10^{-3}$		$\phi_r = 3 \times 10^{-5}$
		F	" " " " " " " " " " " "		$\phi_r = 3 \times 10^{-6}$

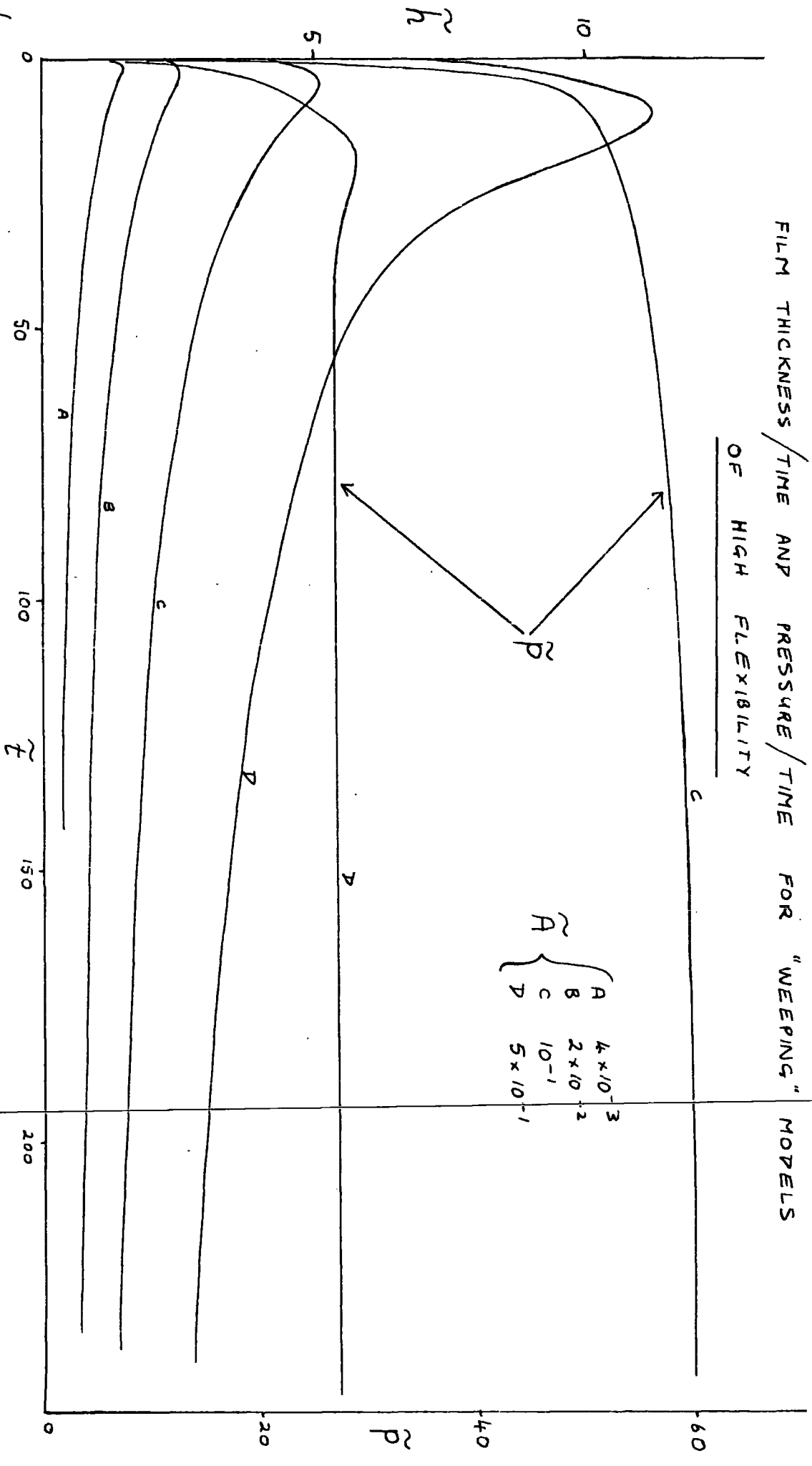
COMPARISON OF "WEEPING" MODEL WITH
EXTREMELY NON-ISOTROPIC PERMEABLE
MODELS IN WHICH $u_0 \eta_0 / \phi_{rT} \neq 0$



$\tilde{A} = 10^{-3}$

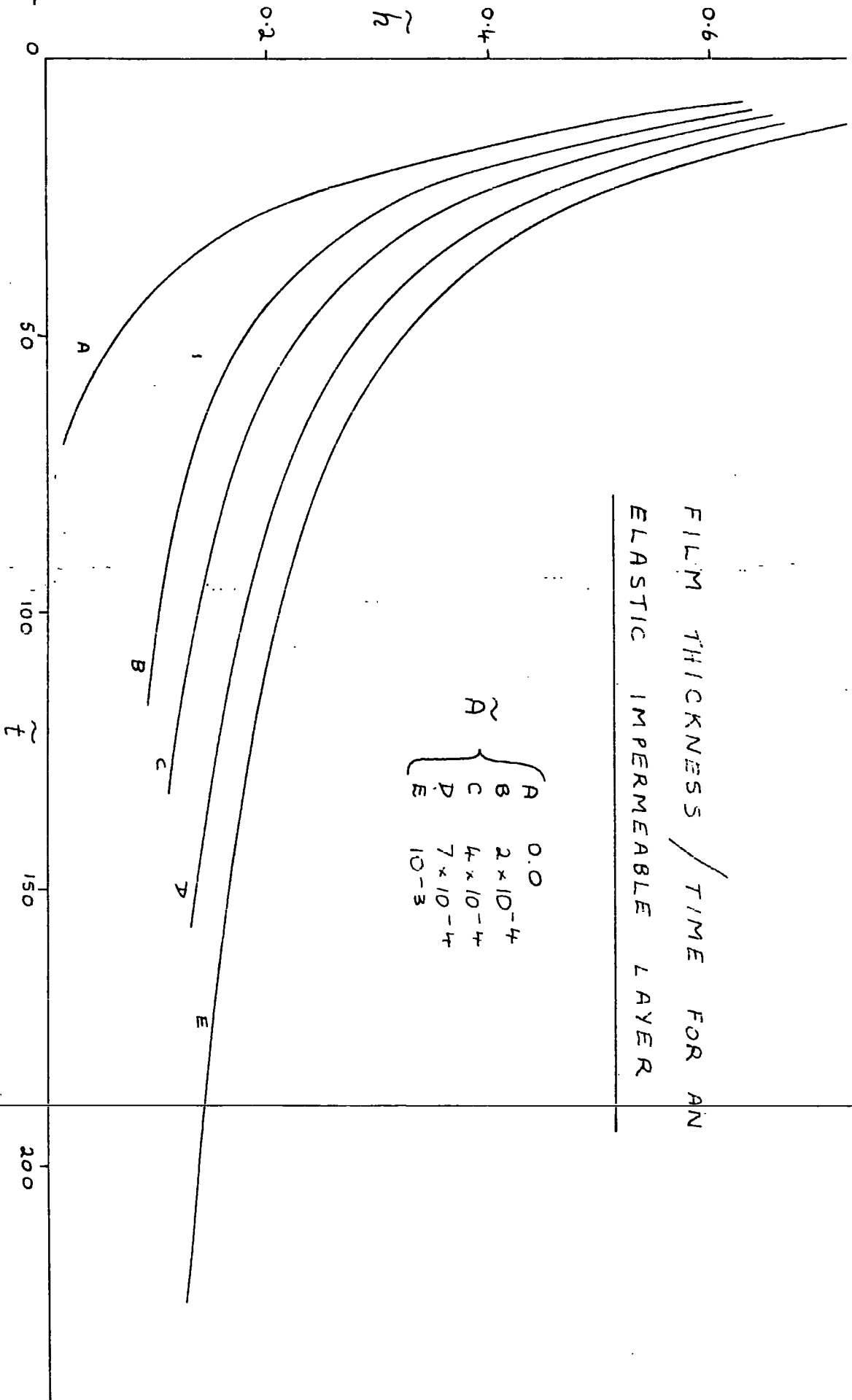
A	}	"WEEPING" MODEL
B		$\tilde{\phi} = 0$
C		$\phi_z = \phi_r = 10^{-3}$
D		" " = 10^{-2}
E		$\phi_z = 3 \times 10^{-3}$, $\phi_r = 3 \times 10^{-5}$
F		" " , $\phi_r = 3 \times 10^{-6}$

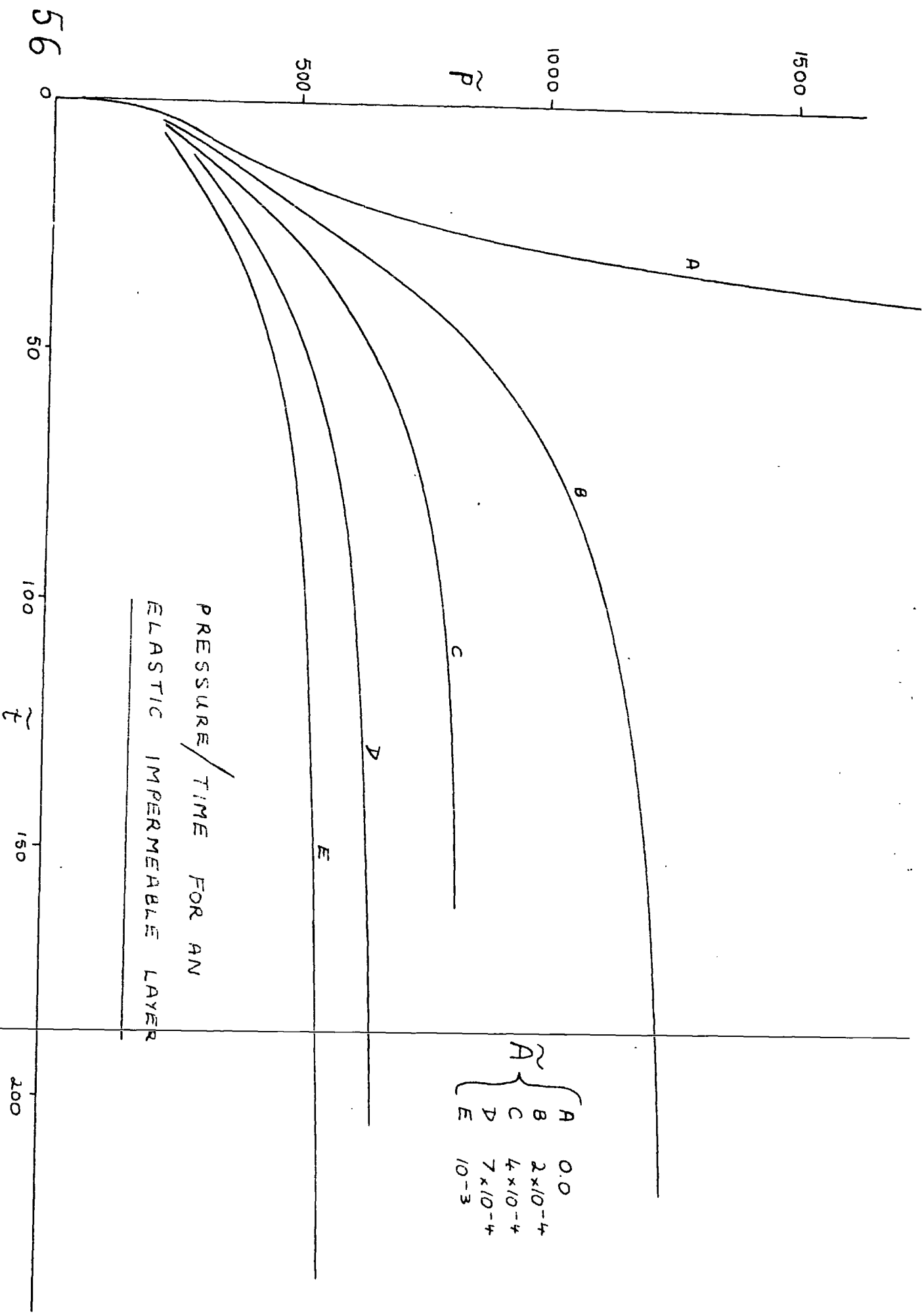
FILM THICKNESS / TIME AND PRESSURE / TIME FOR "WEEPING" MODELS
 OF HIGH FLEXIBILITY



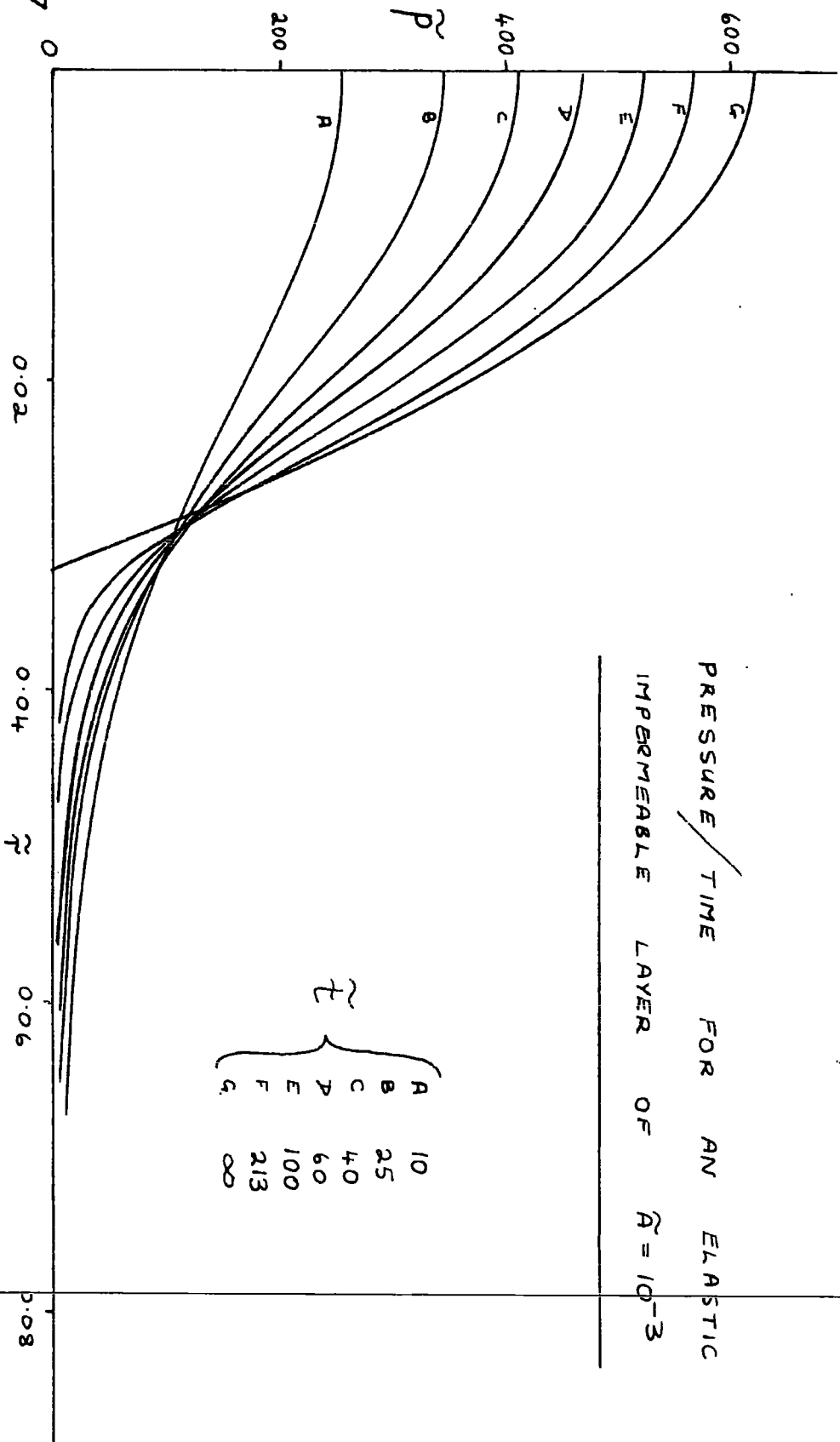
FILM THICKNESS / TIME FOR AN
ELASTIC IMPERMEABLE LAYER

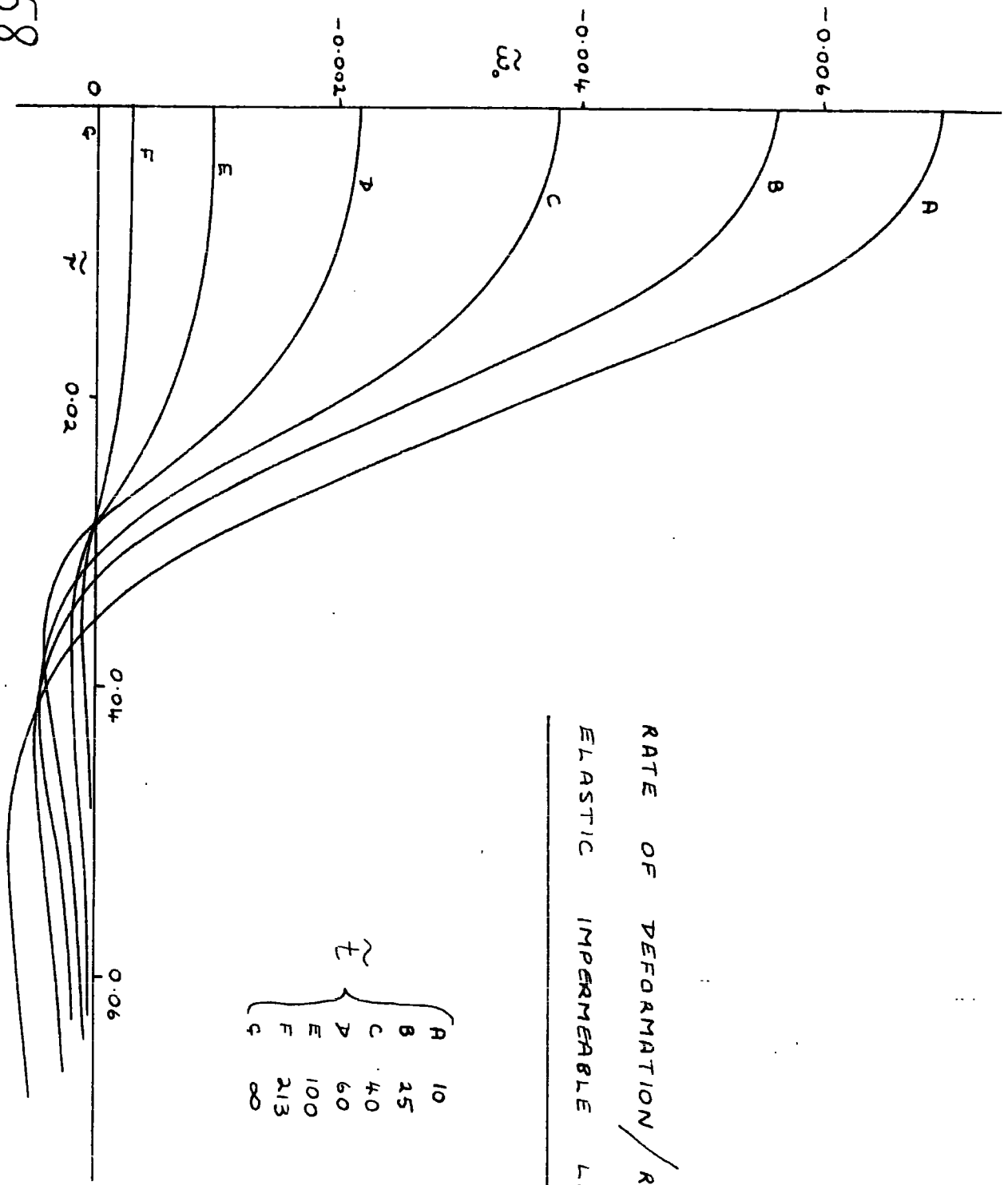
\tilde{h}	{	A	0.0
		B	2×10^{-4}
		C	4×10^{-4}
		D	7×10^{-4}
		E	10^{-3}





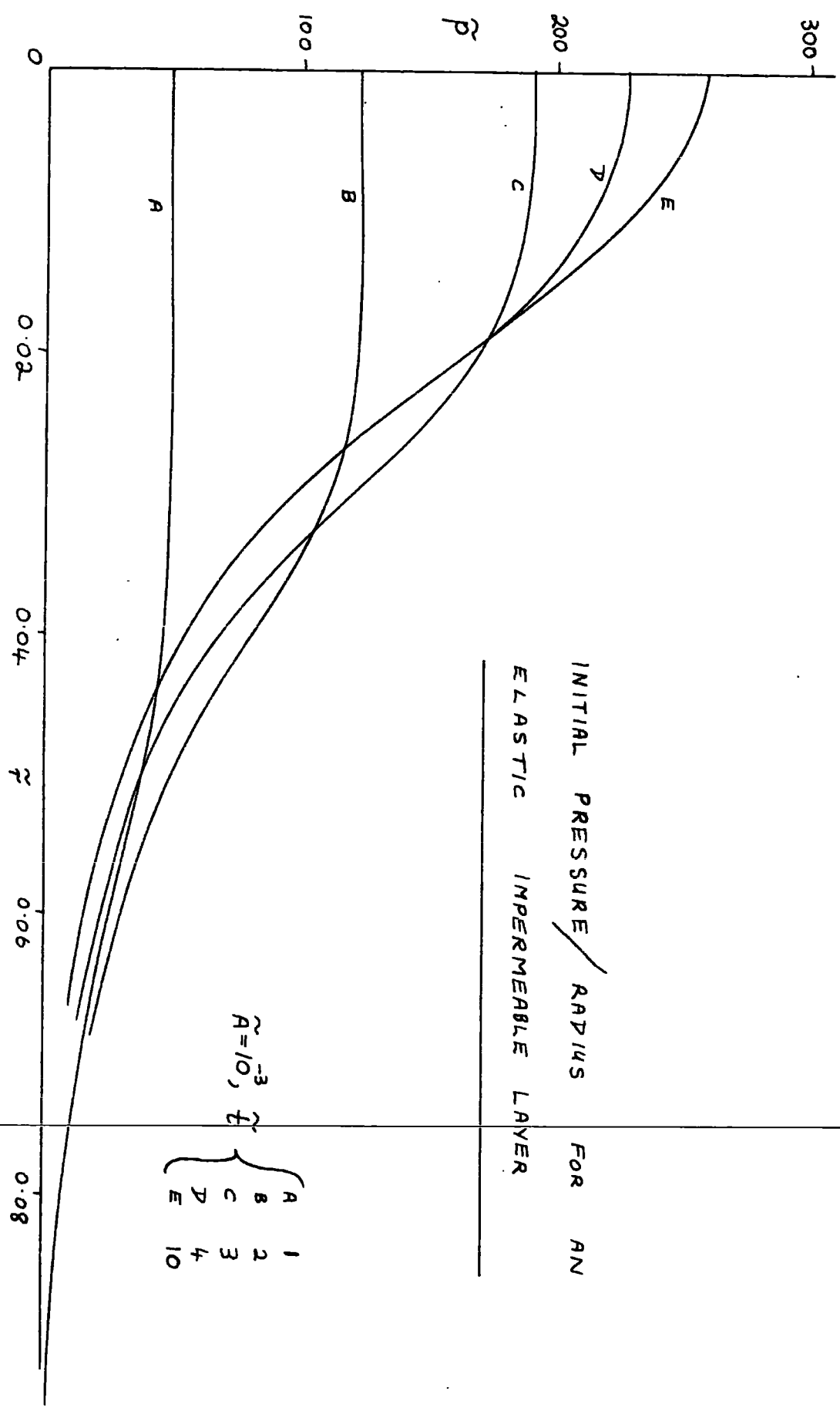
PRESSURE / TIME FOR AN ELASTIC IMPERMEABLE LAYER OF $\tilde{A} = 10^{-3}$

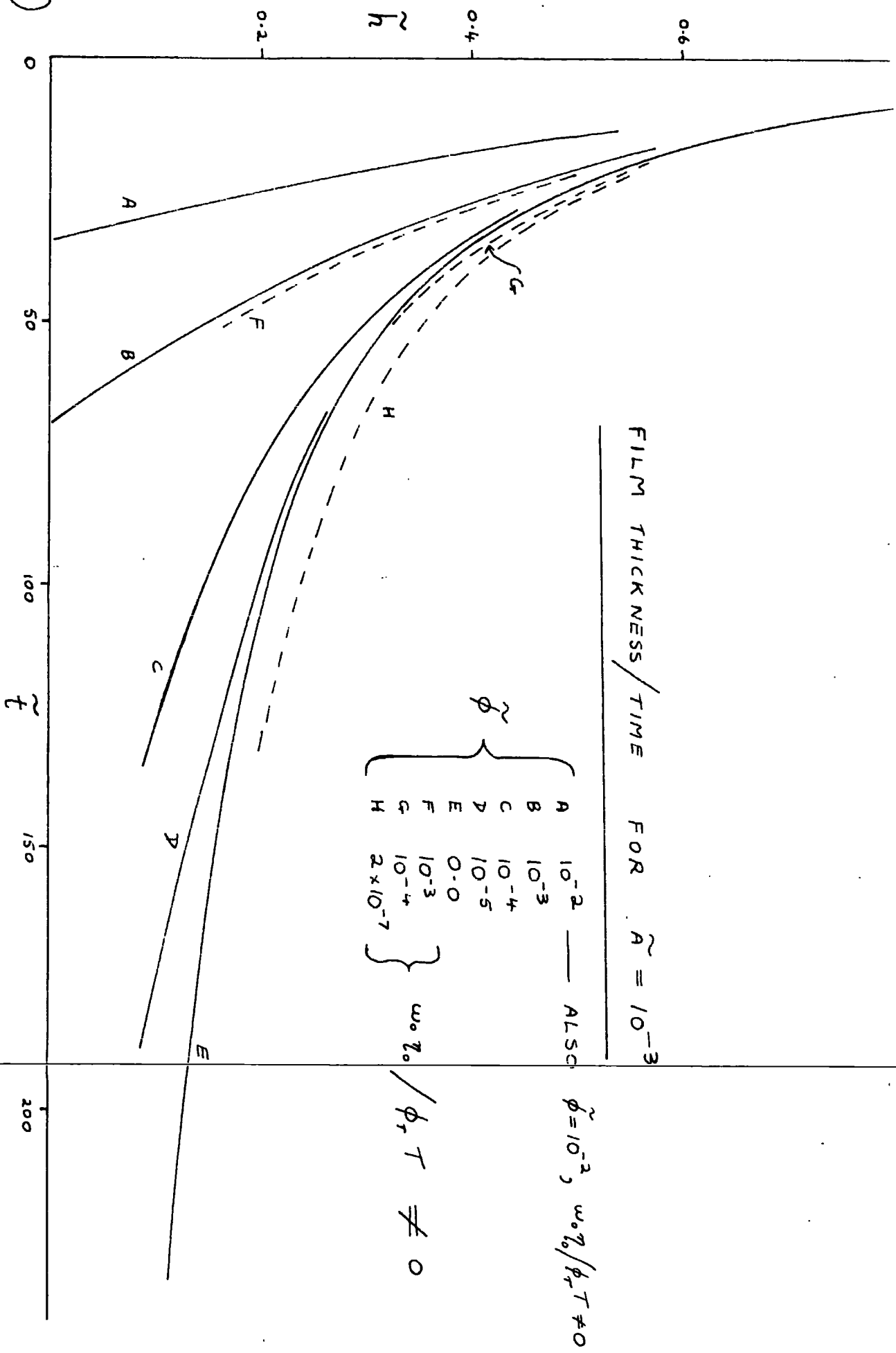


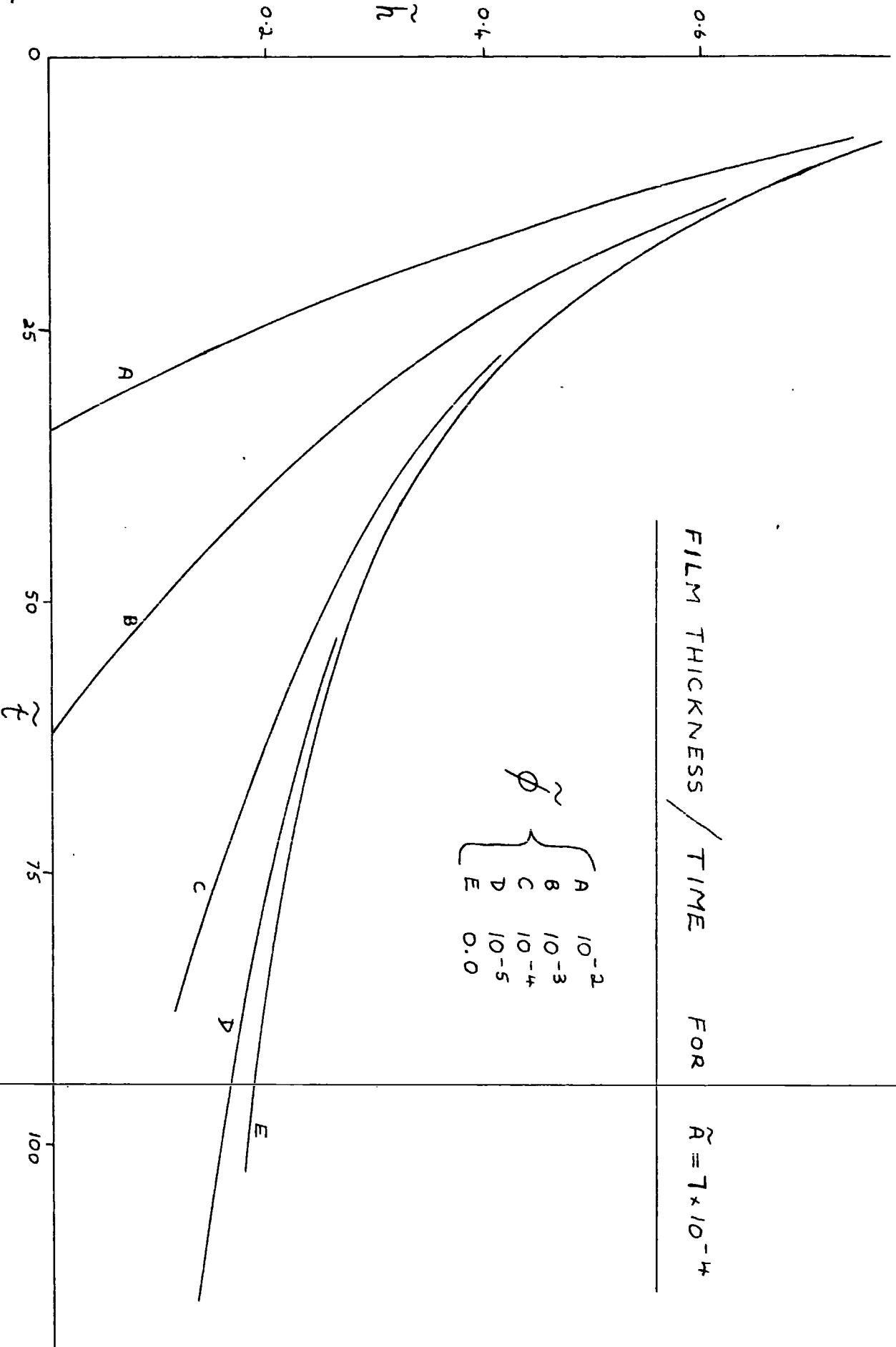


RATE OF DEFORMATION / RADIUS FOR AN ELASTIC IMPERMEABLE LAYER OF $\tilde{A} = 10^{-3}$

\tilde{F}	Curve	Value
A	10	10
B	25	25
C	40	40
D	60	60
E	100	100
F	213	213
G	∞	∞

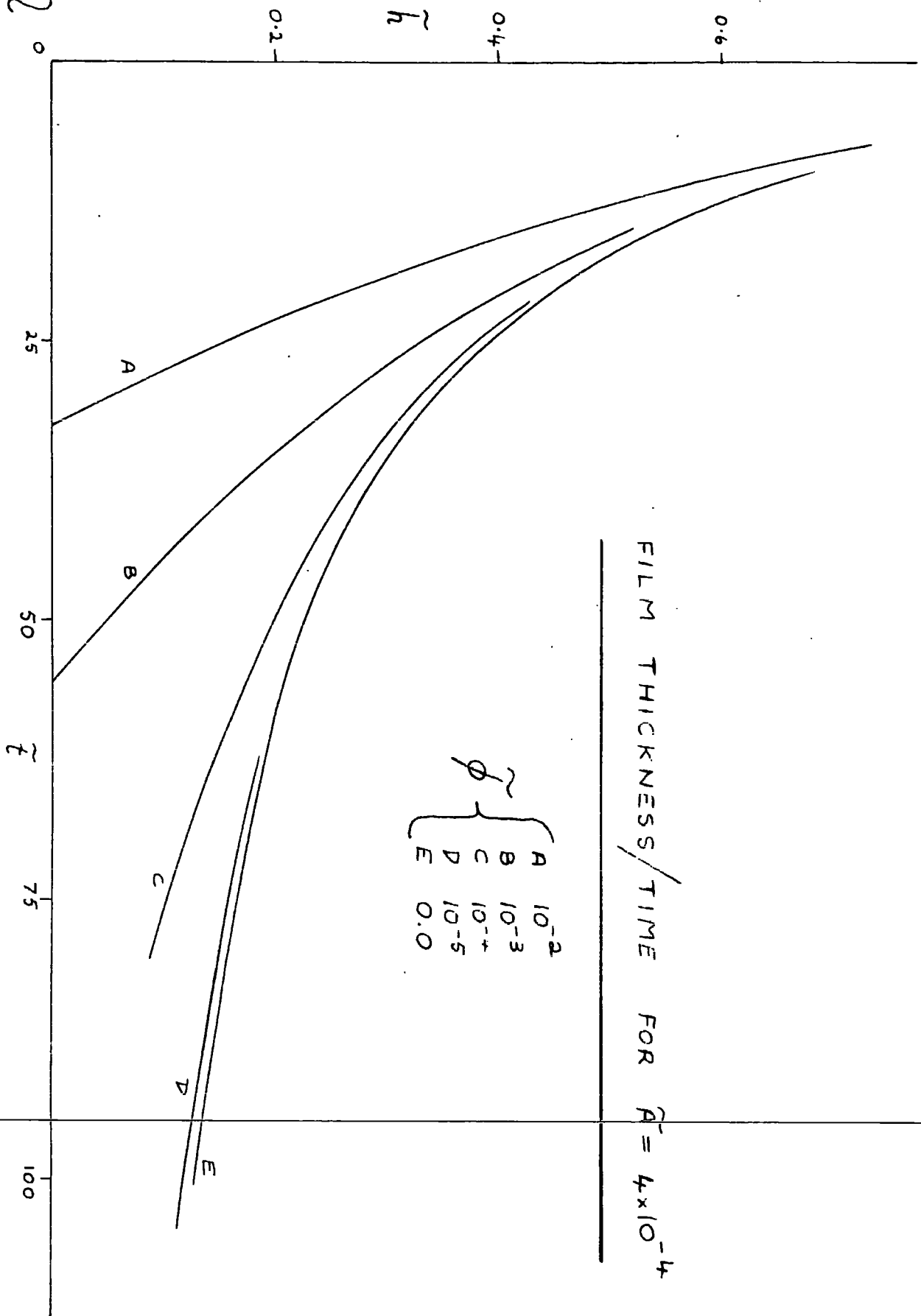


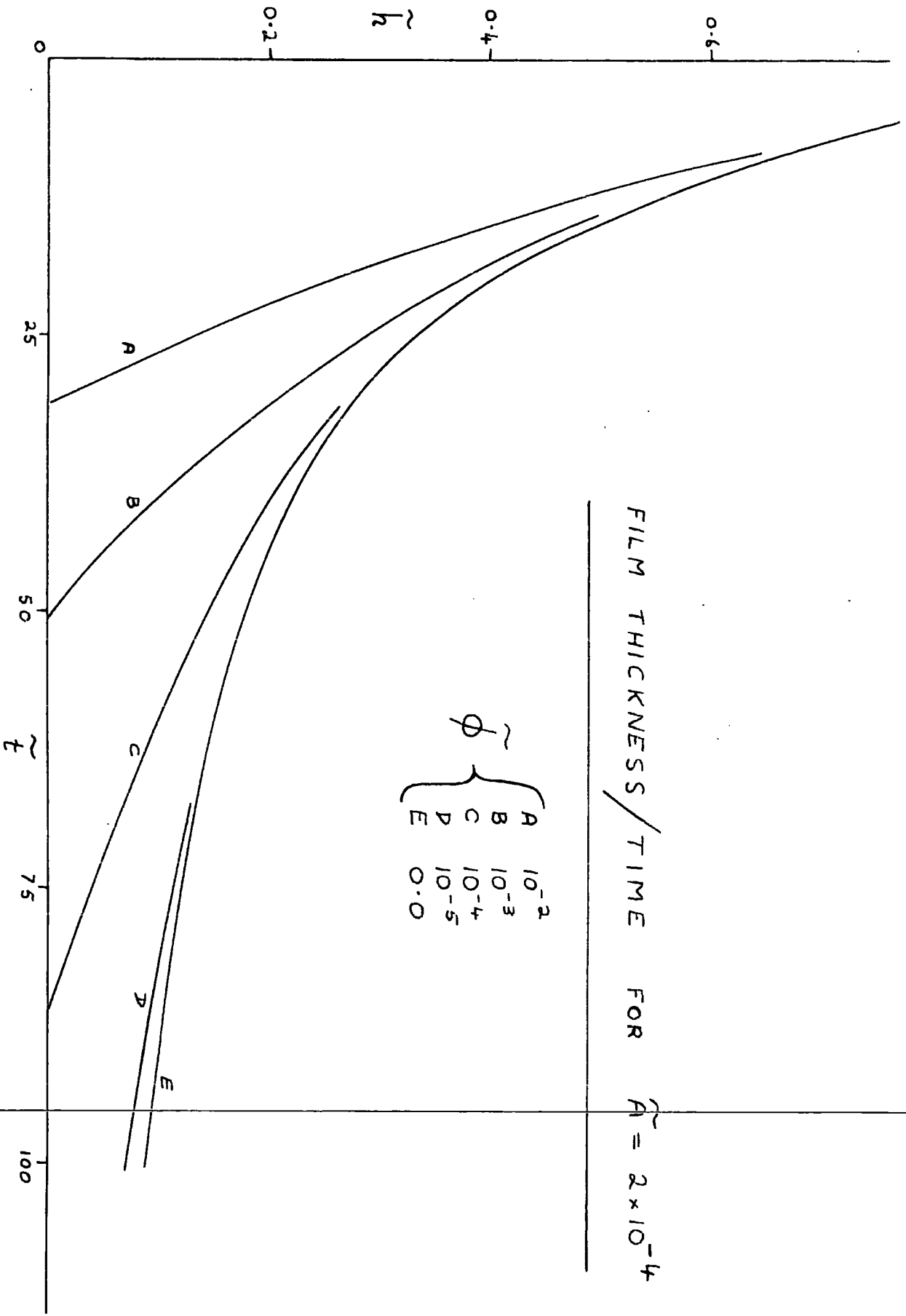


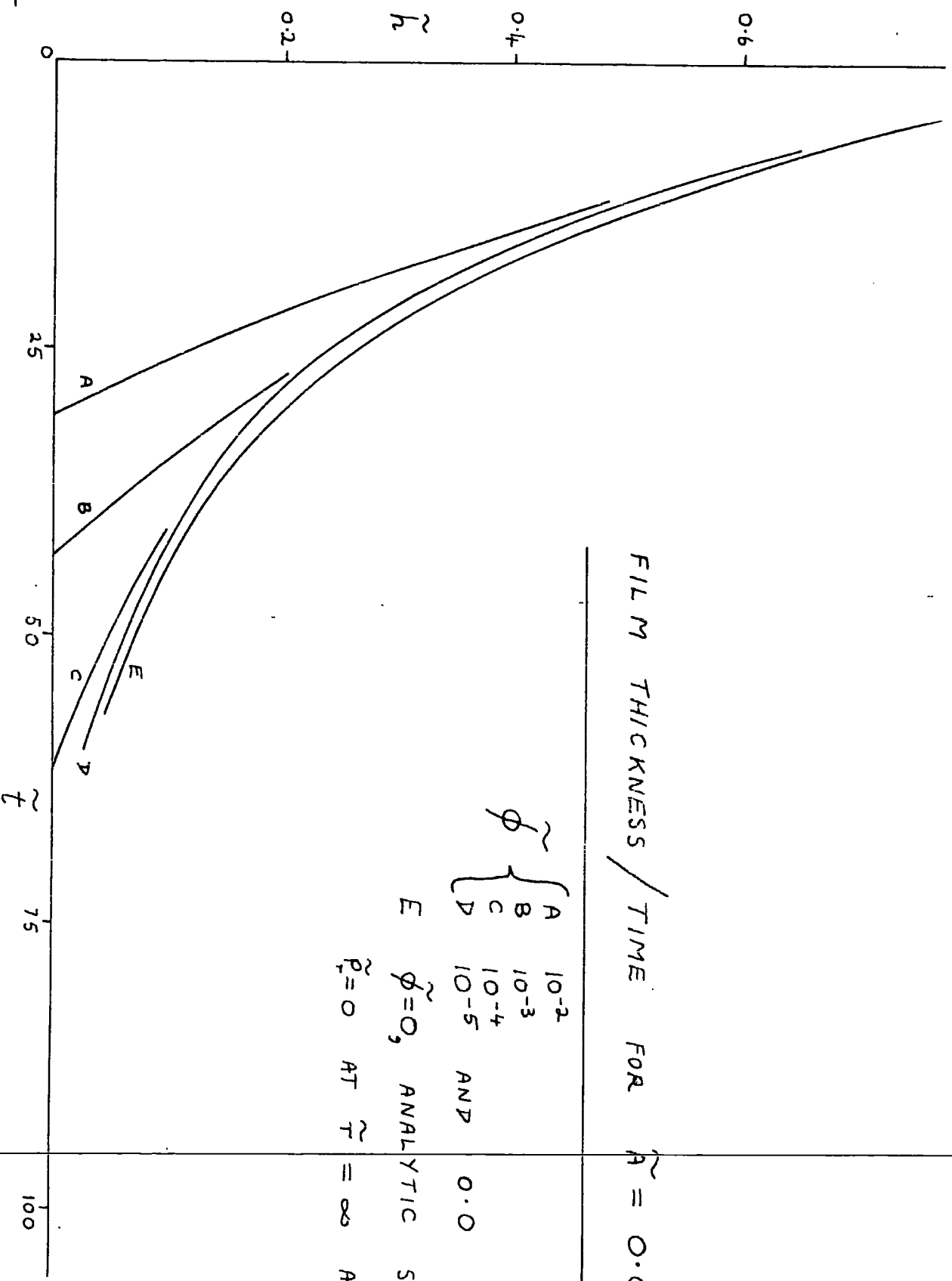


FILM THICKNESS / TIME FOR $\tilde{\Lambda} = 7 \times 10^{-4}$

$\tilde{\phi}$	Case	Value
}	A	10^{-2}
	B	10^{-3}
	C	10^{-4}
	D	10^{-5}
	E	0.0



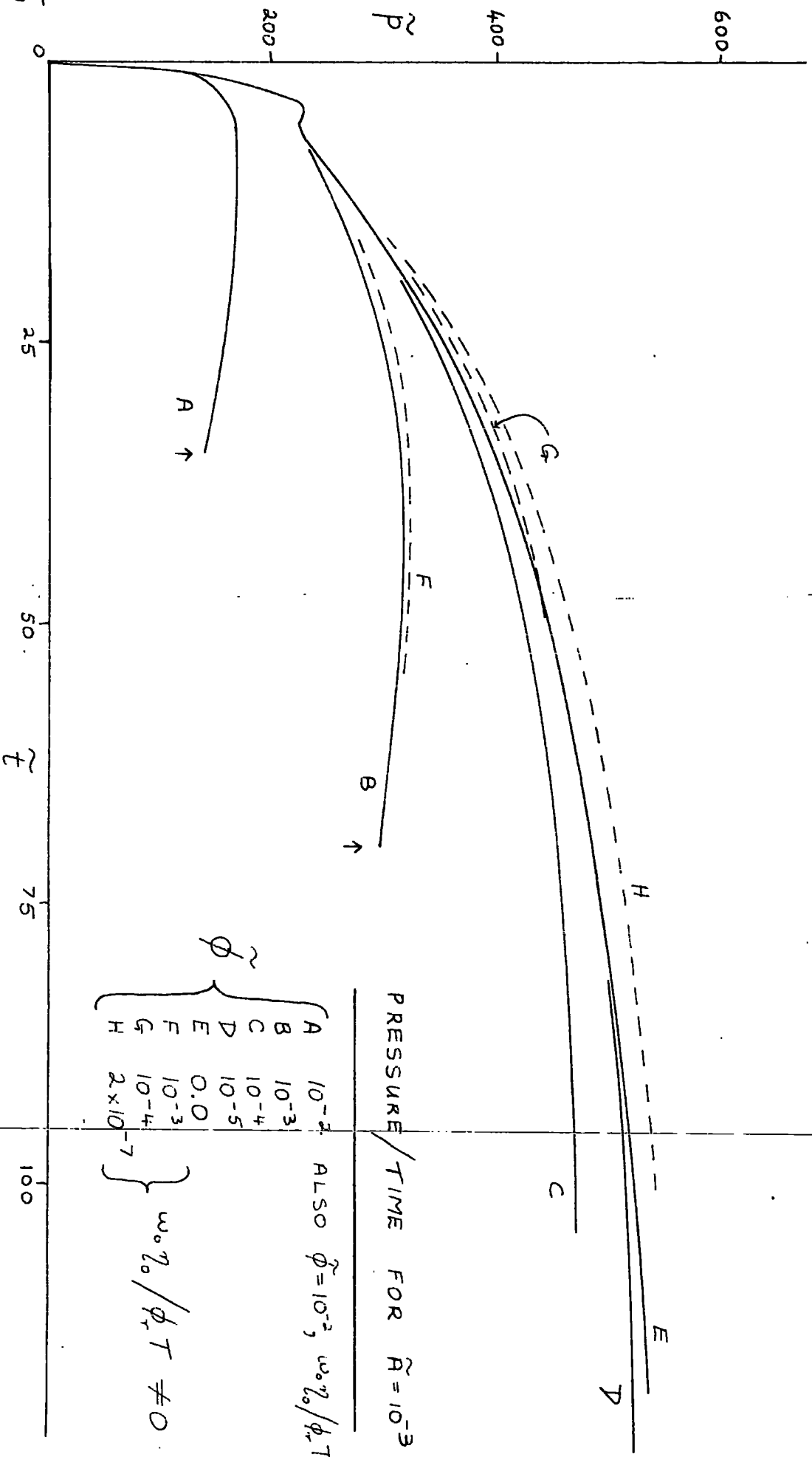


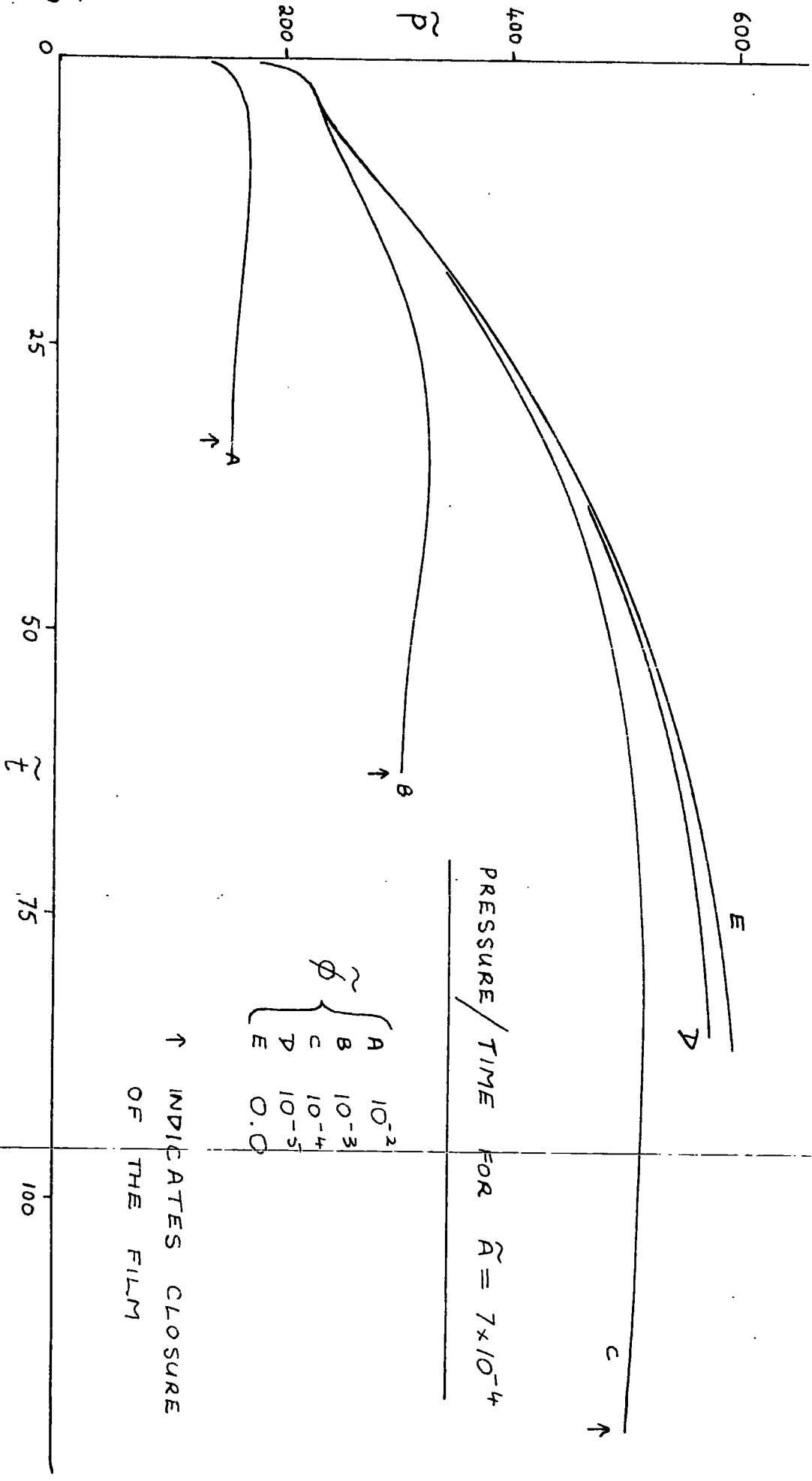


FILM THICKNESS / TIME FOR $\tilde{h} = 0.0$

$\tilde{\phi}$	A	10^{-2}	
	B	10^{-3}	
	C	10^{-4}	
	D	10^{-5}	
	E		0.0

E $\tilde{\phi} = 0$, ANALYTIC SOLUTION WITH $\tilde{p}_z = 0$ AT $\tilde{\tau} = \infty$ AND ZERO INERTIA

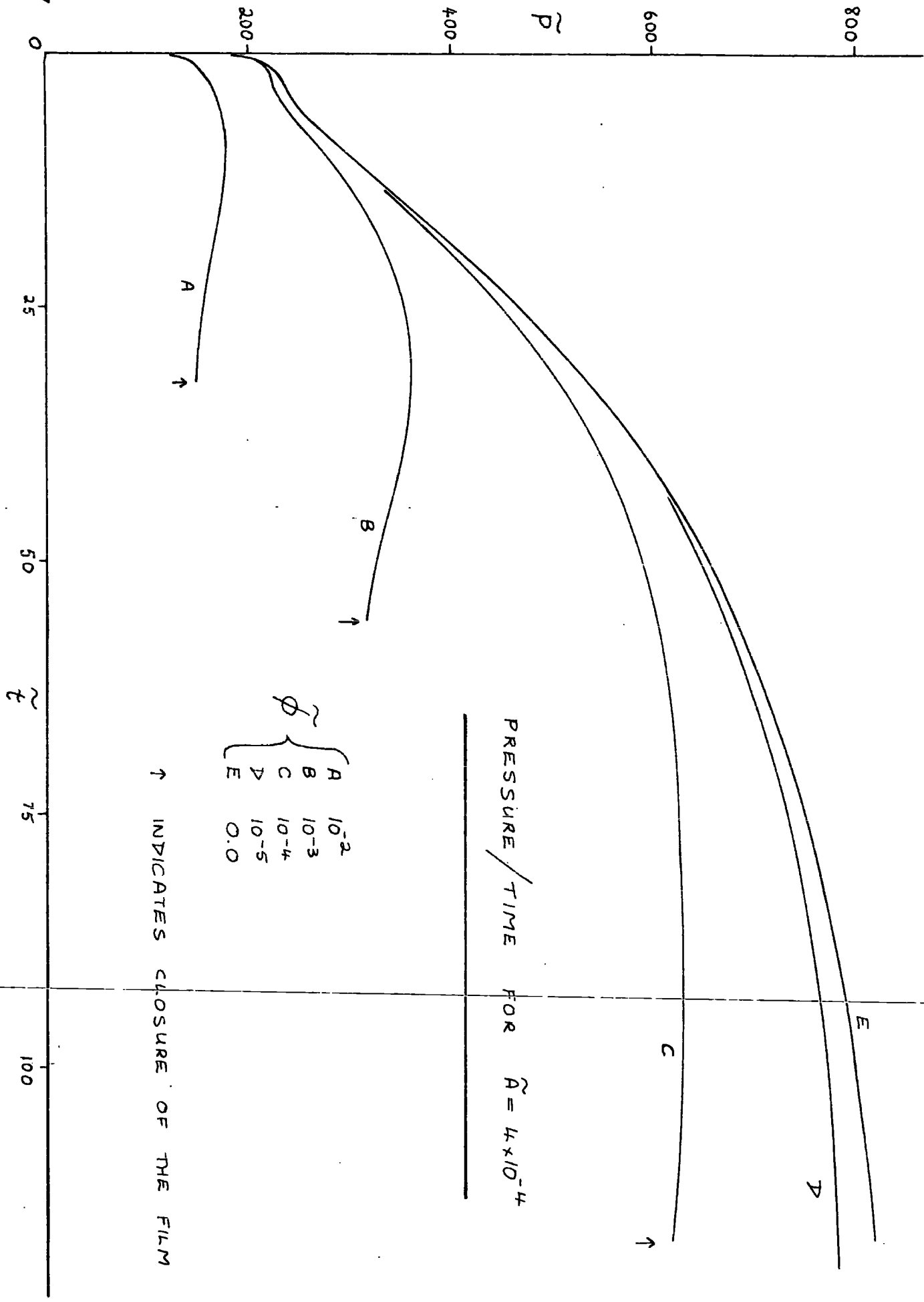




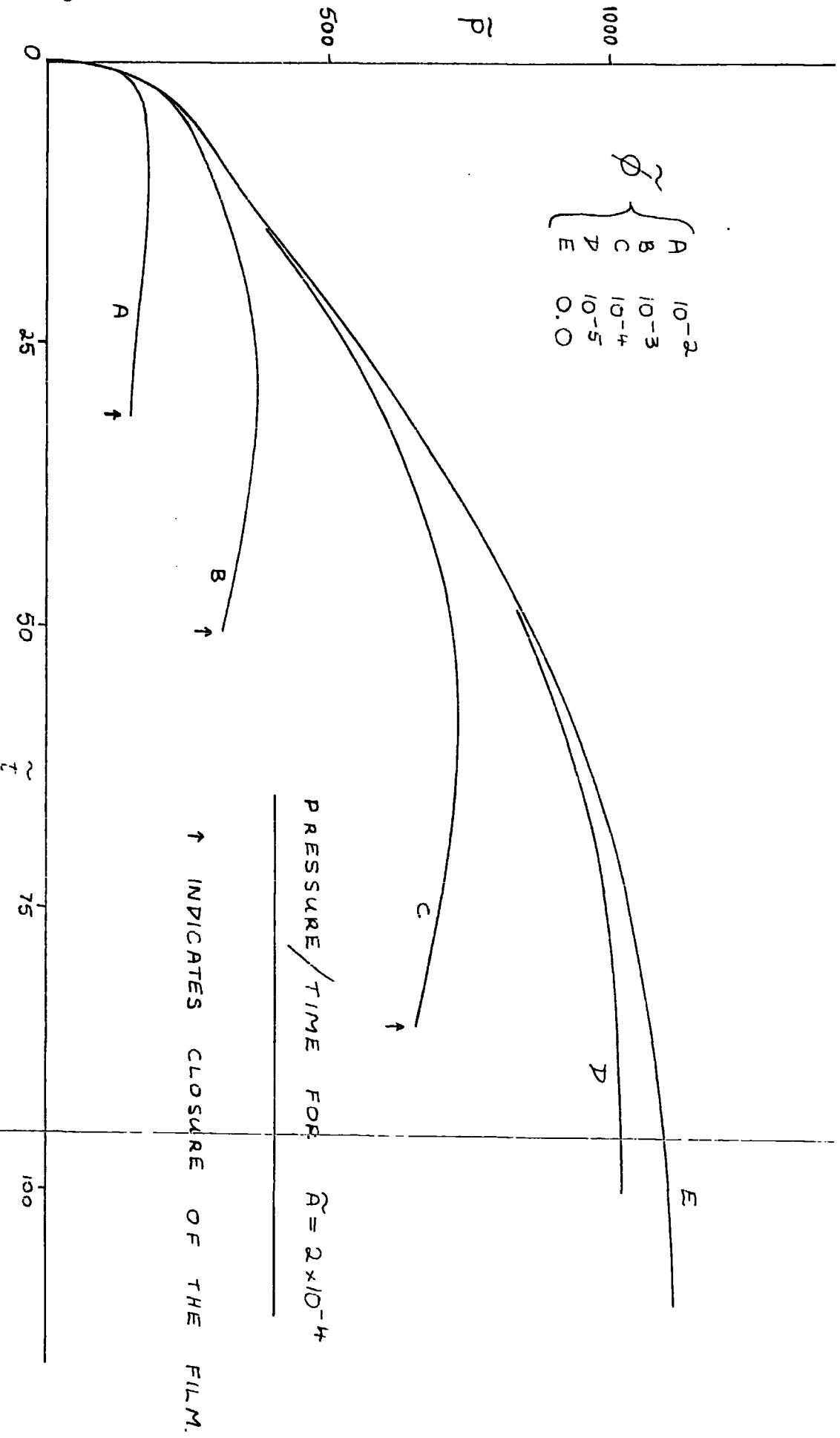
↑ INDICATES CLOSURE OF THE FILM

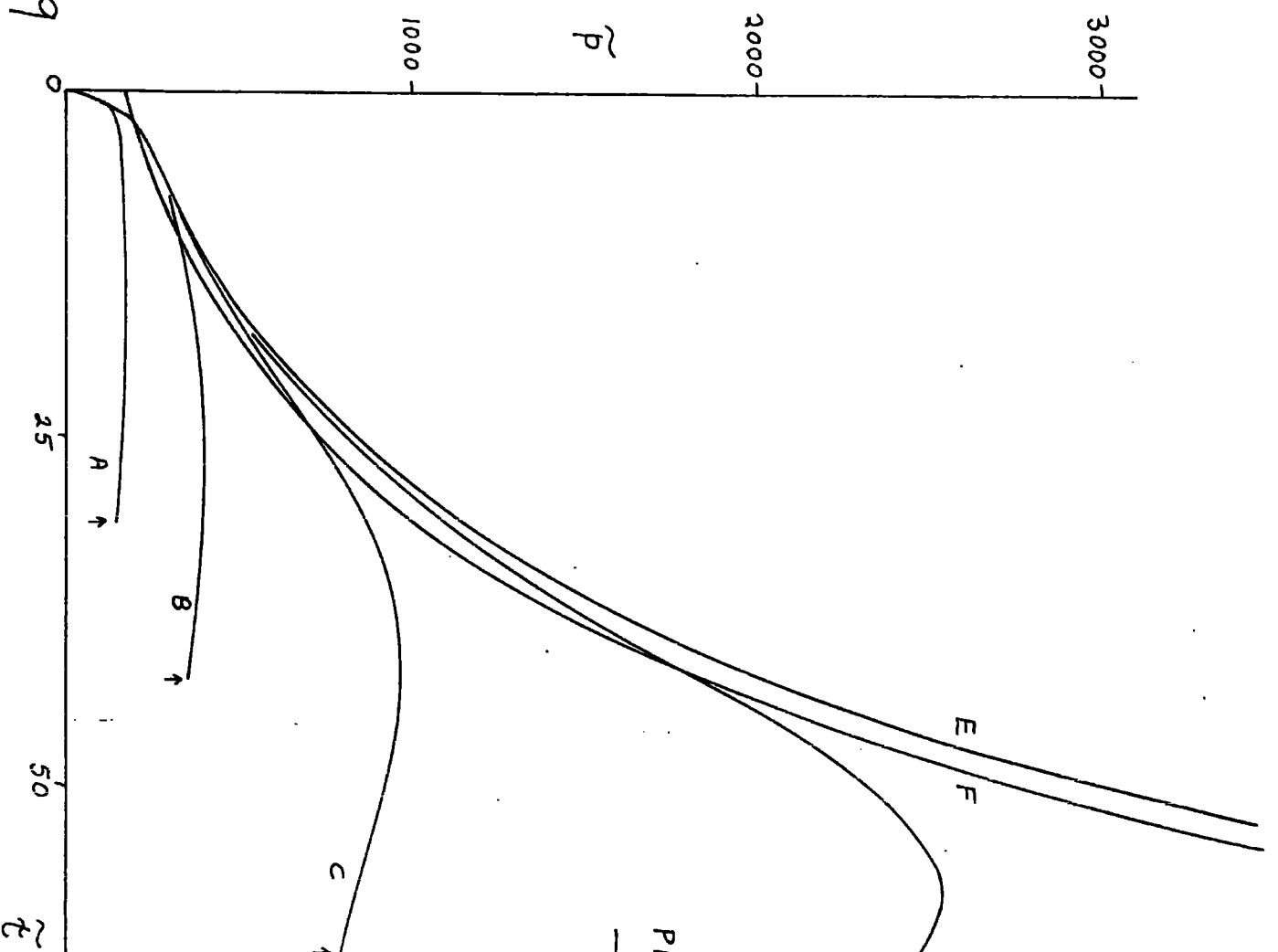
PRESSURE / TIME FOR $\tilde{A} = 7 \times 10^{-4}$

$\tilde{\phi}$	
A	10^{-2}
B	10^{-3}
C	10^{-4}
D	10^{-5}
E	0.0



{	$\tilde{\alpha}$	
	A	10^{-2}
	B	10^{-3}
	C	10^{-4}
	D	10^{-5}
E	0.0	





PRESSURE / TIME FOR $\tilde{A} = 0.0$

$\tilde{\phi}$	
A	10^{-2}
B	10^{-3}
C	10^{-4}
D	10^{-5}
E	0.0

F $\tilde{\phi} = 0$, ANALYTIC SOLUTION WITH
 $\tilde{p} = 0$ AT $\tilde{\tau} = \infty$ AND ZERO INERTIA
 ↑ INDICATES CLOSURE OF THE FILM

DIA GRAM 71

EXPERIMENTAL DATA

RADIUS OF SPHERICAL SURFACE (R) = 300 mm

INITIAL SEPARATION OF CENTRES OF SURFACES (D) NOMINALLY 0.25 mm

At 25°C, VISCOSITIES OF HVI 160, HVI 650, LVI 1100 were 0.21, 1.28, 6.3 Ns/m² respectively.

IMPERMEABLE RUBBER LAYER

THICKNESS, T = 5.34 mm

MASS OF TOP SURFACE, M (kg)	4.33	6.15	7.96
EXPERIMENTAL A (mm ³ /N)	0.42	0.38	0.38
THEORETICAL A (mm ³ /N)	0.34	0.32	0.31

"WEEPING" RUBBER LAYER

THICKNESS, T = 5.34 mm

MASS OF TOP SURFACE, M (kg)	4.33	6.15	7.96
EXPERIMENTAL A (mm ³ /N)	0.53	0.51	0.50
THEORETICAL A (mm ³ /N)	0.45	0.44	0.42

DIAGRAM 71 (CONTINUED)

THE "HIGH PERMEABILITY" MATERIAL

VOID RATIO, V = 0.29

THICKNESS, T = 5.11 mm

A (EXPERIMENTAL AND THEORETICAL) = $1.53 \times 10^{-2} \text{ mm}^3/\text{N}$

RADIAL PERMEABILITY, ϕ_r = $1.28 \times 10^{-5} \text{ mm}^2$

AXIAL PERMEABILITY, ϕ_z = $2.9 \times 10^{-5} \text{ mm}^2$

$$\left(\frac{\phi_z}{\phi_r}\right) = 2.26$$

THE "LOW PERMEABILITY" MATERIAL

VOID RATIO, V = 0.12

THICKNESS, T = 4.46 mm

A (EXPERIMENTAL AND THEORETICAL) = $1.46 \times 10^{-2} \text{ mm}^3/\text{N}$

RADIAL PERMEABILITY, ϕ_r = $9 \times 10^{-7} \text{ mm}^2$

AXIAL PERMEABILITY, ϕ_z = $2.08 \times 10^{-6} \text{ mm}^2$

$$\left(\frac{\phi_z}{\phi_r}\right) = 2.31$$